1  MILBANK, TWEED, HADLEY & McCLOY LLP
   Mark C. Scarsi (SBN 183926)
2  Chris L. Holm (SBN 249388)
   601 South Figueroa Street, 30th Floor
3  Los Angeles, CA   90017-5735
   Telephone:  (213) 892-4000
4  Facsimile:  (212) 822-5796
   F-N-wg@milbank.com
5
   MILBANK, TWEED, HADLEY & McCLOY LLP
6  Christopher E. Chalsen
   Michael M. Murray
7  Lawrence T. Kass
   1 Chase Manhattan Plaza
8  New York, NY   10005
   Telephone:  (212) 530-5000
9  Facsimile:  (212) 822-5796
   F-N-wg@milbank.com
10
   Attorneys for Defendants,
11 FUJITSU LIMITED and
   FUJITSU MICROELECTRONICS AMERICA, INC.
12
                    **UNITED STATES DISTRICT COURT**
13                 **NORTHERN DISTRICT OF CALIFORNIA**
                        **OAKLAND DIVISION**
14
   KLA-Tencor Corporation,                Case No.   4:08-CV-01254 (CW)
15
              *Plaintiff*,                 **DECLARATION OF FRANK A. BRUNO**
16
         -against-
17
   FUJITSU LIMITED and
18 FUJITSU MICROELECTRONICS
   AMERICA, INC.
19
              *Defendants*.
20
21
22
23
24
25
26
27
28

1    I, Frank A. Bruno, declare:

2        1.    I am a member of the Bar of the State New York, an attorney with

3 Milbank, Tweed, Hadley & McCloy LLP, 1 Chase Manhattan Plaza, New York, NY 10005, and

4 counsel for Defendants Fujitsu Limited and Fujitsu Microelectronics America, Inc. in this

5 action.

6

7        2.    I have first hand knowledge of the facts set forth herein, or have learned

8 these facts first hand, and, if called and sworn as a witness, I could and would testify

9 competently and from personal knowledge as to these facts.

10        3.    Attached are true and correct copies of the following exhibits:

11 Ex. A    U.S. Patent No. 6,104,486.

12 Ex. B    Fujitsu's First Set of Requests for Production to KLA (Nos. 1-14).

13 Ex. C    "Infineon, Nanya begin 90 nm 300 mm    Volume Production", Electronic News, June 2, 2005.

14 Ex. D    T. Hingst et al., *Spectroscopic Ellipsometry based Scatterometry enabling 193 nm Litho and Etch process control for the 110 nm technology node and beyond,* 5038 PROC. OF SPIE, 274-85 (2003).

16 Ex. E    SpectraCD Product Page, www.kla-tencor.com/j/servlet/Product?prodID=43&focus=1, June 24, 2008.

18 Ex. F    J.N. Hilfiker et al., Generalized spectroscopic ellipsometry and Mueller-matrix study of twisted nematic and super twisted nematic liquid crystals, Thin Solid Films 455-456 (2004) 569-600.

20 Ex. G    J.A. Woollam, et al., VUV and IR spectroellipsometric studies of polymer surfaces, Nuclear Instruments and Methods in Physics Research B 208 (2003) 35–39.

21 Ex. H    J.A. Woollam, Emerging Applications of Spectroscopic Ellipsometry, Glass Coatings, (1/2007) 24-27.

22 Ex. I    J. Wagner, Spectroscopic Ellipsometry Analysis of InGaN/GaN and AIGaN/GaN Heterostructures Using a Parametric Dielectric Function Model, MRS Internet J. Nitride Semicond. Res. XX, WY.Y (2000).

24 Ex. J    Excerpts from Fujitsu's Responses and Objections to Third-Party Defendant KLA-Tencor Corporation's First Set of Requests for Admissions to Plaintiffs Fujitsu Limited and Fujitsu Microelectronics America, Inc. (1-90), June 30, 2008.

26

27

28

1        I declare under penalty of perjury that the foregoing is true and correct.   Executed at New

2   York, NY, on July 1, 2008.

3

4   Dated:   July 1, 2008            By:   _____

                                           Frank A. Bruno
5

6

7

8

9

10

11

12

13

14

15

16

17

18

19

20

21

22

23

24

25

26

27

28

**DECLARATION OF FRANK A. BRUNO**
4:08-CV-01254 (CW)

# Exhibit A

US006104486A

# United States Patent [19]

## Arimoto

[11] **Patent Number:** **6,104,486**

[45] **Date of Patent:** **\*Aug. 15, 2000**

[54] **FABRICATION PROCESS OF A SEMICONDUCTOR DEVICE USING ELLIPSOMETRY**

[75] Inventor: **Hiroshi Arimoto**, Kawasaki, Japan

[73] Assignee: **Fujitsu Limited**, Kawasaki, Japan

[ * ] Notice: This patent issued on a continued prosecution application filed under 37 CFR 1.53(d), and is subject to the twenty year patent term provisions of 35 U.S.C. 154(a)(2).

[21] Appl. No.: **08/774,272**

[22] Filed: **Dec. 27, 1996**

[30] **Foreign Application Priority Data**

Dec. 28, 1995 [JP] Japan ..................................... 7-343924

[51] **Int. Cl.$^7$** ....................................................... **G01J 3/00**
[52] **U.S. Cl.** .......................... **356/300**; 356/305; 356/310; 356/322; 356/337; 356/340; 356/345; 356/351; 356/364; 356/128; 250/492.1; 250/492.2; 250/492.22; 250/492.3
[58] **Field of Search** ..................................... 356/300, 305, 356/310, 322, 337, 340, 345, 351, 364, 128; 250/492.1, 492.2, 492.22, 492.3

[56] **References Cited**

### U.S. PATENT DOCUMENTS

4,653,924  3/1987  Itonaga et al. ........................... 356/369

5,349,197  9/1994  Sakamoto et al. .................. 250/492.22
5,404,019  4/1995  Ohno et al. ......................... 250/492.22

### FOREIGN PATENT DOCUMENTS

57-132039   8/1982   Japan .
58-206120  12/1983   Japan .
61-4905    1/1986    Japan .

### OTHER PUBLICATIONS

"Ultraviolet–visible ellipsometry for process control during the etching of submicrometer features", N. Blayo et al., AT&T Bell Laboratories, Murray Hill, New Jersey (Sep. 28, 1994); Optical Society of America, vol. 12, No. 3/Mar. 1995, pp. 591–599.

*Primary Examiner*—Christopher L. Chin
*Assistant Examiner*—Bao-Thuy L. Nguyen
*Attorney, Agent, or Firm*—Armstrong, Westerman, Hattori, McLeland & Naughton

[57] **ABSTRACT**

A method of fabricating a semiconductor device includes the steps of illuminating a structure formed on a surface of a substrate by an incident optical beam incident to the structure with a predetermined incident angle with respect to the surface, measuring a polarization state of an exiting optical beam exiting from the structure in response to an illumination of the structure by the incident optical beam, and evaluating a size of the structure in a direction parallel to the surface from the polarization state of the exiting optical beam, and adjusting a parameter of production of a semiconductor device in response to the size.

**11 Claims, 24 Drawing Sheets**

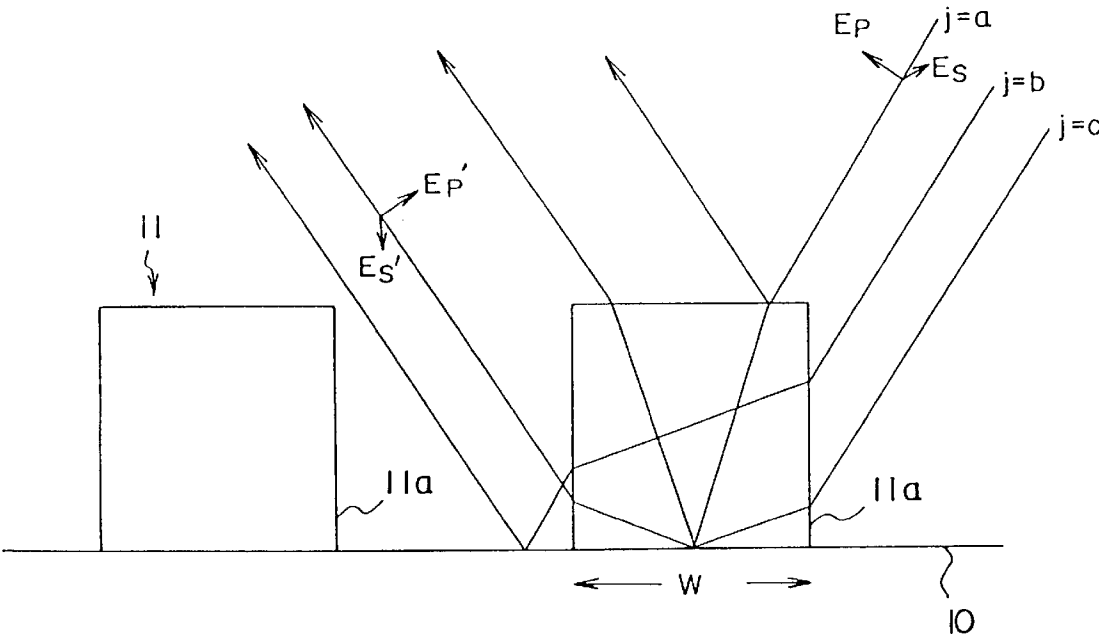**U.S. Patent**          Aug. 15, 2000          Sheet 1 of 24          **6,104,486**
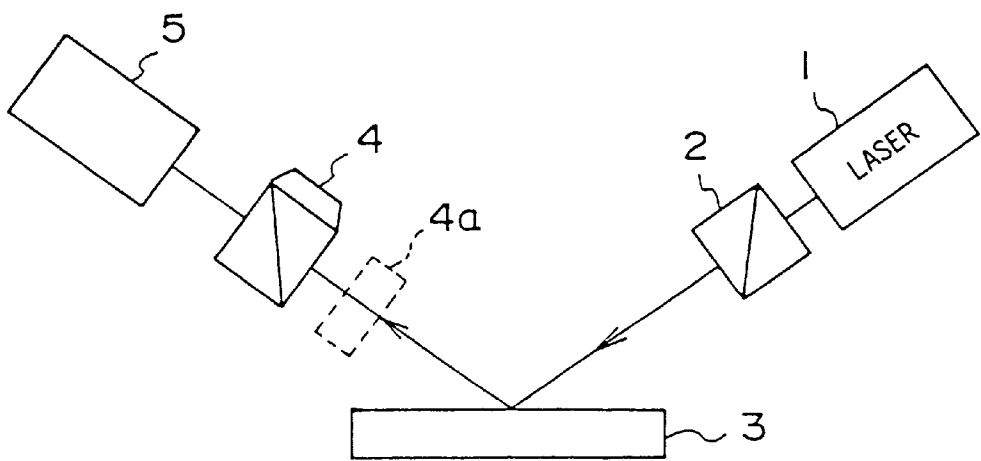
FIG. 1A PRIOR ART



FIG. 1B PRIOR ART

# FIG. 2 PRIOR ART



$$\tan \psi = \frac{\rho_P}{\rho_S}$$

FIG. 3

FIG. 4
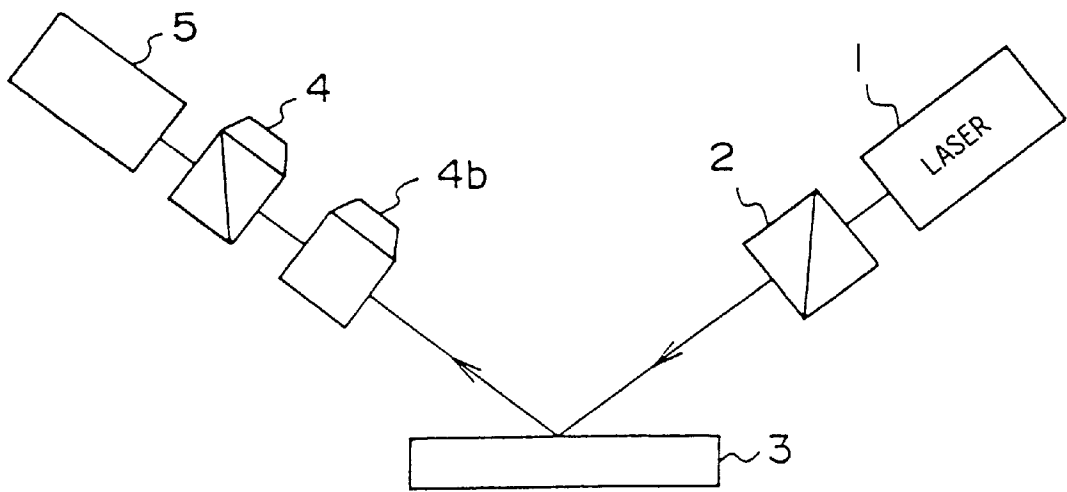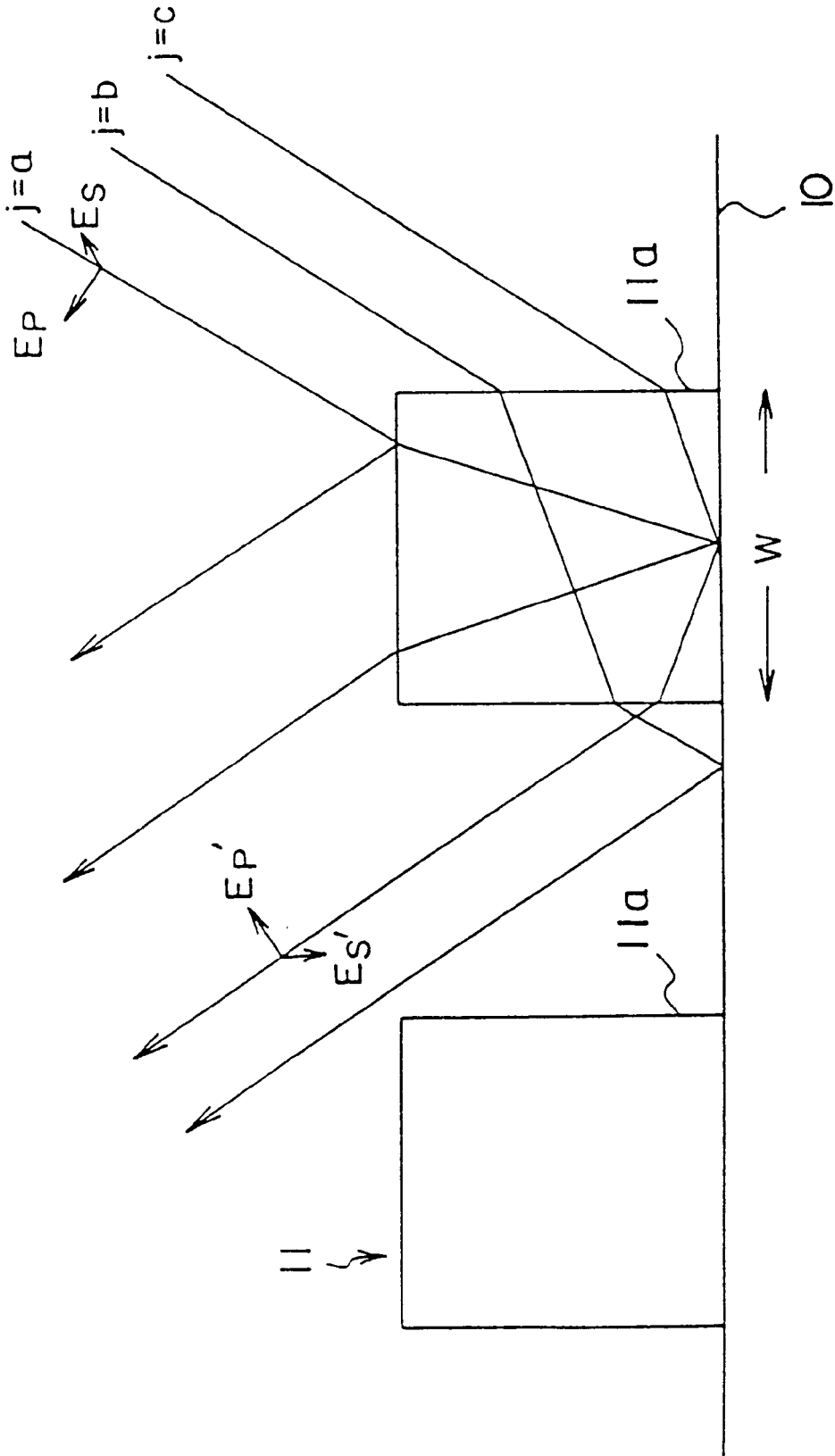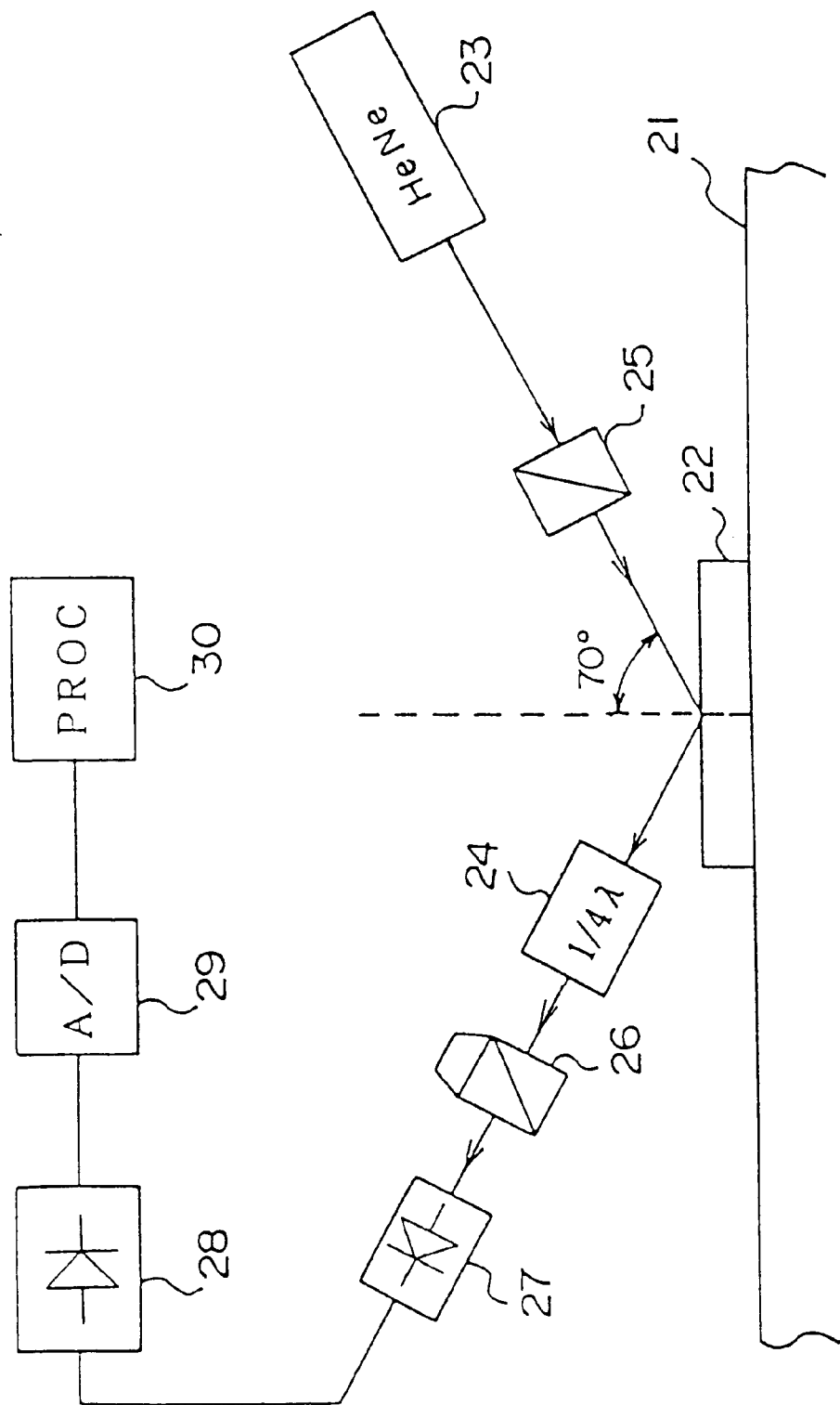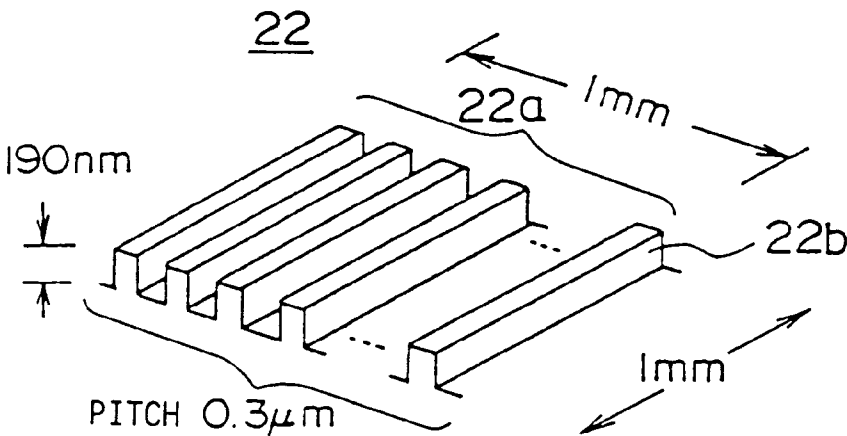
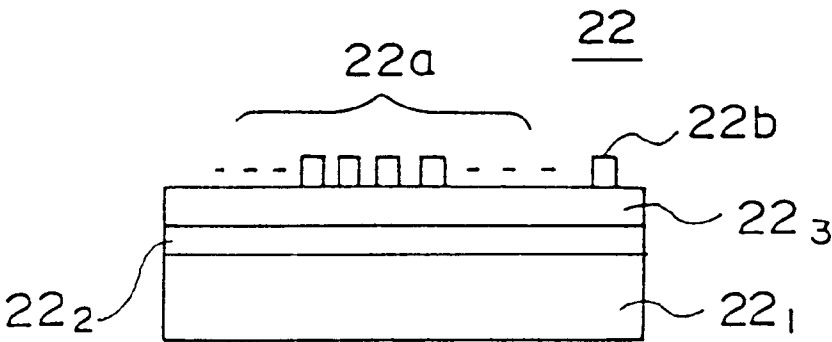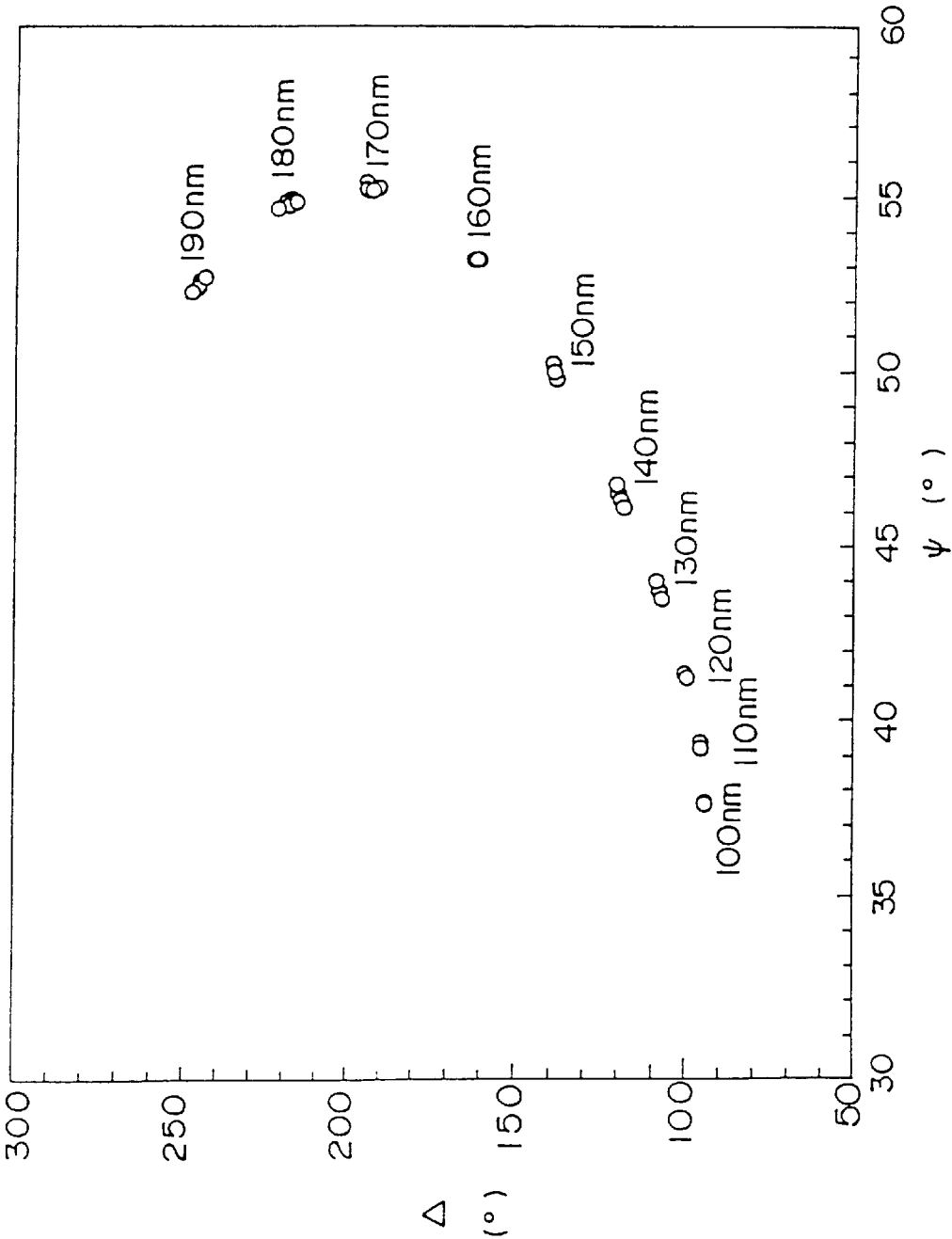**U.S. Patent**      Aug. 15, 2000      Sheet 5 of 24      **6,104,486**
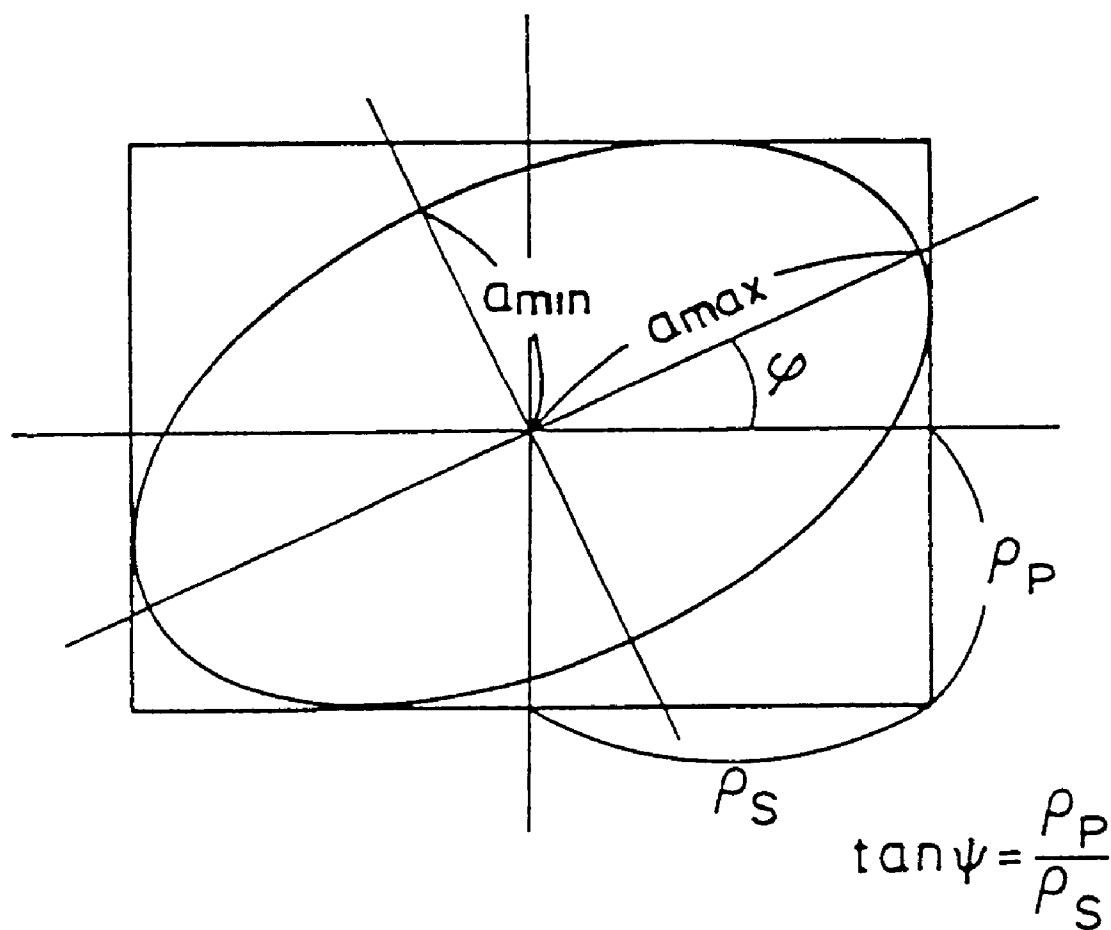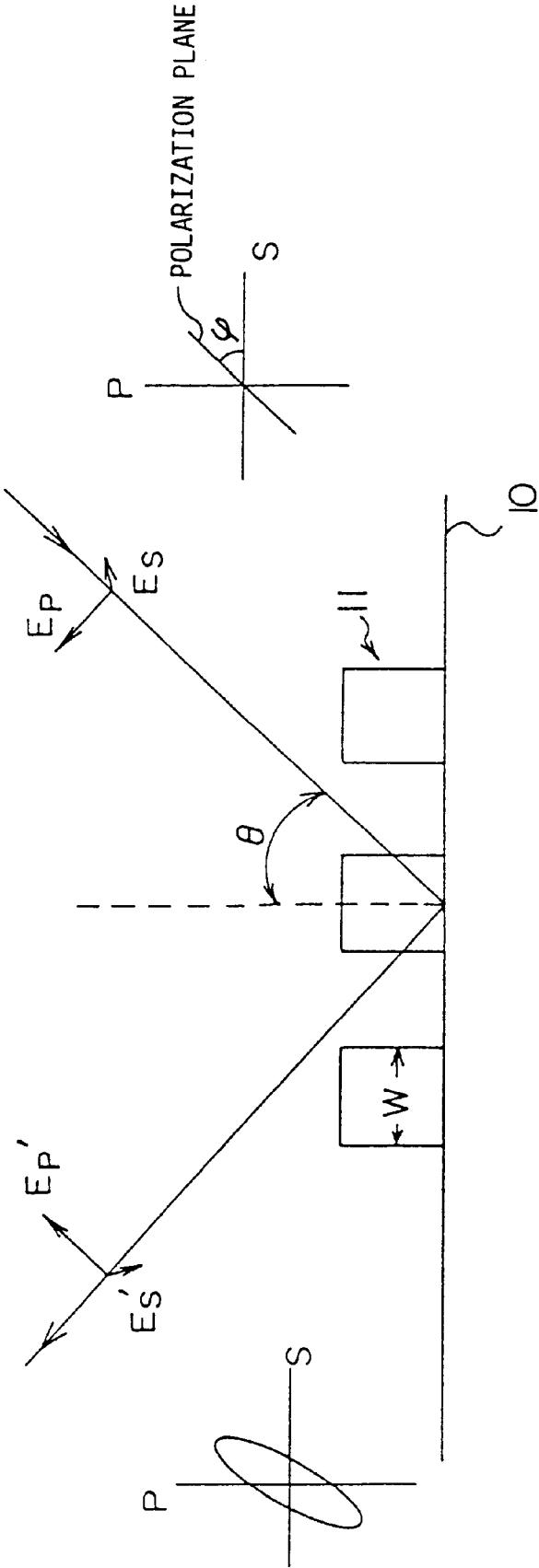
FIG.5

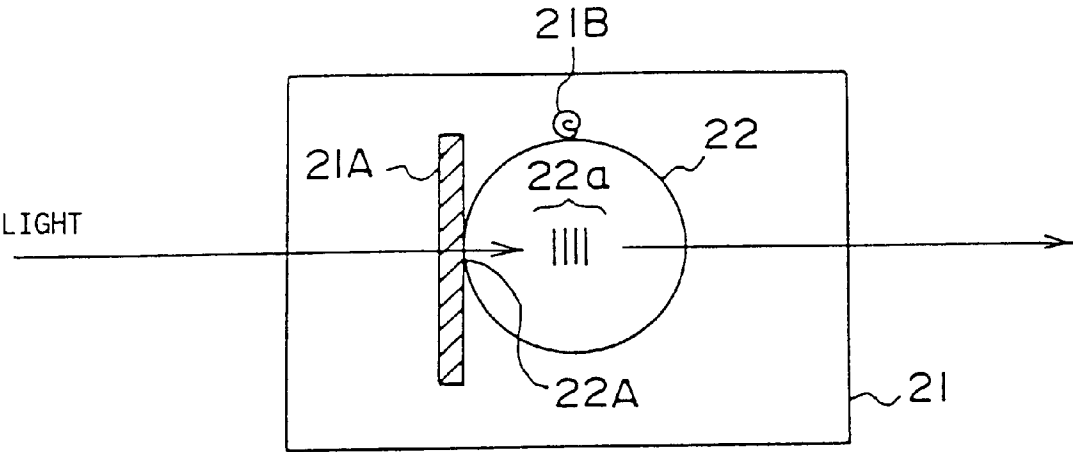# FIG. 6A



# FIG. 6B

FIG. 7

# FIG. 8

FIG. 9
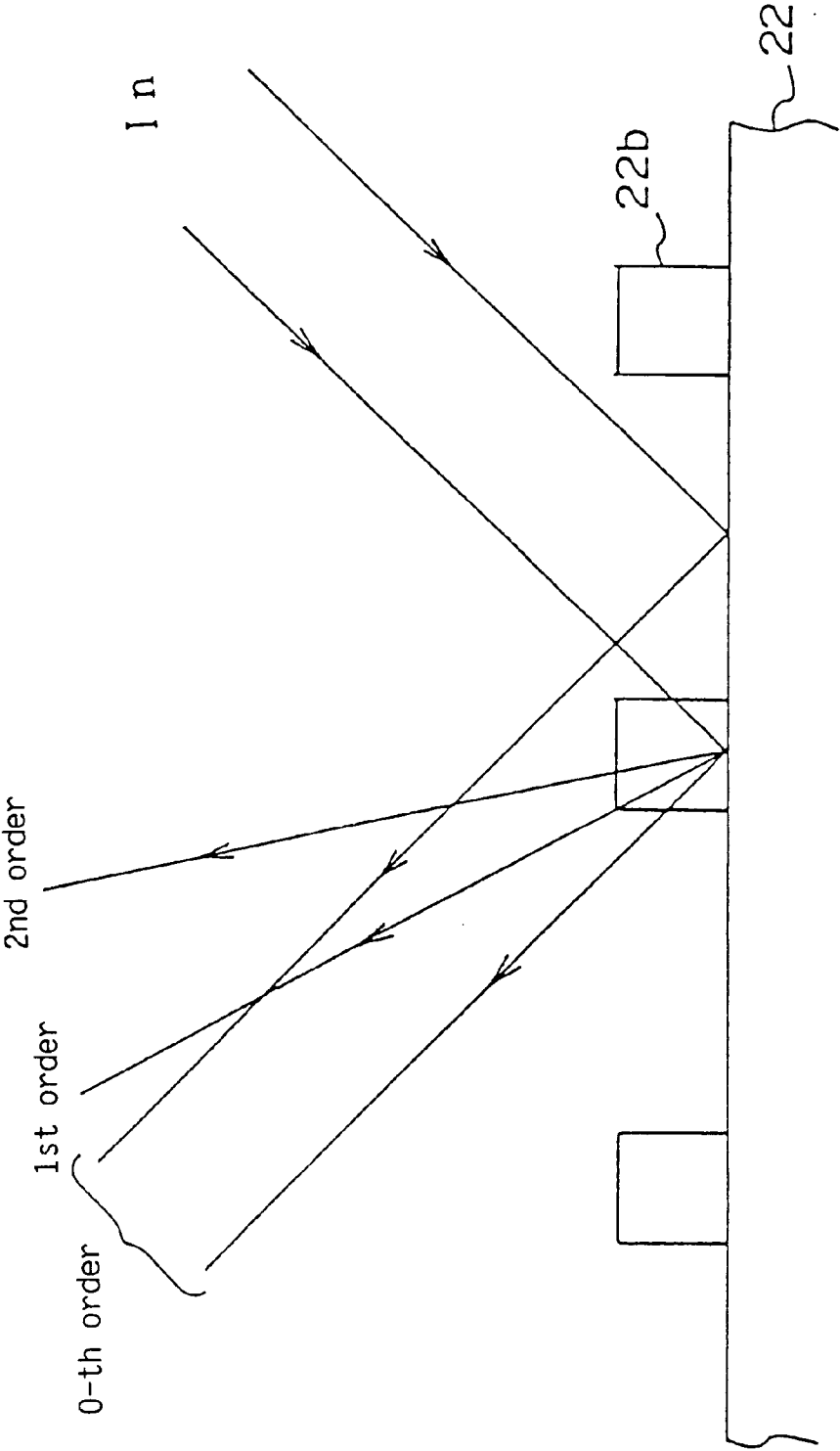
FIG.10

## FIG. 11

FIG.12

FIG. 13

# F I G. 1 4



| | |
|---|---|
| PARAMETER INPUT<br>PATTERN/UNDERGROUND | STEP 1 |
| DIVIDE INTO RAYS | STEP 2 |
| $I_p (i)'$, $I_s (i)'$    $i = 1 \sim n$ | STEP 3 |
| $\Sigma I_p (n)'$, $\Sigma I_s (n)'$ | STEP 4 |
| $\rho = R_p / R_s$ | STEP 5 |
| $\Psi$, $\Delta$ | STEP 6 |
| DATABASE | STEP 7 |

# FIG. 15

# FIG. 16

PolySi / SiO2

Just etch
10% Over etch
30% Over etch

Resist width = 150 nm

$\Delta$ (°)

$\Psi$ (°)
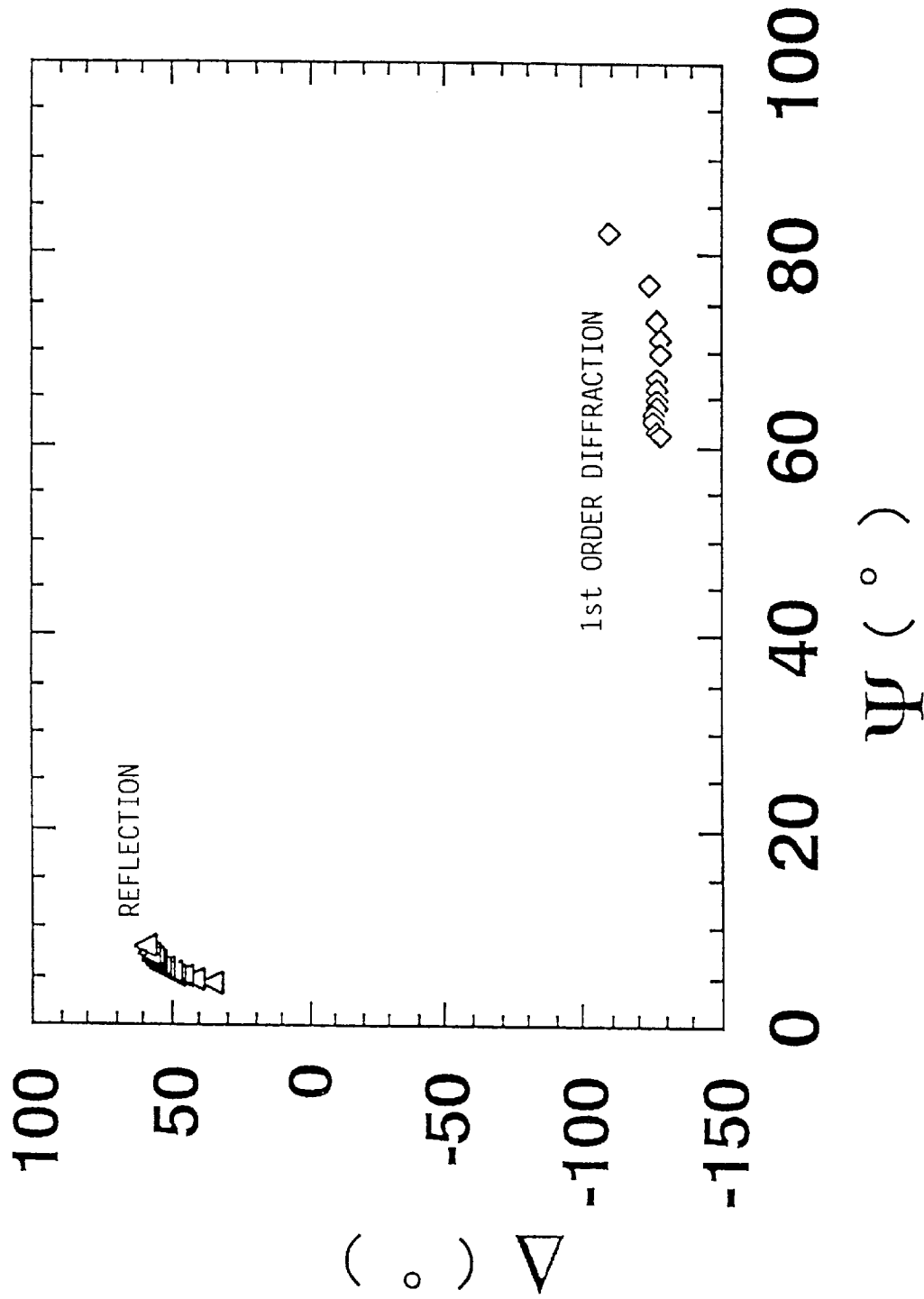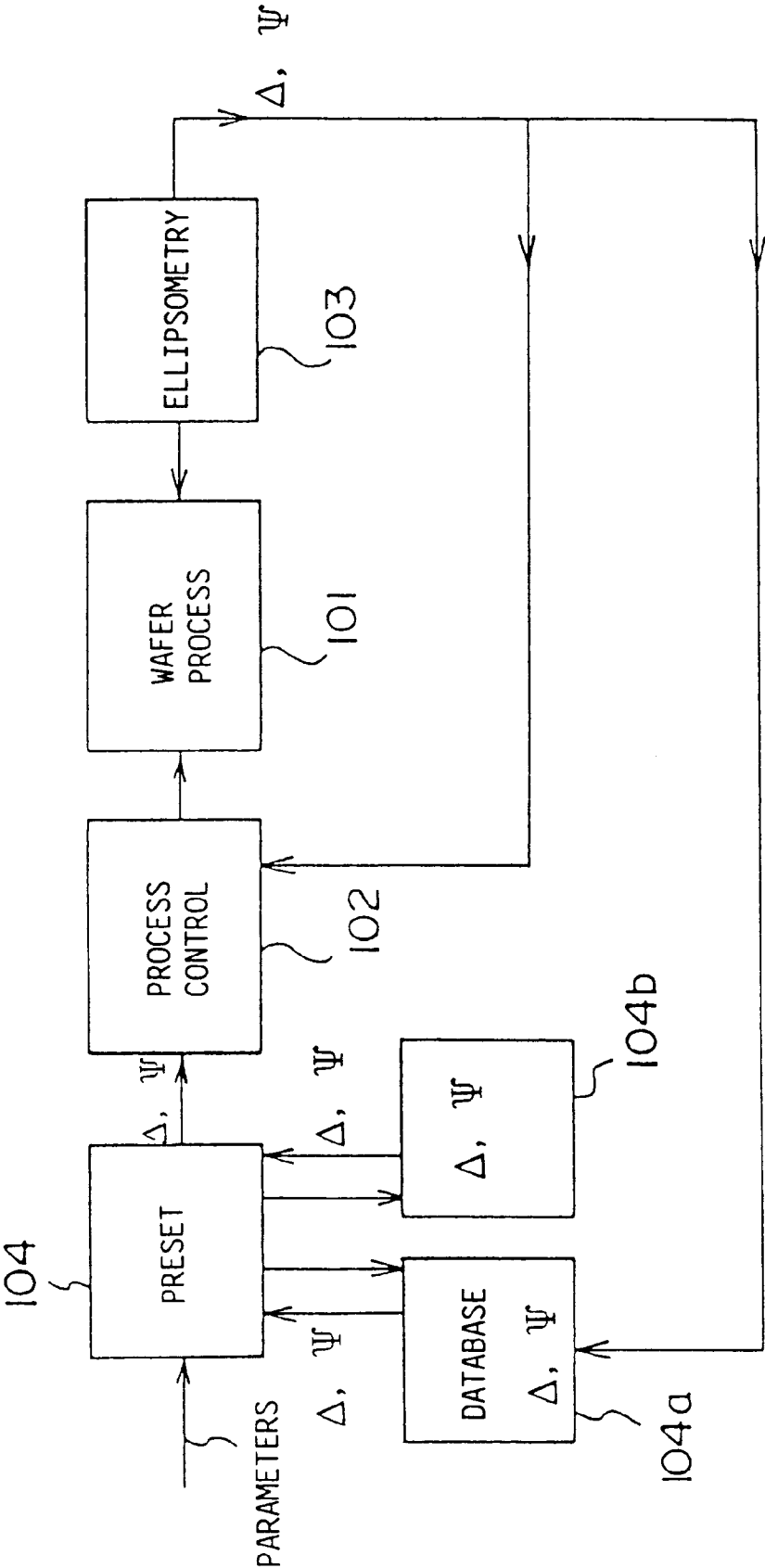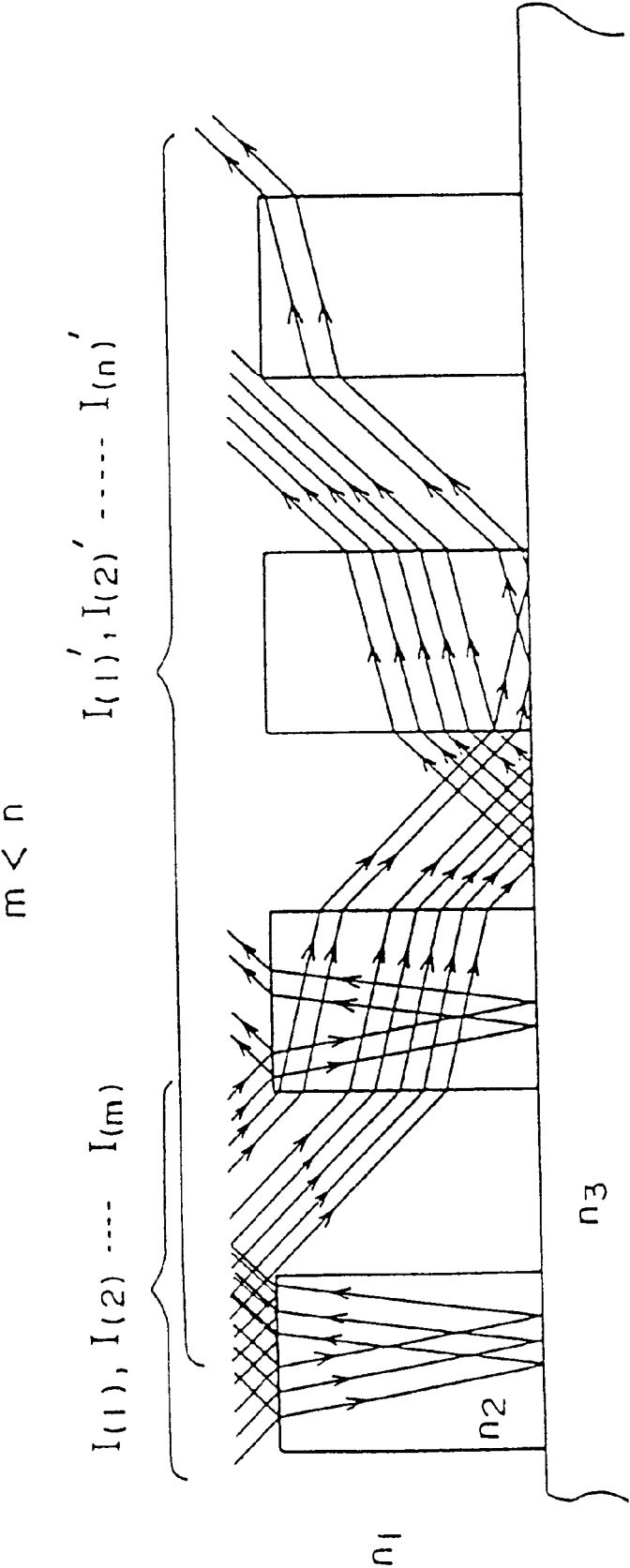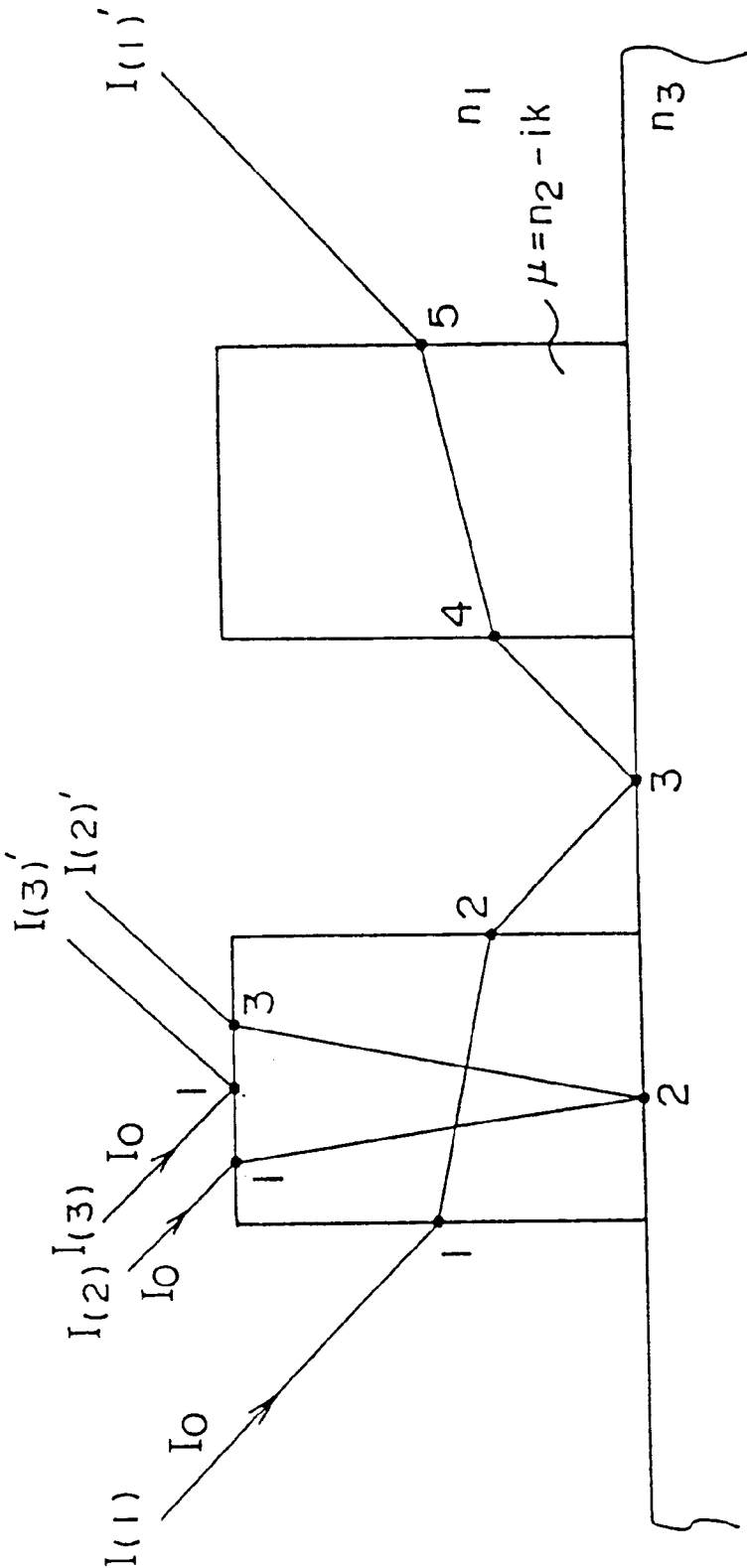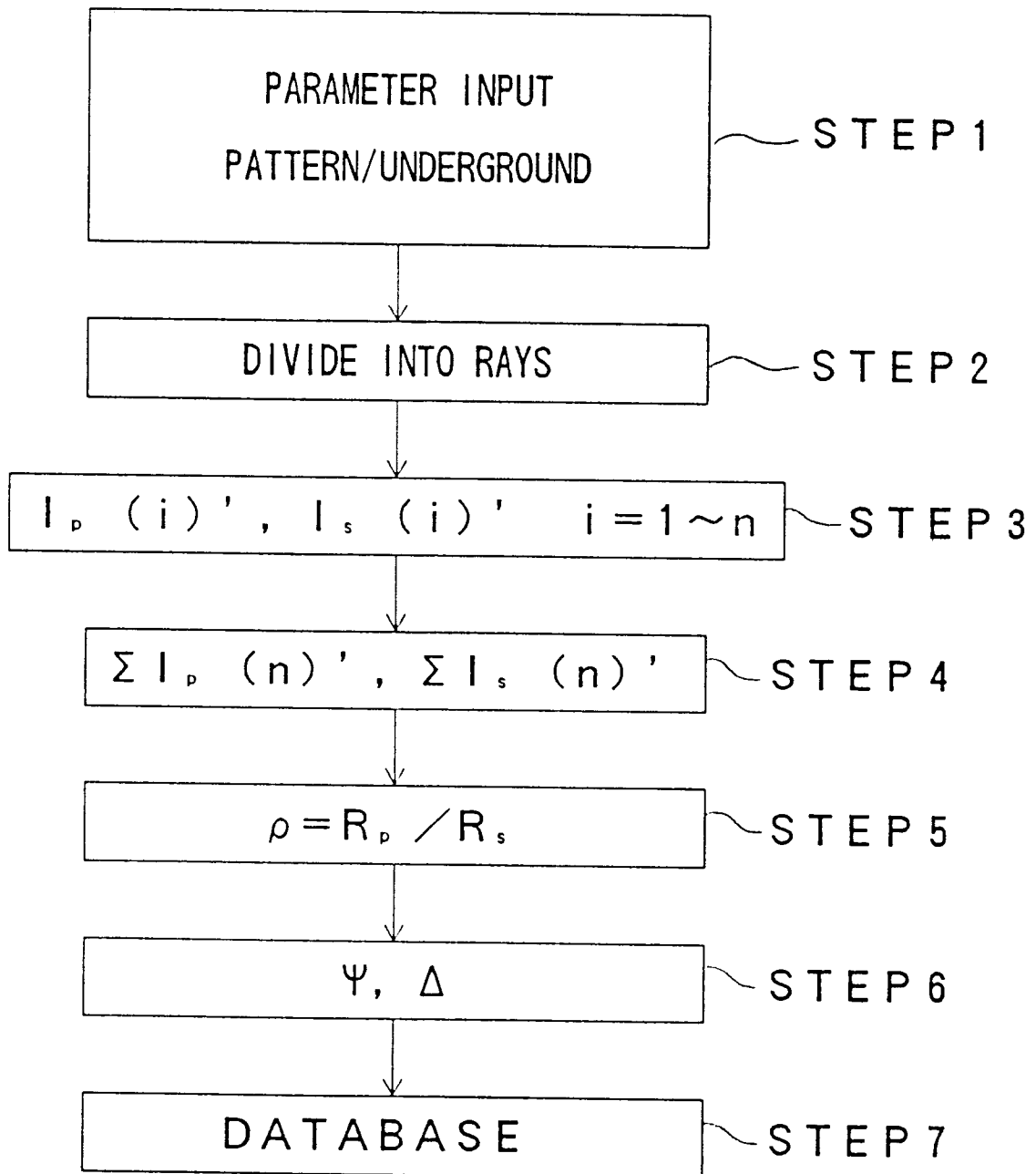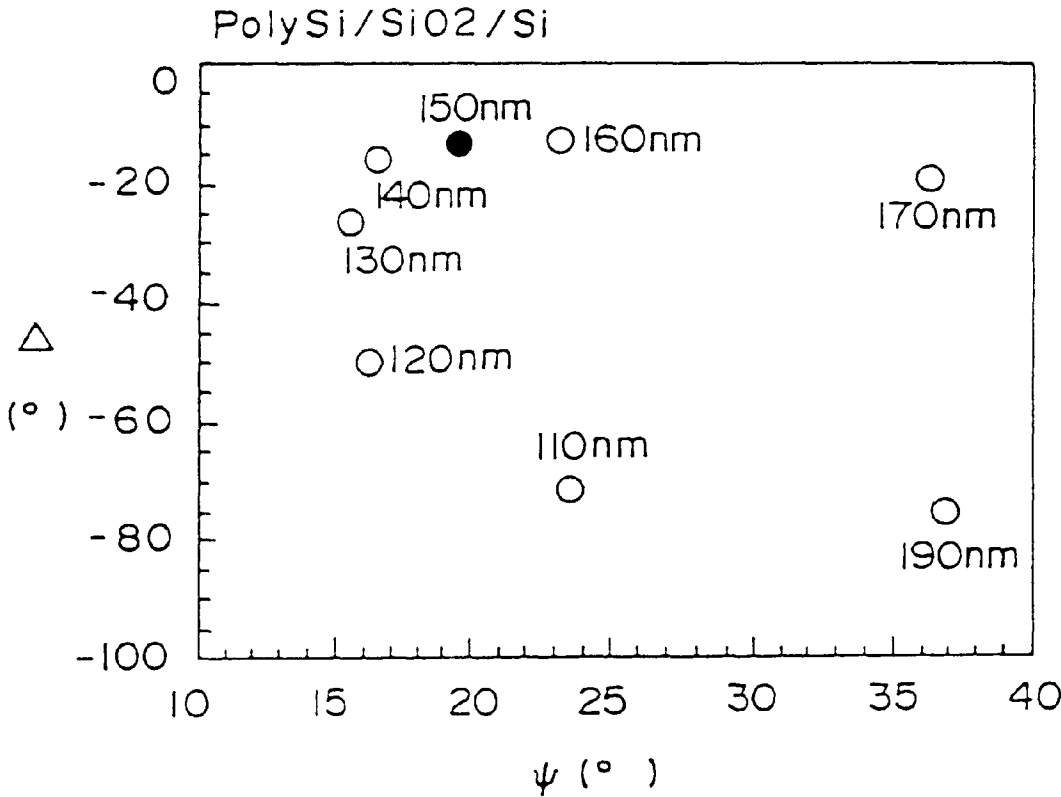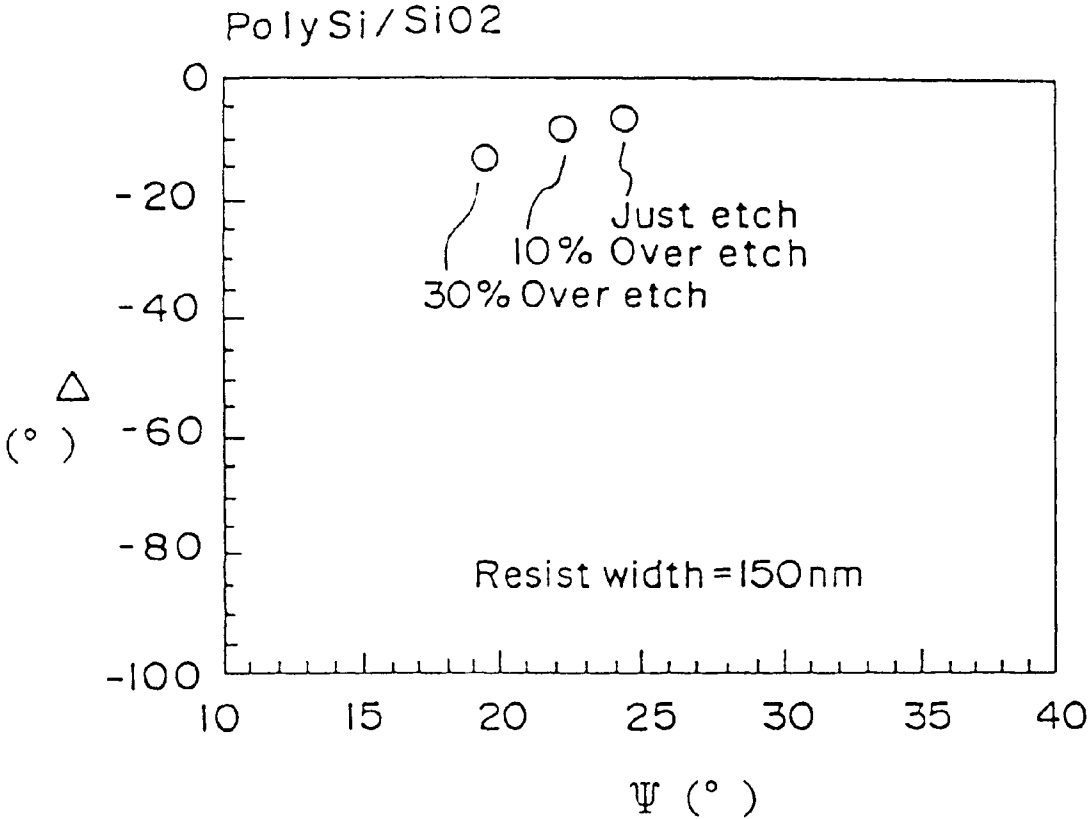
FIG.17

FIG. 18

# FIG. 19

FIG.20

0% O.E.

FIG. 21A



150 nm
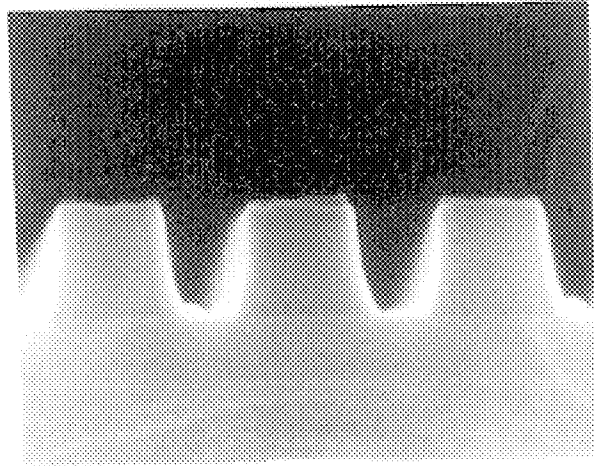
30% O.E.

FIG. 21B



150 nm
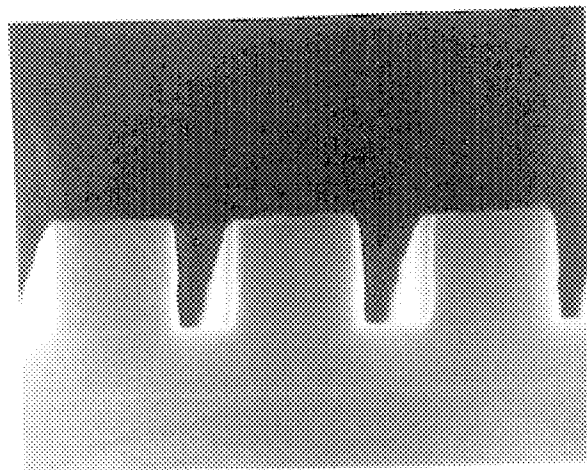
FIG. 21C

80% O.E.



150 nm

FIG. 22

**U.S. Patent**          Aug. 15, 2000          Sheet 24 of 24          **6,104,486**
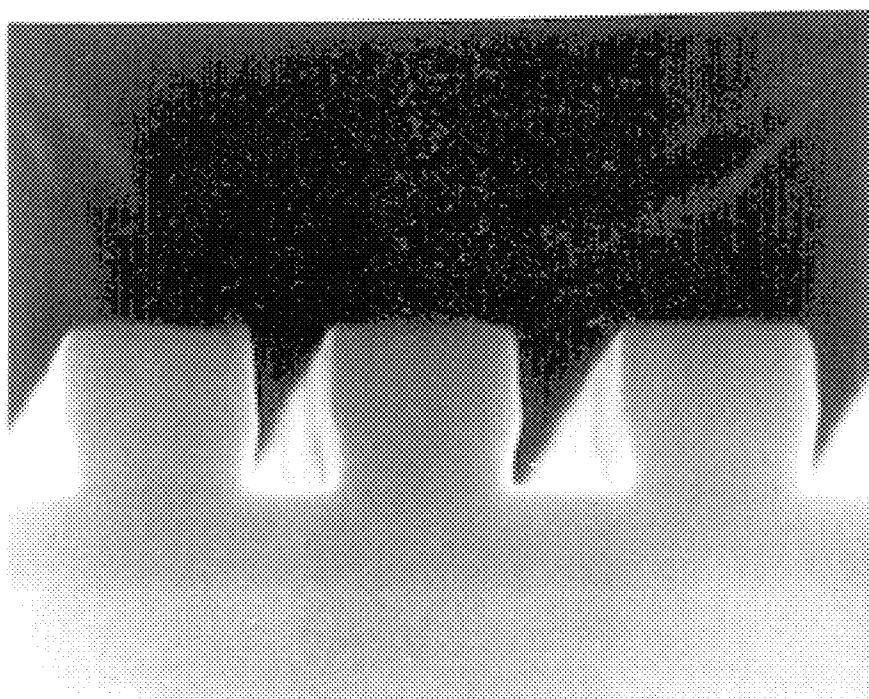
# F I G.   2 3

6,104,486

# 1

## FABRICATION PROCESS OF A SEMICONDUCTOR DEVICE USING ELLIPSOMETRY

### BACKGROUND OF THE INVENTION

The present invention generally relates to fabrication of semiconductor devices and more particularly to a measurement of profile of a semiconductor structure formed on a wafer during a fabrication process of the semiconductor device.

In a production line of semiconductor devices, it is necessary to examine the size of the structures such as agate pattern formed on a wafer quickly, without contacting to or destroying the structure, such that the result of the measurement is fed back immediately to the production line for optimizing various parameters of the production line. Particularly, there is a demand for an exact control for gate lengths, as a gate length provides a profound effect on the threshold characteristic of the semiconductor device that uses a gate structure.

Conventionally, a wafer carrying thereon a structure such as a gate pattern is subjected to a scanning process conducted under a scanning electron-microscope (SEM) for evaluation of the size of the structure. Further, there is a known process for evaluating the gate pattern size by measuring a resistance of the wafer by a bridge circuit that is formed commonly to the gate pattern on the same wafer.

However, the examination process that uses a SEM takes a substantial time due to the need of transporting each wafer on the production line consecutively to a vacuum chamber of the SEM. Thus, it is not practical to apply such an SEM process to all of the wafers on the line. Further, even when the SEM process is applied only to selected wafers, a decrease of throughput is inevitable for the production of the semiconductor devi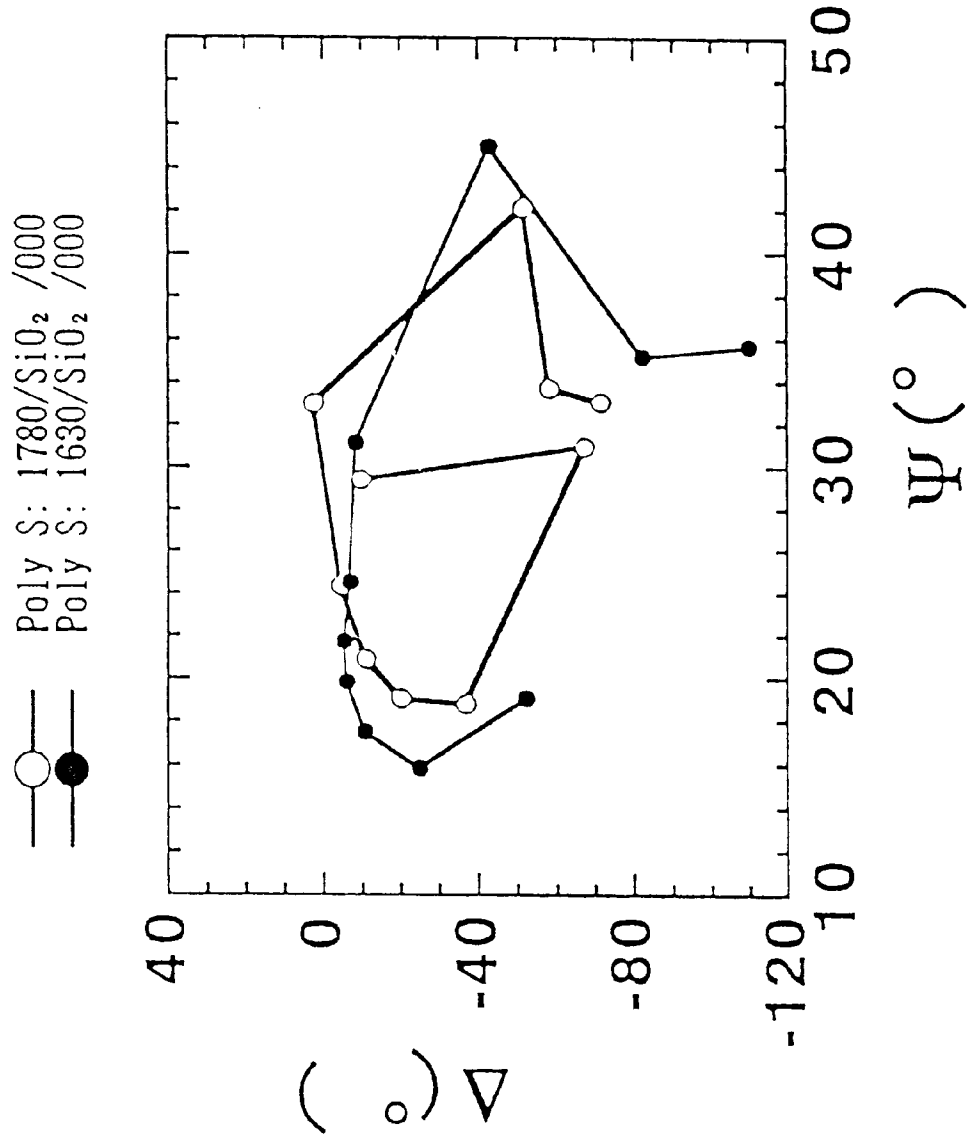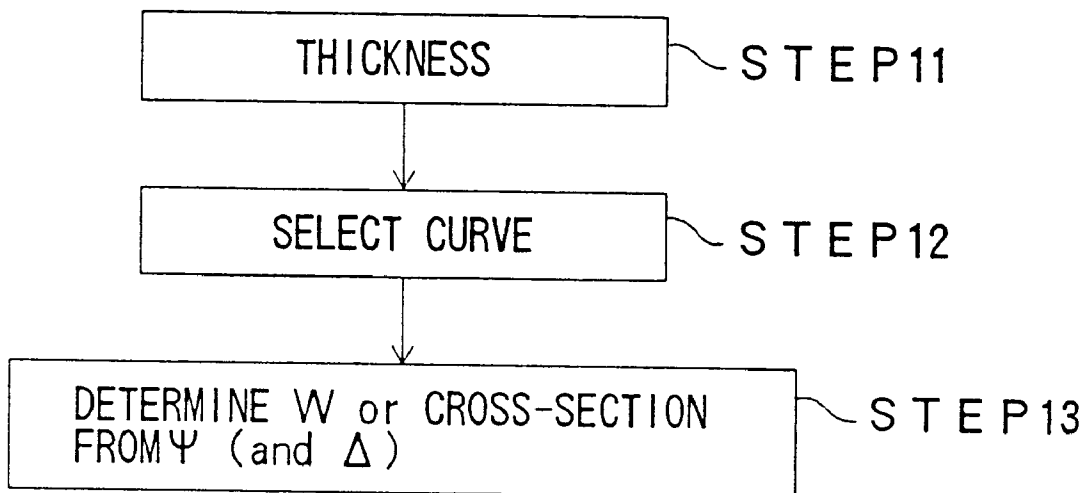ces. In the case of recent miniaturized semiconductor devices having a gate length, or other structural parameters, of 0.1 $\mu$m or less, in particular, the foregoing SEM process tends to cause an error in the result of the measurement due to the finite or non-infinitesimal diameter of the focused electron beam used in the SEM as compared with the size of the structure, wherein the magnitude of the error can reach as much as 10 nm.

In the case of measuring the resistance by using the bridge circuit, on the other hand, the result of the measurement cannot be obtained until the fabrication of the semiconductor devices on the wafer is completed, although the problem pertinent to the case of using a SEM such as the poor accuracy or reproducibility of the measurement may be resolved successfully. Thus, the process cannot be used for an in-situ feedback control of the production line.

Meanwhile, the art of ellipsometry has been used in the fabrication of semiconductor devices for measurement of thickness of semiconductor films and insulation films. Further, the ellipsometry is used also for controlling an etching process at the time of formation of line-and-space patterns (Blayo, N., et al., "Ultraviolet-visible ellipsometry for process control during the etching of submicrometer features,", J. Opt. Soc. Am., A, vol. 12, no. 3, 1995, pp. 591–599).

FIGS. 1A and 1B show the construction of an ellipsometer using conventionally for ellipsometry, wherein FIG. 1A shows a rotary-photometry type apparatus while FIG. 1B shows an extinction-photometry type apparatus.

# 2

Referring to FIG. 1A, the ellipsometer includes an optical source **1** for emitting an optical beam, wherein the optical beam emitted from the optical source **1** is converted to a linearly polarized beam having a predetermined plane of polarization and the linearly polarized beam thus formed hits a specimen **3** on which a film to be measured is formed. After reflection by the specimen **3**, the linearly polarized beam is converted to an elliptically polarized beam characterized by an angle ø indicating the direction of the major axis of the ellipse and an ellipticity k defined as $k=a_{min}/a_{max}$ as indicated in FIG. **2**, wherein the parameters ø and k are related to ellipsometric parameters $\psi$ and $\Delta$ to be used later in the description according to the relationship

$$\tan 2\psi = \tan 2\text{ø} \cdot \cos \Delta \text{ and}$$

$$\sin 2\chi = \sin 2\text{ø} \cdot \sin \Delta,$$

where there holds a relationship of

$$\tan \psi = \rho_p / \rho_s \text{ and}$$

$$\tan \chi = k = a_{min}/a_{max}.$$

In other words, it is possible to convert the set of the parameters (k, ø) obtained by the photometry to the parameters ($\psi$, $\Delta$). It should be noted that the parameter $\Delta$ represents the phase shift of the optical beam.

The elliptically polarized beam thus formed is then detected by a detector **5** after passing through a rotatable analyzer **4**, wherein the ellipsometer of FIG. 1A carries out the detection of the intensity of the optical beam reaching the detector **5** while rotating the analyzer **4**. Further, a quarter-wavelength plate **4**a, which induces a phase shift of a one-quarter of wavelength in the optical beam passing therethrough, may be inserted between the analyzer **4** and the specimen **3** as necessary.

In the ellipsometer of FIG. 1B, on the other hand, a rotary quarter-wavelength plate **4**b is inserted between the rotary analyzer **4** and the specimen **3**, and the elliptically polarized beam reflected by the specimen **3** is converted once to a linearly polarized beam. The rotary analyzer **4** is thereby rotated in search of the extinction angle in which the optical beam reaching the detector **5** is interrupted.

As explained previously, the ellipsometer of FIGS. 1A or 1B has been used successfully for the measurement of film thickness in the fabrication process of semiconductor devices. On the other hand, it should be noted that such conventional ellipsometry has hitherto discarded the information about the lateral size of the structure, which the polarized optical beam has inherently picked up when passing through the structure laterally. In conventional ellipsometry, there has been no proposal to make use of the ellipsometry for measuring the lateral size of the structure such as a line-and-space pattern formed on the specimen based upon the polarization state of the optical beam passed through the structure laterally.

### SUMMARY OF THE INVENTION

Accordingly, it is a general object of the present invention to provide a novel and useful fabrication process of a semiconductor device wherein the foregoing problems are eliminated.

Another object of the present invention is to provide a fabrication process of a semiconductor device that uses ellipsometry for measuring the size of a structure formed on a wafer efficiently with high precision, without destroying or causing a damage to the structure.

6,104,486

3

Another object of the present invention is to provide a method of fabricating a semiconductor device, comprising the steps of:

illuminating a structure formed on a surface of a substrate by an incident optical beam incident to said structure with a predetermined angle with respect to said surface;

measuring a polarization state of an exiting optical beam exiting from said structure in response to an illumination of said structure by said incident optical beam; and

evaluating a size of said structure in a direction parallel to said surface from said polarization state of said exiting optical beam;

said method further including a step of adjusting a parameter of production of a semiconductor device in response to said size.

Another object of the present invention is to provide a method of measuring a size of a structure formed on a surface of a substrate, comprising the steps of:

illuminating said structure by an incident optical beam incident to said structure with a predetermined angle with respect to said surface;

measuring a polarization state of an exiting optical beam exiting from said structure in response to an illumination of said structure by said incident optical beam; and

evaluating a size of said structure in a direction parallel to said surface from said polarization state of said exiting optical beam.

Another object of the present invention is to provide a method for controlling a quality of a semiconductor device, comprising the steps of:

illuminating a structure formed on a surface of a substrate by an incident optical beam incident to said structure with a predetermined angle with respect to said surface;

measuring a polarization state of an exiting optical beam exiting from said structure in response to an illumination of said structure by said incident optical beam; and

evaluating a size of said structure in a direction parallel to said surface from said polarization state of said exiting optical beam.

According to the present invention, it becomes possible to measure the size of the pattern formed on a wafer easily in a short time during the fabrication process of a semiconductor device, without contacting to or without damaging the fabricated device. Further, the result of the measurement can be fed back immediately and in real time to the production line for controlling the quality of the semiconductor devices produced by the production line.

Other objects and further features of the present invention will become apparent from the following detailed description when read in conjunction with the attached drawings.

### BRIEF DESCRIPTION OF THE DRAWINGS

FIGS. 1A and 1B are diagrams showing the construction of a conventional ellipsometer;

FIG. 2 is a diagram explaining the elliptical polarization measured by the ellipsometer of FIGS. 1A or 1B.

FIG. 3 is a diagram showing the principle of the present invention;

FIG. 4 is a diagram showing a part of FIG. 3 in an enlarged scale;

FIG. 5 is a diagram showing a first embodiment of the present invention;

FIGS. 6A and 6B are diagrams showing a line-and-space pattern to which an ellipsometry of FIG. 5 is applied;

4

FIG. 7 is a diagram showing an example of a database used in the ellipsometry of FIG. 5;

FIG. 8 is a diagram showing a positioning of a wafer in the construction of FIG. 5;

FIG. 9 is a diagram showing an ellipsometry according to a second embodiment of the present invention;

FIG. 10 is a diagram showing an example of using a reflection beam and a first-order diffraction beam in the ellipsometry of FIG. 9;

FIG. 11 is a diagram showing a production line of a semiconductor device in which the ellipsometry of FIG. 5 is used according to a third embodiment of the present invention;

FIG. 12 is a diagram showing the principle for calculating the ellipsometric parameters $\psi$ and $\Delta$ in the ellipsometry of FIG. 11;

FIG. 13 is another diagram showing the principle for calculating the ellipsometric parameters $\psi$ and $\Delta$ in the ellipsometry of FIG. 11;

FIG. 14 is a flowchart showing the process conducted in the system of FIG. 11;

FIG. 15 is a diagram showing the relationship between the ellipsometric parameters $\psi$ and $\Delta$ and a pattern width W obtained in the ellipsometry of FIG. 5 for a line-and-space pattern formed by an etching process;

FIG. 16 is a diagram showing the change of the ellipsometric parameters $\psi$ and $\Delta$ with the progress of etching observed by the ellipsometry of FIG. 5;

FIG. 17 is a diagram explaining the principle of a fourth embodiment of the present invention;

FIG. 18 is a diagram showing the details of the ellipsometry of FIG. 17;

FIG. 19 is a diagram showing an example of a characteristic curve obtained by the ellipsometry of FIG. 18;

FIG. 20 is a diagram showing the effect of pattern cross-sectional shape on the ellipsometric parameters $\psi$ and $\Delta$ according to a fifth embodiment of the present invention;

FIGS. 21A–21C are diagrams showing various cross sectional shapes of the line-and-space patterns corresponding to FIG. 20;

FIG. 22 is a diagram showing the effect of pattern thickness on the ellipsometric parameters $\psi$ and $\Delta$ according to a sixth embodiment of the present invention; and

FIG. 23 is a flowchart showing a process of pattern evaluation according to the sixth embodiment.

### DETAILED DESCRIPTION OF THE PREFERRED EMBODIMENTS

#### Principle

First, the principle of the present invention will be described with reference to FIG. 3 showing the process for obtaining a width W of a pattern 11 formed on a substrate 10 based upon a polarization state of an optical beam incident to the pattern 11.

Referring to FIG. 3, it should be noted that the incident optical beam enters the pattern 11 with an incident angle $\theta$, wherein the optical beam thus entering the pattern 11 is a linearly polarized beam having a polarizing angle $\phi$ and characterized by electric field components Ep and Es crossing with each other perpendicularly.

When the incident optical beam has crossed the pattern 11 from a first side thereof to a second opposite side thereof, the

6,104,486

<table>
<tr><td>5</td><td>6</td></tr>
</table>

electric field components Ep and Es are changed respectively to Ep' and Es' due to the difference of refractive index and reflectance between the pattern **11** and the substrate **10** or between the pattern **11** and the air and further due to the phase difference caused in the optical beam as it passes through the pattern **11**. The electric field components Ep' and Es' form an elliptically polarized beam.

FIG. **4** shows a part of FIG. **3** in an enlarged scale.

Referring to FIG. **4**, the pattern **11** includes pattern elements **11***a* and **11***b,* and linearly polarized optical beams a–c entering the pattern **11***a* exit therefrom as elliptically polarized optical beams after experiencing refraction and/or reflection.

For example, a monochromatic linearly polarized optical beam having a polarization angle of 45° and incident to the pattern of FIG. **4** with an incident angle θ forms an elliptically polarized optical beam after reflection, due to the change of reflectance at the interface between the pattern **11***a* and the underlying substrate **10** for each of the p- and s-components Ep and Es as well as due to the phase difference caused in the optical beam as it passes through the pattern **11***a*. In such a case, it is possible to obtain a complex reflection coefficient ratio Rp/Rs by means of an ellipsometer, wherein the foregoing ration Rp/Rs is determined by the factors such as the refractive index of the substrate **10**, the refractive index of the pattern **11**, the shape of the pattern **11** and the incident angle θ of the incident optical beam.

The ellipsometry using an ellipsometer provides parameters ψ and Δ as a result of the ellipsometric observation, wherein the parameters ψ and Δ are related to the complex reflection coefficient ratio Rp/Rs according to the relationship

$$\rho = Rp / Rs = \sum_{j=1}^{n} Rp \Bigg/ \sum_{J=1}^{n} Rs = \tan\psi \exp(i\Delta), \qquad (1)$$

where the parameter ψ is defined as $\tan\psi = \rho_p/\rho_s$ as indicated in FIG. **2**, while Δ represents the phase difference. Both of the parameters ψ and Δ are the quantities observable by the ellipsometry as noted previously. In EQ. (1), it should be noted that the summation is taken for all of the rays that pass through the pattern **11**.

Summarizing above, the parameters ψ and Δ are obtained from the elliptic polarization state of the exit optical beam that includes the components Ep' and Es' by means of ellipsometry, provided that the refractive index or dielectric constant of the substrate **10** as well as the refractive index or dielectric constant of the pattern **11** are specified and the incident angle of the incident optical beam is specified.

As will be seen in FIG. **4**, the exit optical beam picks up the information bout the lateral size W of the pattern **11***a* in the form of phase difference, as the optical beam passes through the pattern **11***a*. Thus, it becomes possible to estimate the foregoing size W of the pattern **11***a* based upon the parameters ψ and Δ obtained from the polarization state of the exit optical beam. In an embodiment of the present invention to be described later, a number of sets of the parameters ψ and Δ are stored in a database in correspondence to various patterns of which size and shape are known for example by SEM observation. Thereby, the pattern size W is easily obtained by referring to the database based upon the parameters ψ and Δ observed by the ellipsometry.

FIRST EMBODIMENT

FIG. **5** shows the construction of an ellipsometric apparatus sued for an ellipsometric size measurement of a pattern

formed on a substrate according to a first embodiment of the present invention.

Referring to FIG. **5**, a substrate **22** carrying a pattern thereof is mounted upon a stage **21** of the apparatus, and the substrate **22** is illuminated by an optical beam produced by a He-Ne laser **23**. The optical beam thus produced has a wavelength of 6328 Å and is passed through a polarizer **25** such that the optical beam is converted to a linearly polarized optical beam having a predetermined polarization angle, which may be set to 45°. The linearly polarized optical beam thus produced then impinges upon the substrate **22** on the stage **21** with a predetermined incident angle such as 70°. Alternatively, it is possible to dispose the quarter-wavelength plate **24** between the substrate **22** and the polarizer **25**.

The linearly polarized optical beam thus impinged upon the substrate **22** is then reflected after passing through a pattern formed on the substrate **22**, wherein the optical beam, initially being a linearly polarized optical beam, is converted to an elliptically polarized optical beam. The elliptically polarized optical beam thus formed is further passed successively through a quarter-wavelength plate **24** and a rotary analyzer **26**, wherein the rotary analyzer **26** converts the elliptically polarized optical beam again to a linearly polarized optical beam, and the linearly polarized optical beam thus obtained is detected by a photocell **27**. The detection by the photocell **27** is carried out while rotating the analyzer **26**.

The photocell **27** produces an output signal corresponding to the intensity of the optical beam incident thereto and supplies the output signal to a processing apparatus **30** after amplification by an amplifier **28** and an analog-to-digital conversion by an A/D converter **29**. The processing apparatus **30** thereby obtains the polarization state of the optical beam incident to the photocell **27** and produces the foregoing parameters ψ and Δ.

FIGS. **6**A and **6**B show an example of a resist pattern **22***a* formed on the substrate respectively in a perspective view and a cross-sectional view. The pattern **22***a* may be any suitable device pattern formed on the substrate or a line-and-space pattern formed on the substrate **22** at a suitable location such as a scribe line.

Referring to FIGS. **6**A and **6**B, the substrate **22** includes a silicon substrate $22_1$ on which a silicon oxide film $22_2$ and a polysilicon film $22_3$ are deposited successively with respective thicknesses of 100 nm and 153 nm, and the foregoing resist pattern **22***a* is formed on the polysilicon film $22_2$. Various resist materials can be used for the resist pattern **22***a* such as the CMS resist (trade name) for electron beam exposure, which is available from Toyo Soda Manufacturing Company, Japan.

The resist pattern **22***a* may be a line-and-space pattern in which a plurality of mutually parallel pattern elements **22***b* are repeated with a predetermined pitch such as 0.3 $\mu$m and is formed on a suitable location of the substrate **22** with a size of generally 1 mm×1 mm. Each of the pattern elements **22***b* has a height of 150 nm as a result of patterning of a resist film having a thickness of 150 nm. In such a line-and-space pattern, it should be noted that, while the pattern pitch can be controlled exactly, the width of the individual pattern elements **22***b* may vary variously. When such a line-and-space pattern is used for the gate electrode of a MOS transistor, such a variation of the pattern width can cause an unwanted deviation of the threshold voltage of the MOS transistor to be formed.

FIG. **7** shows the relationship between the parameters ψ and Δ obtained experimentally for the case in which the

6,104,486

<table>
<tr><td>7</td><td>8</td></tr>
</table>

apparatus of FIG. **5** is applied to a line-and-space pattern while changing the pattern width W variously. In the experiment, the substrate shown in FIGS. **6**A in **6**B is used for the substrate **22**, and the parameters $\psi$ and $\Delta$ were obtained while changing the width W of the pattern element **22***b* from 100 nm to 190 nm. It should be noted that the value of the width W shown in FIG. **7** is obtained by directly observing the line-and-space pattern by a SEM. The parameters $\psi$ and $\Delta$ were obtained for each pattern width W five times.

As will be seen from FIG. **7**, there is a one-to-one correspondence between each set of the parameters $\psi$ and $\Delta$ and the width W. This means that it is possible to estimate the value of the width W of the line-and-space pattern on the substrate by measuring the parameters $\psi$ and $\Delta$ by referring to the relationship of FIG. **7**. Thus, the relationship of FIG. **7** is stored in a database provided in the processing apparatus **30** of FIG. **5**, and the processing apparatus **30** refers to the database for the evaluation of the width W.

FIG. **8** shows the apparatus of FIG. **5** in a plan view.

Referring to FIG. **8**, the stage **21** carries a positioning member **21**A for engagement with an orientation flat **22**A formed on a wafer that forms the substrate **22** as well as a positioning pin **21**B for engagement with a side wall of the wafer **22**.

In the state of FIG. **8** in which the orientation flat **22**A engages the positioning member **21**A and the side wall of the substrate **22** engages the positioning pin **21**B on the stage **21**, it should be noted that the pattern elements **22***b* forming line-and-space pattern **22***a* on the substrate **22** extend generally perpendicularly to the path of the optical beam traveling from the laser **23** when viewed in a direction perpendicular to the substrate **22**. By disposing the line-and-space pattern **22***a* in such a direction, it should be noted that the optical beam efficiently picks up the information of the line-and-space pattern in the form of the phase of the optical beam. In other words, the sensitivity of detection of the pattern width W becomes maximum for the line-and-space pattern **22***a* by disposing the substrate **22** on the stage **21** in the orientation indicated in FIG. **8**.

It should be noted that the foregoing alignment of the wafer for proper orientation can be made by various other means. For example, the wafer **21** may be formed with a cut with a predetermined orientation such that the cut engages with a positioning pin provided on the stage **21** when the wafer **22** is placed on the stage **21** with a proper orientation. Alternatively, it is possible to use an orientation detection mechanism that uses an LED (light emitting diode) for the detection of the wafer orientation.

It is of course possible to dispose the wafer **22** in the construction of FIG. **8** such that the parallel pattern elements of the pattern **22***a* extend generally parallel to the path of the optical beam. By disposing the wafer **22** as such, it is possible to obtain the information about the wafer underneath the pattern **22***a* is obtained.

SECOND EMBODIMENT

FIG. **9** shows a second embodiment of the present invention, wherein those parts described previously with reference to preceding drawings are designated by the same reference numerals and the description thereof will be omitted.

Referring to FIG. **9**, it will be noted that the pattern elements **22***b* are formed relatively sparsely on the substrate **22**. Thus, the optical beam emitted from the optical source **23** tends to pickup not only the information of the pattern elements **22***b* but also the information of the underlying substrate **22** such as the thickness of a film forming a top part

of the substrate **22**. In such a case, there is a substantial risk that the width W obtained from the ellipsometric parameters $\psi$ and $\Delta$ deviates from the real value of the width W.

Thus, the present invention exploits the coherent nature of the optical beam **23**, which is a He–Ne laser, and obtains the pattern width W from diffraction optical beams that are produced by the line-and-space pattern **22***a* as a result of Bragg diffraction. In this case, one or more photocells are disposed so as to detect one or more of such diffraction optical beams. Thereby, the pattern width W is obtained based upon the observed ellipsometric parameters $\psi$ and $\Delta$ similarly to the previous embodiment. In the present embodiment, it is also possible to obtain the most reliable value from the width W by taking a simple average or weighted average of the width W obtained by various diffraction beams.

FIG. **10** shows the examples of the parameters $\psi$ and $\Delta$ obtained form the diffraction optical beam according to the process of FIG. **9** for a specimen in which a line-and-space resist pattern having a height of 150 $\mu$m is formed with a 5 $\mu$m-pitch, in comparison with the parameters $\psi$ and $\Delta$ obtained from the reflected beam for the same line-and-space pattern. In the example of FIG. **10**, it should be noted that the incident angle of the optical beam is set to 77° and hence the reflection beam is formed with a reflection angle of 77°. On the other hand, the first-order diffraction beam is produced with a diffraction angle of 58°.

FIG. **10** clearly indicates that the value of the parameters $\psi$ and $\Delta$ changes when the width W of the line-and-space pattern is changed in the range between 110 nm–210 nm, wherein it should be noted that the parameters $\psi$ and $\Delta$ change respectively in the range of 5–10° and 30–60° when the reflection beam is used, while the parameters $\psi$ and __ change respectively in the range between 60–85° and –100–110° when a first-order diffraction optical beam is used. The result of FIG. **10** indicates further that the change of the phase difference $\Delta$ is small when the first-order diffraction beam is used. In such a case, the width W is generally proportional to the parameter $\psi$.

THIRD EMBODIMENT

FIG. **11** is a block diagram showing the construction of a production line of semiconductor devices according to a third embodiment of the present invention that uses the ellipsometer of FIG. **5**.

Referring to FIG. **11**, the production line includes a wafer processing part **101** that may include in turn processes such as an exposure process and an etching process, and a control part **102** that controls the wafer processing part **101** as usual in a semiconductor process, wherein the production line of FIG. **11** further includes an ellipsometry part **103** that examines the wafer processed by the processing part **101**.

The ellipsometry part **103** includes the ellipsometer of FIG. **5** and obtains the ellipsometric parameters $\psi$ and $\Delta$ based upon the polarization of an optical beam reflected from the wafer that has been processed by the processing part **101**. The ellipsometric parameters $\psi$ and $\Delta$ thus obtained are then supplied to the control part **102**, wherein the control part changes the process condition such as the exposure dose, exposure time, RF power, and the like, based on the comparison of the observed parameters $\psi$ and $\Delta$ with corresponding present values of the parameters $\psi$ and $\Delta$ that are supplied from a presetting part **104**.

As indicated in FIG. **11**, the presetting part **104** is supplied with pattern data such as the thickness and shape of the line-and-space pattern formed in the wafer process part **101** or other various data such as the thickness of the layer formed under the line-and-space pattern, and calculates the

6,104,486

**9**

expected values of the parameters $\psi$ and $\Delta$ be referring to a database **104a** that holds the parameters $\psi$ and $\Delta$ similarly to FIG. **7**. Thereby, the control part **102** compares the parameters $\psi$ and $\Delta$ obtained from the database **104a** with the parameters $\psi$ and $\Delta$ obtained by the ellipsometer **103** and controls the process in the processing part **102** such that the difference between the parameters $\psi$ and $\Delta$ of the database **104a** and the actually observed parameters $\psi$ and $\Delta$ is minimized.

In the production line of FIG. **11**, it should be noted that the database **104a** is constructed by examining the wafers of which pattern size is already known by a SEM scanning, by using the ellipsometer **103** and by storing the ellipsometric parameters $\psi$ and $\Delta$ thus obtained as a function of the shape parameter such as the width W.

Alternatively, the parameters $\psi$ and $\Delta$ may be calculated theoretically in the system of FIG. **11** by using a theoretical calculation unit **104b**, such that the theoretically obtained parameters $\psi$ and $\Delta$ are supplied to the process control part **102** via the presetting part **104**.

The theoretical calculation of the parameters $\psi$ and $\Delta$ in the calculation unit **104b** is conducted generally as follows.

When an optical beam is incident to a specimen carrying thereon a periodic line-and-space pattern with an incident angle $\theta_1$, the incident optical beam experiences refractions and reflections according to the Snell's law as it passes through the specimen as indicated in FIG. **12**, and the optical beam exits from the line-and-space pattern with the same angle $\theta_1$. In FIG. **12**, it should be noted that the environment of the specimen has a refractive index $n_1$ while the line-and-space pattern has a refractive index $n_2$. Further, the substrate on which the line-and-space pattern is formed, has a refractive index $n_3$.

Thus, the incident optical beam is divided into m incident rays $I_{(1)}, I_{(2)}, \ldots, I_{(m)}$ and the optical path is calculated for each of the incident rays $I_{(1)}, I_{(2)}, \ldots I_{(m)}$ by applying the Snell's law. In such a calculation, each of the rays is decomposed into a p-polarization component and an s-polarization component and the effect of attenuation associated with reflection and refraction is calculated for each of the p- and s-components.

More specifically, the effect of attenuation associated with the reflection of an incident ray is evaluated by multiplying Fresnel's amplitude reflectance coefficients $r_p$ and $r_s$ to the amplitude $I_0$ of the p-component and s-component of the incident ray respectively each time the incident ray experiences a reflection. When the incident ray experiences a refraction, on the other hand, Fresnel's amplitude refraction coefficients $t_p$ and $t_s$ are multiplied respectively to the intensity $I_0$ of the p- and s-components of the incident ray each time the incident ray experiences a refraction. Further, the effect of attenuation caused by an opaque medium is evaluated by multiplying an amplitude transmittance coefficient $t_k$.

The final intensity Ip(n)' and Is(n)' respectively of the p- and s- components are then obtained by further multiplying the effect of phase retardation $\delta$ associated with the optical path length, wherein the amplitude reflectance coefficients $r_p$ and $r_s$, the amplitude refraction coefficients $t_p$ and $t_s$, the amplitude transmittance coefficient $t_k$, and the phase retardation $\delta$ are given respectively as

$$r_p=\tan(\theta_1-\theta_2)/\tan(\theta_1+\theta_2),$$

$$r_s=-\sin(\theta_1-\theta_2)/\sin(\theta_1+\theta_2),$$

$$t_p=2\ \sin\theta_2\ \cos\theta_1/\sin(\theta_1+\theta_2)\cos(\theta_1-\theta_2),$$

**10**

$$t_s=2\ \sin\theta_2\ \cos\theta_1/\sin(\theta_1+\theta_2),$$

$$t_k=\exp(-2\pi kd/\lambda),\text{ and}$$

$$\delta=\exp(-i2\pi nd/\lambda),$$

wherein $\lambda$ represents the wavelength of the incident optical beam while d represents the optical path length of the optical beam in the specimen.

In the example of FIG. **13**, incident rays **(1)–(3)** having an initial intensity $I_0$ form exiting rays having p-components Ip(1)'–Ip(3)' and s-components Is(1)'–Is(3)' given as

$$Ip(1)'=t_{p1}t_{p2}r_{p3}t_{p4}t_{p5}\times\exp(-2\pi k_2 d_1/\lambda)\ \exp(-i2\pi n_2 d_1/\lambda)\cdot I_0,$$

$$Is(1)'=t_{s1}t_{s2}r_{s3}t_{s4}t_{s5}\times\exp\ (-2\pi k_2 d_1/\lambda)\ \exp(-i2\pi n_2 d_1/\lambda)\cdot I_0,$$

$$Ip(2)'=t_{p1}r_{p2}t_{p3}\times\exp(-2\pi k_2 d_2/\lambda)\ \exp(-i2\pi n_2 d_2/\lambda)\cdot I_0,$$

$$Is(2)'=t_{s1}r_{s2}t_{s3}\times\exp(-2\pi k_2 d_2/\lambda)\ \exp(-i2\pi n_2 d_2/\lambda)\cdot I_0,$$

$$Ip(3)'=r_{p1}\cdot I_0,\text{ and}$$

$$Is(3)'=r_{s1}\cdot I_0,$$

wherein $n_2$ and $k_2$ represent the refractive index and absorption coefficient of the line-and-space pattern, while $d_1$ and $d_2$ represent respectively the optical path lengths of the rays (1) and (2) in the line-and-space pattern. Further, the suffices 1–5 represent the point of reflection or refraction counted from the side where the rays enter the line-and-space pattern. See FIG. **13**.

After the intensities I(1)'–I(n)' are thus obtained, the complex reflection coefficient ratio (Rp/Rs) is obtained according to the relationship

$$Rp/Rs=\Sigma Ip(n)'/\Sigma Is(n)'=\tan\psi\ \exp(i_{66})$$

and the parameters are obtained according to the relationships of

$$\psi=\tan^{-1}(|Rp/Rs|)\text{ and}$$

$$\Delta=\arg(Rp/Rs).$$

In the construction of FIG. **11**, the calculation unit **104b** carries out the foregoing calculation and supplies the obtained parameters $\psi$ and $\Delta$ to the process control unit **102** via the presetting unit **104** as noted already.

FIG. **14** is a flowchart showing the processing carried out by the calculation unit **104b**.

Referring to FIG. **14**, the process starts with a step **1** in which various structural data such as the thickness, refractive index and absorption of the pattern, the thickness, refractive index and absorption of the underlying layer, the pattern pitch, and the like are given in the form of input.

Next, in a step **2**, the incident optical beam is decomposed into individual rays 1–n, and the optical path is obtained for each of the rays thus decomposed. Further, the intensities Ip(i)' and Is(i)' of the p- and s- components are obtained in a step **3** for each of the rays i(=1–n).

Further, in the step **4**, the intensities Ip(i)' and Is(i)' obtained previously for the rays i are summarized respectively for all of the rays 1–n, and integral intensities $\Sigma Ip(n)'$ and $\Sigma Is(n)'$ are obtained. The integral intensities thus obtained are then used in the step **5** to obtain the complex reflection coefficient ratio $\Sigma Ip(n)/\Sigma Is(n)$, and the complex reflection coefficient ratio $\Sigma Ip(n)/\Sigma Is(n)$ thus obtained is used in a step **6** to calculate the parameters $\psi$ and $\Delta$. Further, in a step **7**, a reference is made to the database for the specific combination of the parameters $\psi$ and $\Delta$ obtained in

6,104,486

11

the step **6**, and the value of the pattern W is obtained as a result of such a reference of the database.

FIG. **15** shows the relationship between the parameter ψ and Δ obtained by the ellipsometer of FIG. **5** for the substrate **22** described previously with reference to FIGS. **6A** and **6B**, for a state in which an RIE (reactive ion etching) process is applied to the polysilicon layer $22_2$ while using the resist pattern **22***a* as a mask and the resist pattern **22***a* is removed subsequently. In the example of FIG. **15**, it should be noted that the incident angle of the incident optical beam is set to 55°, not 70°. By accumulating the relationship of FIG. **15** for various patterns, the database **104***a* is constructed.

FIG. **16**, on the other hand, indicates the relationship of the parameters ψ and Δ observed for the case in which the line-and-space pitch of the mask pattern **22***a* is set to 150 nm in the embodiment of FIGS. **6A** and **6B**. In FIG. **16**, it should be noted further that the duration of the etching process is changed variously. Thus, FIG. **16** shows the results in which an excessive etching is applied to the polysilicon layer $22_2$ by 10% and 30%, in addition to the case in which the etching is terminated exactly upon the exposure of the underlying $SiO_2$ layer $22_1$.

When such an excessive etching process is applied in such an RIE process for forming the line-and-space pattern in the polysilicon layer $22_2$, it is known that the line-and-space pattern thus formed experiences a substantial side wall etching. For example, when an excessive etching of 30% is made, it is known, from a SEM observation, that the line-and-space pattern thus formed experiences a side wall etching of as much as 20 nm. The result of FIG. **16** clearly indicates that the present invention for applying ellipsometry to line-and-space patterns for the measurement of the pattern width W is effective also for detecting the side wall etching of the pattern within a precision of about 10 nm.

FOURTH EMBODIMENT

FIG. **17** shows the principle of a fourth embodiment of the present invention.

Referring to FIG. **17**, the present embodiment obtains the foregoing ellipsometric parameters ψ and Δ based upon the scattering of an incident optical beam In caused by the pattern **22***b* on the substrate **22**, rather than using a reflection beam or diffraction beam of the incident optical beam.

FIG. **18** shows the construction for carrying out the measurement of a scattered light indicated in FIG. **17**, wherein those parts described previously are designated by the same reference numerals and the description thereof will be omitted.

In the apparatus of FIG. **18**, the coherent optical beam emitted from the optical source **23** reaches the wafer **22** which carries thereon the pattern **22***a,* after passing through the polarizer **25** and further through a beam chopper **25A**, wherein the beam chopper **25A** is a rotary disk formed with a cutout at a part thereof for turning on and turning off the optical beam incident to the wafer **22** from the optical source **23**.

Further, the construction of FIG. **18** includes a lens **31** and a beam splitter **32** cooperating with the lens **31**, wherein the lens **31** is disposed so as to avoid the reflection beam or diffraction beam produced by the pattern **22***a* on the wafer **22**. Thereby, the beam splitter **32** decomposes the scattered light produced by the pattern **22***a* and focused by the lens **31** into the p-component and the s-component and supplies the p- and s-components thus decomposed to a detector **27A** and a detector **27B** respectively. The detectors **27A** and **27B** are supplied with a control signal from the beam chopper **25A** as a synchronizing signal SYNC and detect the intensities Ip and Is of the scattered light respectively, wherein the control

12

signal is used in the beam chopper **25A** for controlling the rotation thereof and hence the on-off control of the optical beam. According to such a construction, it becomes possible to detect the intensities Ip and Is of feeble scattering light with high precision, by comparing the detected intensity with the background intensity in which the incident optical beam is interrupted.

The intensities Ip and Is of the scattered light thus obtained is then processed in the processing apparatus **30**, wherein a calculation is made in the processing apparatus **30** to divide the intensity Ip by the intensity Is (Ip/Is), to obtain a reflection coefficient ratio tanψ and hence the ellipsometric parameter ψ.

FIG. **19** shows the relationship between the reflection coefficient ratio (tanψ=Rp/Rs) and the pattern width W obtained according to the construction of FIG. **18** that uses the scattering of the incident optical beam. In the example of FIG. **19**, it should be noted that a wafer carrying a line-and-space pattern having a thickness of 180 nm and a pattern pitch of 300 nm on a $SiO_2$ film of a thickness of 100 nm is used as the substrate **22**, wherein the pattern width W is changed between 120 nm and 180 nm. The ellipsometric measurement was made by using a linearly polarized beam having a polarization angle of 45° as the incident optical beam.

As will be seen from FIG. **19**, the reflectance coefficient ratio tanψ clearly shows a dependency on the pattern width W. This in turn means that it is possible to obtain the pattern width W of the line-and-space pattern from the reflection coefficient ratio tanψ of the scattered light.

FIFTH EMBODIMENT

In any of the ellipsometers of FIG. **5**, FIG. **9**, FIG. **11** or FIG. **17**, the incident angle of the optical beam emitted from the optical source **23** is by no means limited to 70° but other incident angle may also be used. Further, by changing the incident angle variously, it is possible to evaluate not only the pattern width W but also the inclination angle of the pattern side wall by referring to a database that includes the incident angle as a parameter in addition to the foregoing ellipsometric parameters ψ and Δ.

FIG. **20** shows the ellipsometric parameters ψ and Δ obtained from a reflection beam produced by a wafer in which a polysilicon film is formed with a thickness of 182 nm on a $SiO_2$ film having a thickness of 102 nm.

Referring to FIG. **20**, it should be noted that the parameters ψ and Δ are obtained as indicated in the upper left curve of FIG. **20** in the state in which the etching of the polysilicon film is not started yet and only a line-and-space resist pattern is formed on the polysilicon film with pattern widths W of 175 nm, 150 nm and 125 nm. In FIG. **20**, it should be noted that three measurements, represented by an open circle, an open triangle and an open square, were made for each of the pattern widths W of 175 nm, 150 nm and 125 nm, wherein it is noted that the convergence of these measurements are excellent. The data of FIG. **20** was taken by setting the incident angle of the optical beam to 70°.

Next, an etching is applied to the foregoing polysilicon film wile using the line-and-space resist pattern as a mask and the ellipsometric measurement was made upon the structure thus obtained, wherein the solid triangles represent the parameters ψ and Δ obtained for the structure in which the etching is stopped immediately upon exposure of the underlying $SiO_2$ film (0% prolonged etching). On the other hand, the solid squares represent the parameters ψ and Δ obtained for the structure in which the etching is continued for a duration of 30% the nominal duration of etching (30% prolonged etching), after the underlying $SiO_2$ film is

6,104,486

**13**

exposed. Further, the solid circles represent the parameters $\psi$ and $\Delta$ for the structure in which the etching is continued for a duration of 80% the nominal duration of etching (80% prolonged etching), after underlying $SiO_2$ film is exposed.

The structure corresponding to the solid triangles is represented in FIG. **21A** for the case in which the pattern width W is 150 nm, the structure corresponding to the solid squares is represented in FIG. **21B** for the case in which the pattern width W is also 150 nm, and the structure corresponding to the solid circles is represented in FIG. **21C** for the case in which the pattern width W is again 150 nm, wherein FIGS. **21A–21C** show the cross-section of the polysilicon line-and-space patterns obtained by a SEM observation.

As will be seen clearly from FIG. **20**, the curves for the various prolonged etchings are different from each other, except for the case where the pattern width W is set to 175 nm. Only in this case, the curves overlap partially. This means that it is generally possible to evaluate also the cross sectional shape of the polysilicon patterns as represented in FIGS. **21A–21C**, from the combination of the ellipsometric parameters $\psi$ and $\Delta$, when it is possible to estimate the structural parameters of the line-and-space pattern such as the pattern width W, film thickness, refractive index, and the like, by some other means.

SIXTH EMBODIMENT

FIG. **22** shows the relationship between the ellipsometric parameters $\psi$ and __ of the same polysilicon line-and-space pattern for the case in which the thickness of the polysilicon film is changed variously on the $SiO_2$ film of which thickness is set to 100 nm, wherein the curve represented in FIG. **22** by solid circles represent the case in which the polysilicon line-and-space pattern has a thickness of 178 nm, while the curve represented by open circles represent the case in which the polysilicon line-and-space pattern has a thickness of 163 nm. In any of these cases, the line-and-space pattern was formed to have a pitch of 300 nm, and the width W is changed in the range between 110–200 nm.

As will be seen clearly in FIG. **22**, the curve for the 178 nm thickness is distinctly different from the curve for the 163 nm thickness. This in turn means that it is possible to apply the ellipsometric process of the present invention for the patterns of various thicknesses by measuring the pattern thickness before proceeding to the ellipsometric process.

FIG. **23** shows the flowchart of such a process that includes the step of measuring the film thickness according to a sixth embodiment of the present invention.

Referring to FIG. **23**, a step **11** is conducted at first for determining the thickness of the line-and-space pattern, and a step **12** is conducted subsequently for selecting the characteristic curve for the measured thickness of the line-and-space pattern. Further, an ellipsometric process is conducted in a step **13** for the parameters $\psi$ and $\Delta$, and the pattern width W or the cross sectional shape thereof is obtained based upon the characteristic curve thus selected.

Further, the present invention is not limited to the embodiments described heretofore, but various variations and modifications may be made without departing from the scope of the invention.

What is claimed is:

**1**. A method of measuring a size of a structure formed on a surface of a substrate, comprising the steps of:

storing in a database data representing a relationship between lateral size and polarization;

illuminating said structure by an incident optical beam incident to said structure with a predetermined angle with respect to said surface;

**14**

measuring a polarization state of an exiting optical beam from said structure in response to an illumination of said structure by said incident optical beam; and

evaluating a lateral size of said structure from said polarization state of said exiting optical beam according to said data stored in said database.

**2**. A method as claimed in claim **1**, wherein said polarization state is represented in terms of a rotation of a polarization plane and an ellipticity of said exiting optical beam, and wherein said measuring step is carried out by an ellipsometer.

**3**. A method as claimed in claim **1**, wherein said illuminating step is carried out for different incident angles of said incident optical beam, and wherein said evaluating step includes a step of evaluating an angle of a side wall of said structure with respect to said surface of said substrate from a combination of said polarization state and said incident angle.

**4**. A method as claimed in claim **1**, wherein said measuring step is carried out by using a reflection beam of said incident optical beam as said exiting optical beam.

**5**. A method as claimed in claim **1**, wherein said measuring step is carried out by using a diffraction optical beam of said incident optical beam diffracted by said structure as said exiting optical beam.

**6**. A method as claimed in claim **1**, wherein said measuring step is carried out by using a scattered light of said incident optical beam scattered by said structure as said exiting optical beam.

**7**. A method as claimed in claim **1**, wherein said evaluating step includes the substeps of measuring a thickness of said structure, selecting a database corresponding to said measured thickness, and evaluating one of a width and a cross-sectional shape of said structure by referring to said selected database.

**8**. A method as claimed in claim **1**, wherein said illuminating step includes a step of switching said incident optical beam on and off, and wherein said evaluating step measures said polarization state of said exiting optical beam for each of a state in which said incident optical beam is turned on and a state in which said incident optical beam is turned off.

**9**. A method for controlling a quality of a semiconductor device, comprising the steps of a semiconductor device, comprising the steps of:

storing in a database data representing a relationship between lateral size and polarization;

illuminating a structure formed on a surface of a substrate by an incident optical beam incident to said structure with a predetermined angle with respect to said surface;

measuring a polarization state of an exiting optical beam exiting from said structure in response to an illumination of said structure by said incident optical beam;

evaluating a lateral size of said structure from said polarization state of said exiting optical beam according to said data stored in said database; and

adjusting a parameter of production of a semiconductor device in response to said size.

**10**. A method as claimed in claim **1**, wherein said database stores said relationship in the form of curves.

**11**. A method as claimed in claim **9**, wherein said database stores said relationship in the form of curves.

\*    \*    \*    \*    \*

# Exhibit B

MILBANK, TWEED, HADLEY & McCLOY LLP
Mark C. Scarsi (SBN 183926)
Chris L. Holm (SBN 249388)
601 South Figueroa Street, 30th Floor
Los Angeles, CA  90017-5735
Telephone:     (213) 892-4000
Facsimile:     (212) 822-5796
F-N-wg@milbank.com

MILBANK, TWEED, HADLEY & McCLOY LLP
Christopher E. Chalsen (*Pro Hac Vice*)
Michael M. Murray (*Pro Hac Vice*)
Lawrence T. Kass (*Pro Hac Vice*)
1 Chase Manhattan Plaza
New York, NY  10005
Telephone:  (212) 530-5000
Facsimile:   (212) 822-5796
F-N-wg@milbank.com

Attorneys for Plaintiffs
FUJITSU LIMITED and FUJITSU
MICROELECTRONICS AMERICA, INC.

UNITED STATES DISTRICT COURT
NORTHERN DISTRICT OF CALIFORNIA
OAKLAND DIVISION

| | |
|---|---|
| FUJITSU LIMITED and FUJITSU MICROELECTRONICS AMERICA, INC., | Case No.   4:06-CV-06613 (CW) (JCS)<br>4:07-CV-03672 (CW)<br>4:08-CV-01254 (CW) |
| *Plaintiffs and Counterclaim-Defendants,* | **PLAINTIFFS' FIRST SET OF REQUESTS FOR PRODUCTION TO DEFENDANT KLA-TENCOR CORP. (Nos. 1-14)** |
| -against- | |
| NANYA TECHNOLOGY CORP. and NANYA TECHNOLOGY CORP. U.S.A., | Date:      April 24, 2008<br>Time:      n/a<br>Location:  n/a |
| *Defendants and Counterclaim-Plaintiffs.* | |
| NANYA TECHNOLOGY CORP. and NANYA TECHNOLOGY CORP. U.S.A., | |
| *Third-Party Plaintiff,* | |
| -against- | |
| KLA-TENCOR CORPORATION, | |
| *Third-Party Defendant.* | |

MILBANK, TWEED, HADLEY & MᶜCLOY LLP
ATTORNEYS AT LAW

1    Pursuant to Rules 26 and 34 of the Federal Rules of Civil Procedure and the Local Civil

2   Rules of this Civil Court, Plaintiffs Fujitsu Limited and Fujitsu Microelectronics America, Inc.

3   (collectively "Fujitsu" or "Plaintiffs") hereby serve the following Requests for Production of

4   documents, electronically stored information and things upon Third-Party Defendant KLA

5   Tencor Corp. ("KLA"), and request that KLA produce the requested documents, electronically

6   stored information and things within thirty (30) days of service, in accordance with the

7

8   definitions and instructions provided below.  KLA is subject to a duty to supplement all

9   responses to these Requests for Production in accordance with Federal Rule of Civil Procedure

10   26(e).  These Requests for Production are continuing to the extent provided by the applicable

11   rules.

12                          **INSTRUCTIONS**

13

14       A.    These document requests require you to produce all materials that are in your

15   actual or constructive possession, custody, or control.

16       B.    Materials are to be produced in the same form and same order as they are kept in

17   the ordinary course of business.  The documents are to be produced in the boxes, file folders,

18   bindings, or other containers in which the documents are found.  The titles, labels, or other

19   descriptions on the boxes, file folders, bindings, or other containers are to be left intact.

20   Documents from any single file should be produced in the same order as they were found in such

21   file.  If copies of documents are produced, such copies should be legible and bound or stapled in

22   the same manner as the original.  Electronically stored information is to be produced in the

23   the same manner as the original.  Electronically stored information is to be produced in the

24   directory and file structure in which the electronically stored information is found.  Where e-mail

25   with attachments are produced as electronically stored information, the attachments are to remain

26   associated with the e-mail message.

27

**PLAINTIFFS' FIRST SET OF REQUESTS FOR
PRODUCTION TO KLA-TENCOR CORP. (Nos. 1-14)**

C.    In the event you claim that a request is over-broad, you are requested to respond to that portion of the request which is unobjectionable and specifically identify the respect in which the request is allegedly overly broad.

D.    In the event you claim that responding to a request is unduly burdensome, you are requested to respond to that portion of the request that is unobjectionable and specifically identify the respect in which the request is allegedly unduly burdensome.

E.    With respect to any materials that you are unwilling to produce for inspection by Plaintiff's counsel because the material is asserted to be immune from discovery on the basis of the claim of attorney-client privilege, attorney work product or any other privilege or immunity, you are requested to produce no later than the day on which materials are produced pursuant to these requests and state, separately with respect to each such material, sufficient information to disclose:

    (a)    the names and job titles of the persons making and receiving the privileged and protected communication;

    (b)    steps taken to ensure the confidentiality of the communication, including affirmation that no unauthorized persons have received the communication;

    (c)    the date of the communication;

    (d)    the number of pages;

    (e)    the subject matter of the communication; and

    (f)    grounds for the claim to privilege or immunity as to each such material.

F.    For any requested materials that has been destroyed after the commencement of this suit, you are requested to identify each such material, set forth the contents of each destroyed material, the date of such destruction, the identity of any individuals who authorized the destruction, and other circumstances related to such destruction.

**PLAINTIFFS' FIRST SET OF REQUESTS FOR**
**PRODUCTION TO KLA-TENCOR CORP. (Nos. 1-14)**

-3-

G.      The use of a verb in any tense shall be construed as the use of the verb and all other tenses whenever necessary to bring within the scope of the request all materials that might otherwise be construed outside its scope.

H.      A plural noun shall be construed as a singular noun, and a singular noun, shall be construed as a plural noun whenever necessary to bring within the scope of the request all materials that might otherwise be construed outside its scope.

I.       The singular form or masculine gender, when used herein, shall include respectively, the plural and feminine or neuter as appropriate.

J.       For purposes of these requests, terms not specifically defined shall be given their ordinary meaning as you understand them to be used in the trade.

K.      If you object to any portion of a request, please provide all documents, electronically stored information, and things requested by any portion of the request to which you do not object.

L.      If you object to or disagree with any of the definitions set forth in Attachment B, or if you do not understand any term used in Attachment B, please explain in detail the nature of your disagreement with the definition, or lack of understanding of the term, provide an alternative definition of the term, and respond in accordance with that alternative definition.

## DEFINITIONS

1.      The terms "you," "your," and "KLA-Tencor" each mean KLA-Tencor Corporation and, whether foreign or domestic, (a) all of its divisions, departments, parents, subsidiaries, affiliated entities, assigns, or other organizational or operational units; (b) all of its predecessor or successor companies, corporations, or entities; (c) all companies, corporations, partnerships, associations, or other business entities, which are or have been under its ownership or control, are controlled by it, which control it, or which are under common control in any manner with it; and, for each of the foregoing, its (d) present and former officers, directors,

**PLAINTIFFS' FIRST SET OF REQUESTS FOR
PRODUCTION TO KLA-TENCOR CORP. (Nos. 1-14)**

1  employees, agents, investigators, accountants, consultants, attorneys, other representatives, or

2  any other persons acting or purporting to act on its behalf or under its direction.

3          2.      The term "Infineon" means Infineon AG, Infineon North America Corp, and,

4  whether foreign or domestic, (a) all of its divisions, departments, parents, subsidiaries, affiliated

5  entities, assigns, or other organizational or operational units; (b) all of its predecessor or

6  successor companies, corporations, or entities; (c) all companies, corporations, partnerships,

7  associations, or other business entities, which are or have been under its ownership or control,

8  are controlled by it, which control it, or which are under common control in any manner with it;

9  and, for each of the foregoing, its (d) present and former officers, directors, employees, agents,

10  investigators, accountants, consultants, attorneys, other representatives, or any other persons

11  acting or purporting to act on its behalf or under its direction.

12          3.      The term "Inotera" refers to Inotera Memories, Inc. and (a) any of its divisions,

13  departments, parents, subsidiaries, affiliated entities, assigns, or other organizational or

14  operational units; (b) all predecessor or successor companies or corporations; (c) all companies,

15  corporations, partnerships, associations, or other business entities, which are or have been under

16  common ownership or control, are controlled by Inotera Memories, Inc., which control Inotera

17  Memories, Inc., or which are under common control in any manner with Inotera Memories, Inc.;

18  and (d) each of the present and former officers, directors, employees, agents, investigators,

19  accountants, consultants, attorneys, other representative, or any other persons acting or

20  purporting to act on behalf of any of them.

21          4.      The term "Qimonda" means Qimonda AG, Qimonda North America Corp, and,

22  whether foreign or domestic, (a) all of its divisions, departments, parents, subsidiaries, affiliated

23  entities, assigns, or other organizational or operational units; (b) all of its predecessor or

24  successor companies, corporations, or entities; (c) all companies, corporations, partnerships,

25  associations, or other business entities, which are or have been under its ownership or control,

**PLAINTIFFS' FIRST SET OF REQUESTS FOR
PRODUCTION TO KLA-TENCOR CORP. (Nos. 1-14)**

1  are controlled by it, which control it, or which are under common control in any manner with it;

2  and, for each of the foregoing, its (d) present and former officers, directors, employees, agents,

3  investigators, accountants, consultants, attorneys, other representatives, or any other persons

4  acting or purporting to act on its behalf or under its direction.

5          5.      The terms "Defendants" and "Nanya" all collectively refer to Defendants Nanya

6  Technology Corp. and Nanya Technology Corp. U.S.A., and (a) any of their divisions,

7  departments, parents, subsidiaries, affiliated entities, assigns, or other organizational or

8  operational units; (b) all predecessor or successor companies or corporations; (c) all companies,

9  corporations, partnerships, associations, or other business entities, which are or have been under

10  common ownership or control, are controlled by Defendants, which control Defendants, or

11  which are under common control in any manner with Defendants; and (d) each of the present and

12  former officers, directors, employees, agents, investigators, accountants, consultants, attorneys,

13  other representative, or any other persons acting or purporting to act on behalf of any of them.

14          6.      The term "document" is defined broadly to give the full scope of that term as

15  contemplated by Rule 34 of the Federal Rules of Civil Procedure, and shall include any original

16  (or a copy when an original is not available), each non-identical copy thereof (including those

17  which are non-identical by reason of notations or markings), and any other written, printed,

18  typed, punched, taped, graphic matter, or recorded or tangible thing, of whatever description,

19  however produced or reproduced, and shall include all attachments to and enclosures with any

20  requested item, and each draft thereof. The term Document includes: correspondence, telegrams,

21  memoranda, communications, minutes or records of meetings and conferences, lists of persons

22  attending meetings or conferences, summaries, records of conversations, drafts, notes,

23  notebooks, logs, invention records and disclosures, translations, drawings, graphs, charts,

24  photographs, sound recordings, images, data compilations, computer records or printouts,

25  specifications, reports, opinions, summaries, agreements, forecasts, plan drawings, mask works,

PLAINTIFFS' FIRST SET OF REQUESTS FOR
PRODUCTION TO KLA-TENCOR CORP. (Nos. 1-14)

1   engineering drawings, expressions or statements of policy, consultations, brochures, pamphlets,

2   advertisements, publications, circulars, trade letters, press releases, and drafts of any of the

3   foregoing, whether printed, recorded, written by hand, or stored in some tangible medium of

4   expression from which the information can be retrieved, perceived, or understood.

5       7.    The term "electronically stored information" is defined broadly to give the full

6   scope of that term as contemplated by Rule 34 of the Federal Rule of Civil Procedure, and refers

7   to all computer or electronically stored or generated data and information, and shall include all

8   attachments to and enclosures with any requested item, and all drafts thereof. Electronically

9   stored information includes information stored in any format and on any storage media,

10  including: hard disks; floppy disks; optical disks; flash memory devices; and magnetic tape,

11  whether fixed, portable, or removable. Electronically stored information includes: word-

12  processing documents; electronic spreadsheets; electronic presentation documents; e-mail

13  messages; image files; sound files; and material or information stored in a database, or accessible

14  from a database. Electronically stored information also includes all associated metadata that is

15  maintained or saved, which includes: document title or name; file name; date and time of

16  creation; date and time of last edit; identity of author; identity of owner; identities of editors;

17  identities of recipients; changes; history of changes; e-mail header information; history of who

18  viewed an e-mail and when; and e-mail routing information. Electronically stored information

19  further includes: correspondence, telegrams, memoranda, communications, minutes or records of

20  meetings and conferences, lists of persons attending meetings or conferences, summaries,

21  records of conversations, drafts, notes, notebooks, logs, invention records and disclosures,

22  translations, drawings, graphs, charts, photographs, sound recordings, images, data compilations,

23  computer records or printouts, specifications, reports, opinions, summaries, agreements,

24

25

26

27  forecasts, plan drawings, mask works, engineering drawings, expressions or statements of policy,

consultations, brochures, pamphlets, advertisements, publications, circulars, trade letters, press

**PLAINTIFFS' FIRST SET OF REQUESTS FOR**
**PRODUCTION TO KLA-TENCOR CORP. (Nos. 1-14)**

releases, and drafts of any of the foregoing.  Unless otherwise agreed upon, all electronically

stored information shall be produced in the form in which it is kept in the usual course of

business.  If electronically stored information is produced in the form in which it is kept in the

usual course of business but it is not reasonably useable in that form, then all software,

instructions, or tools necessary to make the information reasonably useable must also be

provided or identified.  To the extent that identical information is available as both a document

and as electronically stored information or in multiple forms of electronically stored information,

KLA-Tencor need only produce the electronically stored information in one reasonably useable

form.  Fujitsu's counsel invites KLA-Tencor's counsel to call to discuss compliance with the

foregoing instructions concerning electronically stored information.

       8.      The term "thing" shall have the broadest meaning prescribed in Rule 34 of the

Federal Rules Of Civil Procedure, and refers to any tangible object, other than documents or

electronically stored information, and includes physical objects of every kind and manner

including: prototypes, models, and specimens.

       9.      The term "materials" means any document, electronically stored information, or

thing as those terms are defined above.

      10.     The term "including" means including but not limited to.  The term "includes"

means includes without limitation.

      11.     The terms "relate," "relating," "refer," "referring," "concerning," and "concern"

shall be construed in the broadest sense to include, in addition to their customary and usual

meanings, describing, evidencing, including, discussing, mentioning, connected with, involving,

commenting on, memorializing, identifying, tending to support, tending to discredit, or

constituting, in whole or in part.

      12.     The terms "any" and "each" include and encompass each other and "all"

whenever such construction will serve to bring within the scope of these Requests and Subjects

**PLAINTIFFS' FIRST SET OF REQUESTS FOR
PRODUCTION TO KLA-TENCOR CORP. (Nos. 1-14)**

-8-

1    any Materials or testimony that would otherwise not be brought within their scope.

2        13.    The terms "and" and "or" shall be construed both conjunctively and disjunctively

3    and each shall include the other whenever such construction will serve to bring within the scope

4    of these Requests any Materials or testimony that would otherwise not be brought within their

5    scope.

6        14.    The term "attorney" includes attorneys (both in-house and outside counsel),

7

8    paralegals, and their secretaries and other support staff whenever necessary to bring within the

9    scope of these Requests any Materials or testimony that would otherwise not be brought within

10    their scope.

11        15.    The terms "communication", "communicated", or "communications" mean, in

12    addition to their customary and usual meanings, any transmission of letters, numbers, images,

13

14    symbols, data, or other information by any means, including any oral, written, or electronic

15    means.

16        16.    The terms "person" or "persons" mean any natural person, agency, association,

17    corporation, firm, individual, joint venture, organization, proprietorship, partnership, trust, or

18    entity.

19        17.    The phrase "KLA-Tencor product" means any and all products made by or on

20    behalf of KLA-Tencor or any and all products sold by or on behalf of KLA-Tencor.

21

22        18.    The phrase "KLA-Tencor measurement system" means any and all KLA-Tencor

23    products that use ellipsometer or spectrometer-based techniques to perform measurements,

24    including, but not limited to, SpectraCD, SpectraFX, SpectraFX with SCD option, KLA1280SE,

25    and KLA-Tencor ASET F5x measurement systems.

26        19.    The phrase "the '486 patent" means United States Patent No. 6,104,486, entitled

27    "Fabrication Process of a Semiconductor Device Using Ellipsometry" and all Fujitsu Related

Patent Applications, including application serial number 08/774,272.

**PLAINTIFFS' FIRST SET OF REQUESTS FOR**
**PRODUCTION TO KLA-TENCOR CORP. (Nos. 1-14)**

1    **REQUESTS FOR DOCUMENTS AND THINGS**

2

3    **REQUEST NO. 1:**    All materials concerning communications with Nanya including, but not

4    limited to, communications concerning sales, use, and operation of KLA-Tencor measurement

5    systems since 2000.

6    **REQUEST NO. 2:**    All materials concerning shipments, sales or marketing of KLA-Tencor

7    products to Infineon including, but not limited to, shipments, sales or marketing of KLA-Tencor

8    measurement systems since 2000.

9

10    **REQUEST NO. 3:**    All materials concerning shipments, sales or marketing of KLA-Tencor

11    products to Inotera including, but not limited to, shipments, sales or marketing of KLA-Tencor

12    measurement systems since 2000.

13    **REQUEST NO. 4:**    All materials concerning shipments, sales or marketing of KLA-Tencor

14    products to Nanya including, but not limited to, shipments, sales or marketing of KLA-Tencor

15    measurement systems since 2000.

16

17    **REQUEST NO. 5:**    All materials concerning shipments, sales or marketing of KLA-Tencor

18    products to Qimonda including, but not limited to, shipments, sales or marketing of KLA-Tencor

19    measurement systems since 2000.

20    **REQUEST NO. 6:**    All materials concerning the use and operation of KLA-Tencor

21    measurement systems including, but not limited to, manuals, data sheets, and marketing

22    materials since 2000.

23    **REQUEST NO. 7:**    Materials sufficient to show and fully describe all physical aspects and

24    features of the KLA-Tencor measurement systems including, but not limited to, design

25    schematics, layout materials, product specifications, maintenance and parts manuals, and quality

26    control documents since 2000.

27

MILBANK, TWEED, HADLEY & McCLOY LLP
ATTORNEYS AT LAW

**REQUEST NO. 8:**    All materials concerning data, data types, and format of data stored in KLA-Tencor measurement systems, for example, stored in a library or database, since 2000.

**REQUEST NO. 9:**    All materials concerning all modes of operation and use and operation of all of the measurement processes of KLA-Tencor measurement systems, including film thickness measurements and grating measurements, since 2000.

**REQUEST NO. 10:**    All materials concerning the processes used and steps taken to evaluate a lateral size of a structure measured by the KLA-Tencor measurement systems since 2000.

**REQUEST NO. 11:**    All materials concerning the processes used and steps taken to match data stored in KLA-Tencor measurement systems, for example, stored in a library or database, with a structure measured by the KLA-Tencor measurement systems since 2000.

**REQUEST NO. 12:**    Materials sufficient to show, for each KLA-Tencor measurement system sold to Inotera, Infineon, Nanya, or Qimonda since 2000:
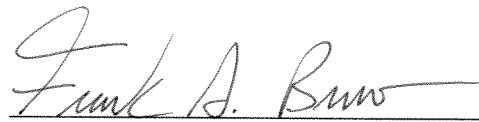
    (a)    all functional diagrams of the KLA-Tencor measurement system;

    (b)    all process diagrams of the KLA-Tencor measurement system;

    (c)    all flowcharts of the KLA-Tencor measurement system;

    (d)    all operation and user manuals of the KLA-Tencor measurement system;

    (e)    all schematics of the KLA-Tencor measurement system;

    (f)    all testing performed on KLA-Tencor measurement system;

    (g)    all information provided to Inotera, Infineon, Nanya, or Qimonda concerning use and operation of the KLA-Tencor measurement system; and

    (h)    all information requested by Inotera, Infineon, Nanya, or Qimonda concerning the use and operation of the KLA-Tencor measurement system.

MILBANK, TWEED, HADLEY & M^cCLOY LLP
ATTORNEYS AT LAW

1    **REQUEST NO. 13:**  All materials concerning the suitability of the KLA-Tencor measurement

2    systems for measuring line shape parameters, such as width, height, and sidewall angle of

3    semiconductor chips.

4    **REQUEST NO. 14:**  All documents, electronically stored information, things, and

5    communications concerning or referring to U.S. Patent No. 6,104,486, including any documents,

6    electronically stored information, things, or communications you sent to or you received from

7    third parties.

8

9

10

11    Dated:  April 24, 2008                    By:

MILBANK, TWEED, HADLEY & MCCLOY LLP
Mark C. Scarsi (SBN 183926)
Chris L. Holm (SBN 249388)
601 South Figueroa Street, 30th Floor
Los Angeles, CA  90017-5735
Telephone:      (213) 892-4000
Facsimile:      (213) 822-5796
F-N-wg@milbank.com

MILBANK, TWEED, HADLEY & MCCLOY LLP
Christopher E. Chalsen (*Pro Hac Vice*)
Michael M. Murray (*Pro Hac Vice*)
Lawrence T. Kass (*Pro Hac Vice*)
1 Chase Manhattan Plaza
New York, NY  10005
Telephone:      (212) 530-5000
Facsimile:      (213) 822-5796
F-N-wg@milbank.com

*Attorneys for Plaintiffs*
FUJITSU LIMITED and FUJITSU
MICROELECTRONICS AMERICA, INC.

12

13

14

15

16

17

18

19

20

21

22

23

24

25

26

27

MILBANK, TWEED, HADLEY & M<sup>c</sup>CLOY LLP
ATTORNEYS AT LAW

MILBANK, TWEED, HADLEY & McCLOY LLP
Mark C. Scarsi (SBN 183926)
Chris L. Holm (SBN 249388)
601 South Figueroa Street, 30th Floor
Los Angeles, CA 90017-5735
Telephone:     (213) 892-4000
Facsimile:     (213) 822-5796
F-N-wg@milbank.com

MILBANK, TWEED, HADLEY & McCLOY LLP
Christopher E. Chalsen (*Pro Hac Vice*)
Michael M. Murray (*Pro Hac Vice*)
Lawrence T. Kass (*Pro Hac Vice)*
1 Chase Manhattan Plaza
New York, NY 10005
Telephone:     (212) 530-5000
Facsimile:     (212) 822-5796
F-N-wg@milbank.com

Attorneys for Plaintiffs,
FUJITSU LIMITED and
FUJITSU MICROELECTRONICS AMERICA, INC.

**UNITED STATES DISTRICT COURT**
**NORTHERN DISTRICT OF CALIFORNIA**
**OAKLAND DIVISION**

| | |
|---|---|
| FUJITSU LIMITED and FUJITSU MICROELECTRONICS AMERICA, INC., | Case No. 4:06-CV-06613 (CW) |
| *Plaintiffs,* | **CERTIFICATE OF SERVICE** |
| -against- | |
| NANYA TECHNOLOGY CORP. and NANYA TECHNOLOGY CORP. U.S.A., | |
| *Defendants.* | |
| NANYA TECHNOLOGY CORP. and NANYA TECHNOLOGY CORP. U.S.A., | |
| *Third-Party Plaintiff,* | |
| -against- | |
| KLA-TENCOR CORPORATION, | |
| *Third-Party Defendant.* | |

1

2
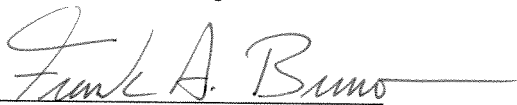
        I hereby certify that on April 24, 2008, a true and correct copy of the foregoing document was caused to be served on the following counsel of record electronically via direct email with a confirmation copy via First Class Mail:

3

4

Martin C. Fliesler, Esq.
FLIESLER MEYER LLP

Justin Kimble, Esq.
SHORE CHAN BRAGALONE, LLP

5

650 California Street
14th Floor

325 N. St. Paul Street
Suite 4350

6

San Francisco, CA  94108
T: (415) 362-3800

Dallas, TX  75201
T: (214) 593-6110

7

F: (415) 362-2928
mcf@fdml.com

F: (214) 593-6111
jkimble@ShoreChan.com
mhenry@ShoreChan.com

8

*Attorneys for Defendants*

9

*Nanya Technology Corp. and*
*Nanya Technology Corp. U.S.A.*

*Attorneys for Defendants*
*Nanya Technology Corp. and*
*Nanya Technology Corp. U.S.A.*

10

Robert Harkins, Esq.

11

HOWREY LLP
525 Market Street

12

Suite 3600
San Francisco, CA  94105

13

T: (415) 848-4935
F: (415) 848-4999

14

harkinsr@howrey.com

15

*Attorneys for Third-Party Defendant*
*KLA-Tencor Corp.*

16

17

18

19

20

NY2:#4735636

21

22

23

24

25

26

27

28

# Exhibit C

**<< Back | Print**

### Infineon, Nanya Begin 90nm 300mm Volume DRAM Production

**Online staff -- 6/2/2005**
**Electronic News**

Infineon Technologies AG and Nanya Technology Corp. today reported the successful qualification of 90nm DRAM technology, jointly developed at Infineon's research center in Dresden, Germany.

Both companies have qualified the 90nm memory products at major customers and have achieved the validation of Intel. Volume production with 90nm process structures on 300mm has begun at Infineon's 300mm production line in Dresden.

As of the end of May, approximately 5 percent of Infineon's total global DRAM production has been converted from 110nm to 90nm.

Also, Inotera Memories, the Taiwan-based manufacturing joint venture of Infineon and Nanya, has begun transitioning to 90nm, the companies said.

Early adoption of 90nm is meant to improve production costs and product performances and is one of the most important factors to increase profitability in DRAM manufacturing, the companies believe.

ADVERTISEMENT

Process structures of 90nm further reduce chip size compared to the previous 110nm technology thereby increasing potential chip output per wafer by more than 30 percent. The expected productivity increase by shrinking the chip size combined with the use of 300mm wafers is the basis for a significant reduction of production cost per chip.

Next, Infineon and Nanya will develop technology for the next node with 70nm structures under their strategic development alliance.

"With the qualification of advanced DRAM products on 90nm process technology we have achieved a major milestone towards product and technology leadership and increased DRAM manufacturing productivity," said Andreas von Zitzewitz, member of Munich-based Infineon's management board and head of its memory products business group, in a statement.

The introduction of 90nm process structures was helped along by the company's experience with advanced 193nm lithography, introduced at the 110nm node, Infineon said.

Further, due to the introduction of so called "checkerboard cell array," a superior storage capacitance could be achieved by just implementing standard surface enhancement methods instead of using complex high-k dielectrics.

Except for its cost advantage, transition to smaller process geometries is crucial for high-speed and low-power DDR2 and DDR3 SDRAM in an increasingly mobile world, the two said.

The companies plan to extend their DRAM offering with a 512Mb DDR2 SDRAM expected in the second half of the year, with a variety of other products including 256Mb DDR2 and 1G DDR2 to follow.

**<< Back | Print**

# Exhibit D

# Spectroscopic Ellipsometry based Scatterometry enabling 193nm Litho and Etch process control for the 110nm technology node and beyond.

Thomas Hingst[a], Thomas Marschner[a], Manfred Moert[a], Jan Homilius[a], Marco Guevremont[b], John Hopkins[b], Assim Elazami[b].

[a] Infineon Technologies GmbH, Unit Process Development Department, Koenigsbruecker Str. 180, 01099 Dresden, Germany;
[b] KLA-Tencor Corp., San Jose, CA.

## ABSTRACT

In the production of sub 140nm electronic devices, CD metrology is becoming more critical due to the increased demands placed on process control. CD metrology using CD-SEM is approaching its limits especially with respect to precision, resolution and depth of field. Potentially, scatterometry can measure structures down to 50nm with the appropriate precision. Additionally, as scatterometry is a model based technique it allows a full reconstruction of the line profile and the film stack. In this work we use SE based scatterometry in the control of a 110nm DRAM WSi$_x$ Gate process at the Litho and the Mask Open step. We demonstrate the use of a single trapezoid as a basic shape model in FEM and field mapping applications as well as in a high volume production test. The scatterometry results are compared to CD-SEM data. We show that for the GC Litho application, n&k variations in some of the stack materials do not affect the scatterometry CD measurement significantly.

**Keywords:** scatterometry, spectroscopic ellipsometry, CD, DRAM, gate control.

## 1. INTRODUCTION

The capability of scatterometry to measure structures with dimensions 0.25μm and below has been demonstrated [1][2][3]. There is, consequently, considerable interest in the application of scatterometry within the semiconductor industry as microfabrication processes continue to be scaled down. Currently, the most advanced fabrication processes are capable of the mass production of devices with a minimum line width of ~0.15μm. Next generation devices are road mapped for target line widths of ~0.1μm and already, scatterometry has been used in the measurement of pilot production structures [4]. In addition to measurement capability, scatterometry offers a number of advantages over competing techniques:

(i)     it is non-destructive - patterned 193nm photoresist layers are known to be irreversibly affected by the electron beam during CD-SEM measurement ("line slimming"),

(ii)    high throughput - a number of process related parameters such as Top-CD (TCD), Middle-CD (MCD), Bottom-CD (BCD), sidewall angle, height/depth and also layer thicknesses can be extracted from a single measurement,

(iii)   low cost of ownership (e. g. there are no costly vacuum systems to maintain),

(iv)    rapid integration into production lines. Fab engineering teams are already experienced in the implementation of similar techniques such as reflectometry and conventional ellipsometry. There is the possibility of integrating scatterometry modules into modular process tools for inline real time measurement [5].

Until now several applications for scatterometry have been successfully demonstrated, e.g. STI [7] and polysilicon gate [6]. More challenging applications such as in the WSi$_x$ containing gate structures used in DRAM manufacturing, are yet to be implemented in production. The main obstacle is the complexity of the profiles, stacks and materials. Key issues for these applications are the modeling of the optical properties of the WSi$_x$ layer, the modeling of possible top rounding effects as well as surface and interface roughness of the structures.

In this work we examine SE based scatterometry [8] in the control of a 110nm DRAM WSi$_x$ Gate process (GC) at the Litho and the Mask Open step.

## 2. METHODOLOGY

In this study all scatterometry measurements were performed using the KLA-Tencor SpectraCD system[**], a spectroscopic ellipsometer based on the ASET F5x platform, a well-established thin film measurement tool present in a number of fabs worldwide.

All scatterometry data presented in this paper use the library matching approach where libraries are built based on nominal process knowledge. In the library building process material dispersions are first determined via the system thin film capabilities, then using a non-linear regression approach line profiles are parameterized and process ranges are established. A library of pre-computed electromagnetic responses is then generated to provide reliable high throughput run-time performance.

In an effort to establish scatterometry as an independent measurement technique, the results obtained are compared to measurements obtained from traditional top-down scanning electron microscopy (SEM) for correlation as well as cross section SEM micrographs for profile information validation.

(**) provided by KLA-Tencor, San Jose, CA.

## 3. RESULTS

### 3.1 GC Litho, 110nm Technology

The nominal film stack for this process step is shown in Figure 1 (a). The film thicknesses within the stack were subsequently confirmed by SE measurement at unpatterned measurement sites (for stack model details see section 3.6). A test reticle was used containing various periodic gratings with different line width and line/space (L/S) ratios. We utilized the following eight L/S gratings per die (all dimensions in nm): (1) 110/110 (target line width for this process technology), (2) 140/140, (3) 160/120, (4) 170/170, (5) 200/140, (6) 250/590, (7) 250/870, and (8) 270/750. The results described in this section were taken from a wafer which had been exposed under focus/exposure type conditions.

Regression analysis of spectra taken from the 110/110, 140/140 and 160/120 gratings at locations around the wafer showed the optimum line shape to be represented by a single trapezoid (Figure 1 (b)). Based upon this single trapezoid shape, two regression libraries were created for measurement of the 220nm pitch and 280nm pitch gratings, respectively. Measurement was made over the 300nm - 700nm wavelength range on a GC Litho wafer with 25 die.

Typically for NGOF > 0.9 the model represents the actual line profile. From Table 1, it is apparent that when measuring the 160/120 gratings, a low NGOF is reported at a significant number of sites. However, when using the same 280nm pitch regression library to measure the 140/140 gratings, higher NGOFs are generally observed. The observation of low NGOFs was attributed to deviation of the particular gratings from the ideal single trapezoid shape and is to be expected in significantly under- or over-exposed die on the FEM wafer. This was later verified by vertical sectioning of the wafer (Figure 2). Based on this information NGOF=0.9 was established as a threshold value to distinguish between good CD measurement and need for disposition.

| Grating (line/space) in nm | Number of dies with NGOF > 0.9 | $\chi^2$ range |
| --- | --- | --- |
| 110/110 | 17 | 1400- 8700 |
| 140/140 | 22 | 3400- 6500 |
| 160/120 | 11 | 3800- 6400 |

Table 1: Numbers of accepted SCD measurements on different gratings of the GC Litho 110nm structure, based on NGOF filtering.

The relationship between NGOF and grating profile is also shown by the 220nm pitch (110/110) gratings. Figure 3 shows the focus/exposure plot for the 110/110 gratings. The measured BCD has varied with exposure conditions in the expected manner and an optimum focus/exposure range to achieve the required process line width, can be identified. Within the optimum range, Spectra-CD has measured the grating BCD with high accuracy (e. g. die 11, 16; see Figure 3) and the grating profile is close to a single trapezoid shape. As a regression library based upon a single trapezoid shape had been demonstrated to give reasonable accuracy at or around the optimum focus/exposure range, the single trapezoid library was applied to the measurement of (i) 110/110 grating arrays (see section 3.4) and (ii) GC Litho 140 nm technology production lots (see section 3.5). Nevertheless, it is clear from studies of the vertical sections that

outside the optimum focus-exposure range, effects such as corner rounding and footing are present. Such effects cannot be reproduced with a single trapezoid model. In order to give the photo engineer a more complete range of information in focus- exposure studies, a more sophisticated shape model was applied (see section 3.2).
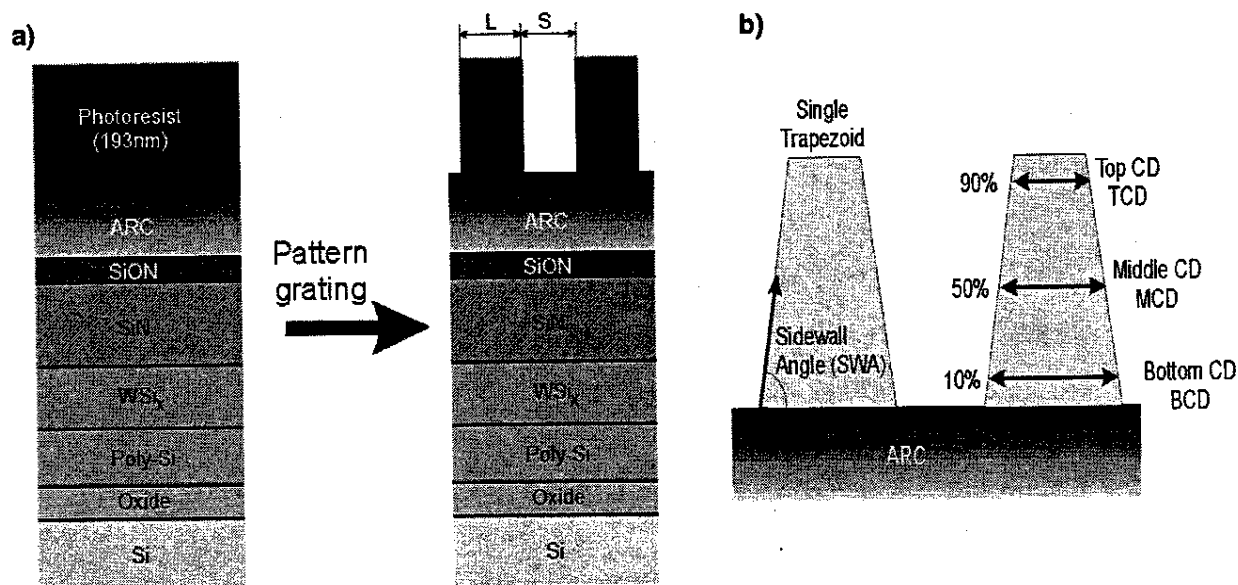
a)

Photoresist (193nm)

ARC
SiON
SiN
WSi$_x$
Poly-Si
Oxide
Si

L    S

Pattern grating

ARC
SiON
SiN
WSi$_x$
Poly-Si
Oxide
Si

b)

Single Trapezoid

90%    Top CD TCD

50%    Middle CD MCD

Sidewall Angle (SWA)

10%    Bottom CD BCD

ARC

Figure 1: (a) Gate Control 110 nm processing: Nominal film stack at photolithography, (b) the single trapezoid shape and definition of the key dimensions.

NGOF>0.9    NGOF>0.9    NGOF<0.9    NGOF<0.9

140/ 140 Grating. Die 6.
Micrograph BCD 114 nm,
Spectra-CD BCD 128.5 nm.

140/ 140 Grating. Die 20.
Micrograph BCD 97 nm,
Spectra-CD BCD 98.1 nm.

160/ 120 Grating. Die 6.
Micrograph BCD 189 nm,
Spectra-CD BCD 127.9 nm.

160/ 120 Grating. Die 20.
Micrograph BCD 144 nm,
Spectra-CD BCD 98.9 nm.
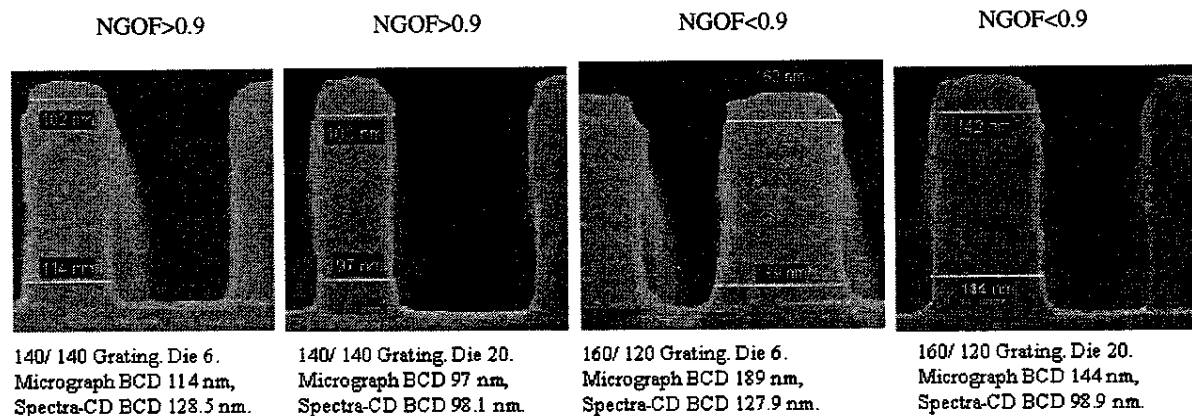
Figure 2: Imaging SEM micrographs of the 110nm GC Litho structure. Vertical sections of 140/140 and 160/120 gratings processed under two different focus-exposure conditions within an FEM-wafer.

In order to determine the correlation between scatterometry and other measurement techniques, regression libraries based on the single trapezoid shape were generated for the remaining gratings pitches (i) 170/170 and 200/140, (ii) 250/590, (iii) 250/870 and (iv) 270/750.

An initial analysis of a plot of Spectra-CD BCD against the BCD as reported by the CD-SEM for the 270/750 gratings (Figure 4) suggested that there was no obvious relationship between the two parameters. However, examination of the original Spectra-CD measurements for this grating showed that sidewall angles > 90° were being reported at several die on an identical wafer. This was later verified by a review of vertical section micrographs (Figure 5). Sidewall angles > 90° are clearly present and it is noticeable that no obvious footer is present. In view of this, the correlation data shown in Figure 4 was reviewed. Although there is no obvious relationship between Spectra-CD BCD

and CD-SEM BCD, plotting the Spectra-CD TCD against the value reported by the CD-SEM shows an almost linear relationship for Spectra-CD reported sidewall angles > 90°. Thus, for such structures, the top down measurement of the CD-SEM is a measurement of the TCD rather than the required BCD. This effect was also observed at certain focus/exposure conditions at the other grating pitches.
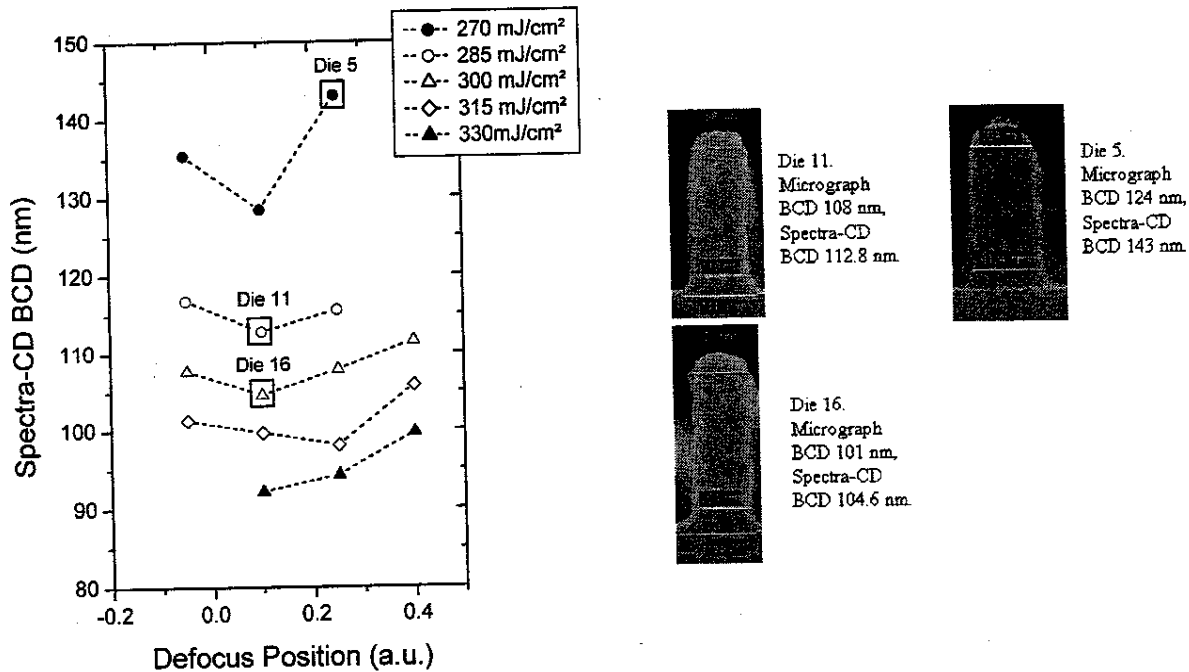


Figure 3: Focus/ exposure plot of BCD as reported by Spectra-CD, for 110/ 110 nm gratings processed with 110 nm technology at GC-Litho. SEM images of vertical sections of the resist structure at a die with non-optimum (die 5) and optimum (die 11, 16) focus/ exposure dose.
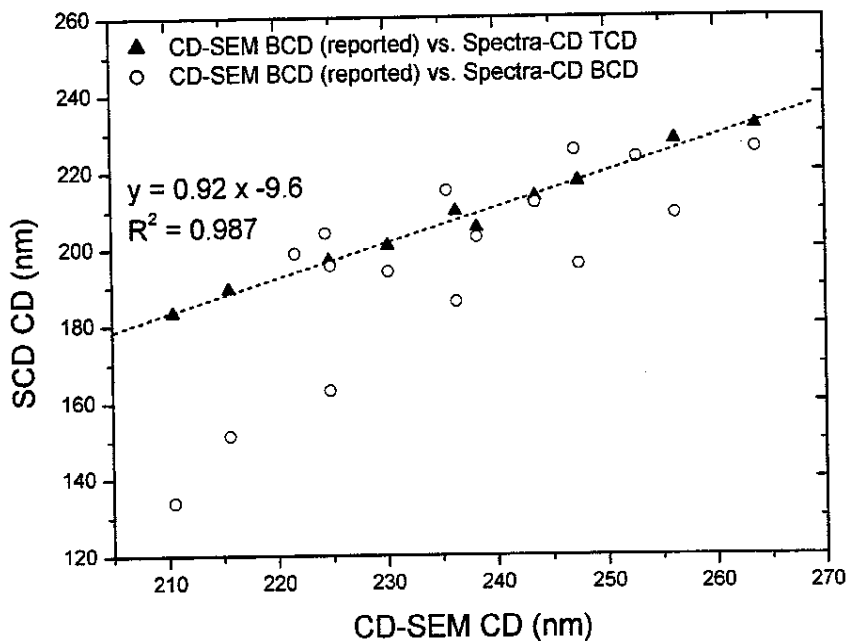


Figure 4: Plot of Spectra-CD BCD and TCD against CD-SEM reported CD for the GC Litho 270/750 resist grating (processing is based on 110nm technology).
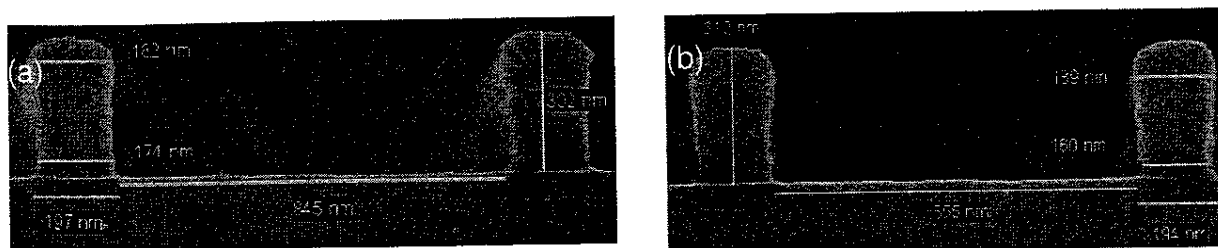
Figure 5: 270/ 750 grating. (a) Die 15 and (b) die 20. Important is that (i) a sidewall angle > 90 degrees is clearly present and (ii) there is no significant footing present.

## 3.2 Advanced Shape Models

In order to more closely reproduce the typical shape across the full focus-exposure range, a refinement on the single trapezoid shape was used. The regression library described in section 3.1 was regenerated but with a shape algorithm that allowed the user to incorporate top and bottom rounding effects (Figure 6)
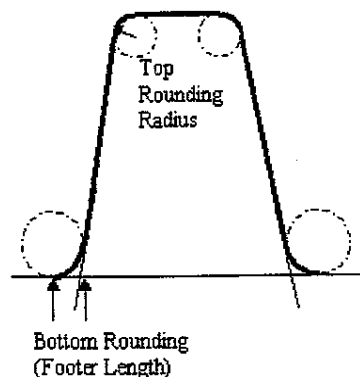


| Grating | Number of Die NGOF > 0.9 | $\chi^2$ range |
|---------|--------------------------|----------------|
| 110/110 | 19/25 | 1100 - 2000 |
| 140/140 | 22/25 | 970 – 2000 |
| 160/120 | 15/25 | 1400 – 2400 |

Table 2: GC Litho S11. Spectra-CD measurement using regression library that incorporates top and bottom rounding

Figure 6: Advanced shape model for GC Litho S11: Trapezoid shape with top and bottom rounding

A marked improvement in the quality of fit (reduced $\chi 2$, Table 2) is observed when compared to the equivalent measurement summarized in Table 1.With application of the rounded trapezoid shape to the 110/110, 140/140 and 160/120 gratings, a general improvement in the quality of fit (lower $\chi 2$) was observed. At some of the gratings in certain die, the bottom footer length was very pronounced, and in some cases the space had not opened completely. The 160/120 gratings were particularly prone to this effect (see Figure 2). Use of the rounded trapezoid shape produced a slight shift in the observed wall angles (Table 3) and it is noticeable that the 110/110 and 140/140 gratings show wall angles slightly greater than 90°.

| Grating | Single Trapezoid, Wall Angle Range (nm) | Rounded Trapezoid, Wall Angle Range (nm) |
|---------|------------------------------------------|-------------------------------------------|
| 110/110 | 88.0 - 89.0 | 88.4 - 90.8 |
| 140/140 | 85.6 - 90.4 | 87.1 - 91.0 |
| 160/120 | 82.2 - 88.2 | 85.8 - 89.3 |

Table 3: GC Litho S11. Wall angle ranges observed with die NGOF > 0.9, using (i) single trapezoid library and (ii) rounded trapezoid library for regression.

Figure 7 shows the Spectra-CD BCD versus CD-SEM BCD correlation plot for the three sets of gratings. The main correlation plot is generated using gratings where the sidewall angle has been reported to be less than 90°. Gratings that show a sidewall angle greater than 90° are displaced from this main plot. This displacement can be attributed to an effect that was originally observed in the measurement of large pitch gratings. The fact that the sidewall angle of the structure is greater than 90° has caused the top down CD-SEM measurement to report TCD rather than BCD and thus contribute significant error.

The correlation relationship shown by the main plot is in reasonable agreement with that found using field mapping techniques (Figure 10). Also, in view of the fact that the target line width for this technology is 110 nm, grating pitch clearly has an influence on the accuracy that can be attained using top down CD-SEM measurement for this line width. The application of advanced shape algorithms within the Spectra-CD measurement ultimately has allowed (i) more accurate measurement of the line width within the process window and (ii) measurement of CD in the FEM matrix at parameter ranges outside the optimum, thus giving the Photolithography engineer a broader range of information.
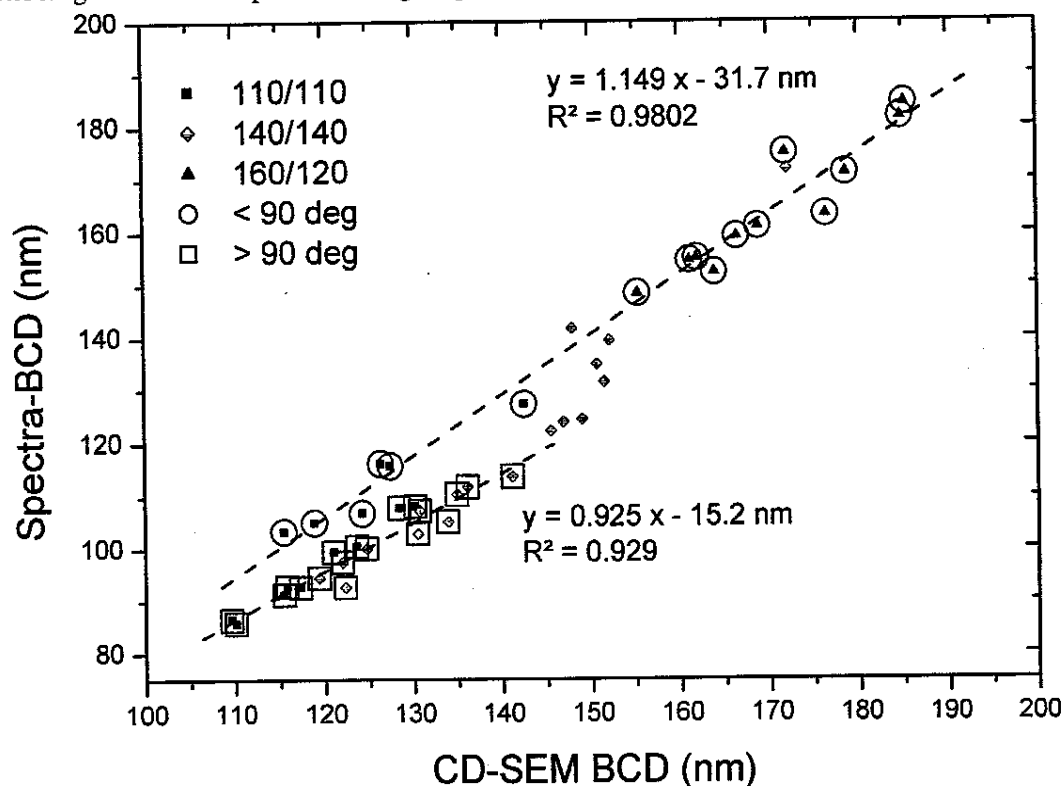


Figure 7: Spectra-CD BCD versus CD-SEM BCD correlation plot for GC-Litho S11 test gratings with advanced model shapes. Square framed datapoints are gratings where SWA > 90 degrees. Round framed data points show SWA < 90 degrees.

### 3.3 GC Mask Open, 110 nm Technology

Once the GC Litho step is completed, the open areas are etched down to the upper surface of the $WSi_x$. The residual photoresist and organic ARC are then removed. The final structure shown in Figure 8 (a) is formed. In practice, an overtech of the $WSi_x$ occurs (Figure 8 (b)). Gratings created at GC Mask Open were analyzed using real-time regression to confirm that the dispersion models used to characterize the relevant layers at GC Litho, still applied at GC Mask Open. It was observed at this point that the $WSi_x$ overetch could be measured. Consequently, an additional trapezoid was added to the regression library shape. With this advanced input, a final regression library could be created. The library showed a high NGOF (low $\chi 2$) for the optimum focus/exposure die (Table 4) and the measured $WSi_x$ overetch was in very good agreement with the overetch thickness observed in micrographs. The fact that such a high NGOF (low $\chi 2$) could be achieved for the optimum focus/exposure case, using shapes based on the single trapezoid confirms the relationship between final best fit and shape.

(a)                                                                 (b)
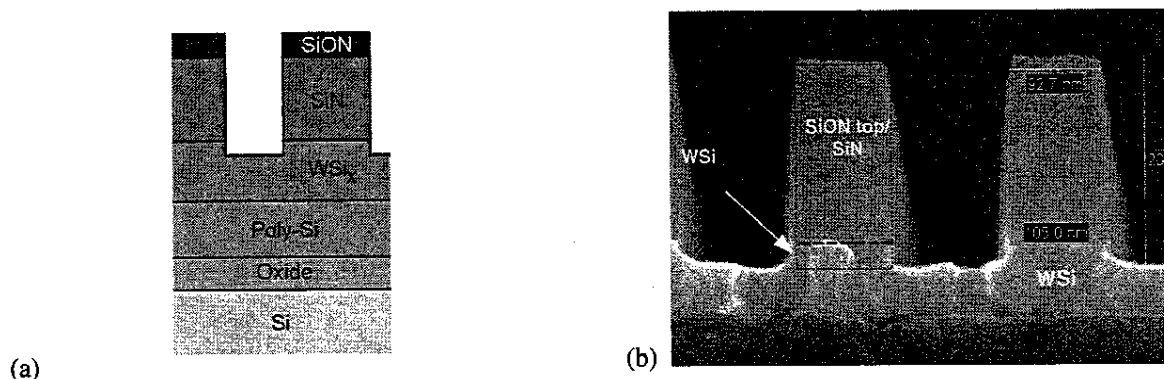
Figure 8: (a) Schematic of structure after gate control mask open (110nm technology). (b) Imaging of the overetch at SiN/WSi$_x$ interface by vertical SEM-section.

| Grating (line/space) in nm | Number of dies with NGOF > 0.9 | $\chi 2$ range |
| --- | --- | --- |
| 110/110 (slot 8) | 23/34 | 1200- 3000 |
| 110/110 (slot 11) | 18/25 | 1000- 3800 |
| 140/140 (slot 11) | 22/25 | 1000- 2500 |
| 160/120 (slot 11) | 13/25 | 1600- 2300 |

Table 4: Numbers of accepted SCD measurements on different gratings. GC Mask Open 110nm. Based on NGOF filtering, for two different FEM wafers.

### 3.4 Field Mapping, 110nm Technology

Irradiation of a surface with an electron beam can result in a number of highly undesirable effects. The localized deposition of energy can cause partial and irreversible change in patterned photoresist films while the widely observed effect of "charging" causes the irradiated area to image darker after repeated scans with the electron beam. Consequently, a quantitative assessment of the precision of a CD-SEM measurement can only be made by measurement of several identical sites at different locations.

To compare the precision attainable in the CD-SEM with that of the Spectra-CD, two wafers were exposed using a mask in which a matrix (5 rows, 9 columns) of 110/110 gratings had been patterned within each die. In order to simulate a process based change, five die close to the wafer centre (Figure 9) were exposed under slightly different conditions but close to the optimum. After exposure and development, the wafers were separated. One wafer remained at litho while the second wafer was moved on to the following process step (GC Mask Open). By mapping the dimensional changes across the wafer centre, the user can assess the behavior of the regression library within a dimensional range which is centred at the process optimum. The measurements were then repeated using a CD-SEM.

The wafers were measured using Spectra-CD recipes based on the libraries described in sections 3.1 and 3.3. Figure 9 shows the BCD for each grating in the matrix within each die for GC Litho and GC Mask Open. As expected, each of the five die shows a different mean BCD due to the different focus/exposure condition. However, variations *within* a die are also clearly present and both CD-SEM and SCD report an anomalously high BCD for gratings within the first row of the matrix at each of the five die.

A full Spectra-CD BCD and CD-SEM BCD correlation is shown in Figure 10 for GC Litho and in Figure 11 for GC Mask Open. It is noticeable that a higher $R^2$ is obtained in the GC Mask Open case when compared to the value obtained for GC Litho.

It is apparent that differences exist in the precision with which both techniques measure and one contributing factor is relative spot size. The CD-SEM measures an individual line and is consequently sensitive to local line width variations while Spectra-CD averages over a larger measurement area (approximately 25μm by 25μm) and therefore requires lower statistical throughput.
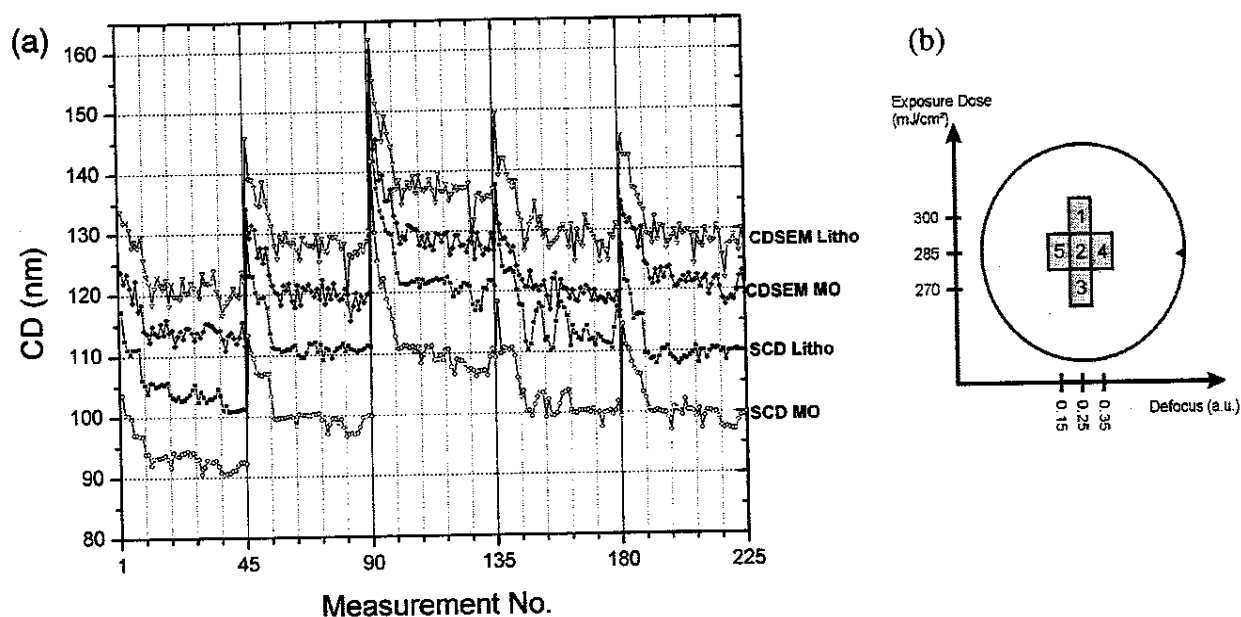
Figure 9: (a) BCD die map measurement of 5 dies of GC Litho and GC Mask Open 110nm processed FEM-wafers on 110/110 grating. (b) Die layout and sequence of the measurements. One 110/110 grating array per die

The similarity in behavior of the two independent regression libraries is illustrated in Figure 12 and Figure 13. Similar dimensional changes have been measured in two separate wafers. Thus, the measurement technique can be eliminated as the cause of the anomalously high CD measurements recorded for the first grating row in each die. Electrical testing of finished die had shown this mask to be defective. Measurements by Spectra-CD and CD-SEM had therefore, confirmed this.
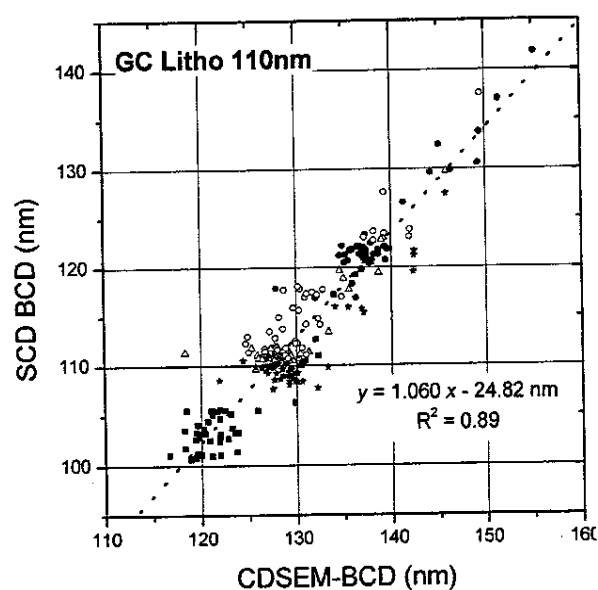


Figure 10: GC Litho, 110nm technology. Spectra-CD BCD against CD-SEM BCD as obtained from 110/110 grating arrays.
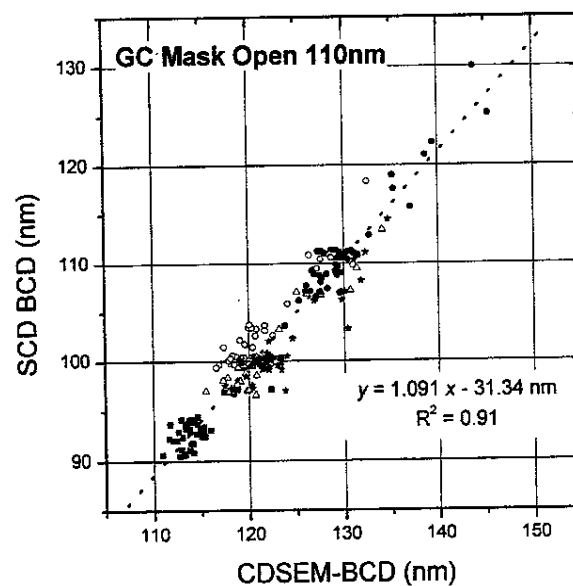
Figure 11: GC Mask Open, 110nm technology. Spectra-CD BCD against CD-SEM BCD as obtained from 110/110 grating arrays.
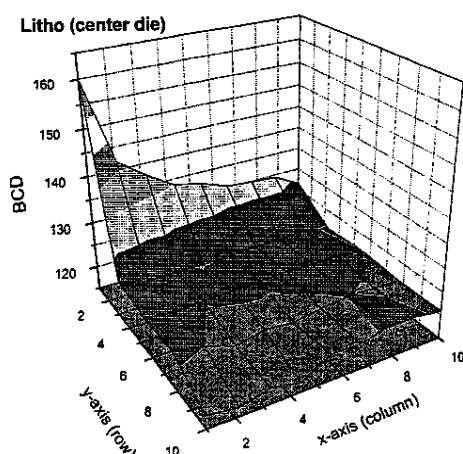
Figure 12: Die mapping of the bottom CD of GC Litho 110nm test structures.
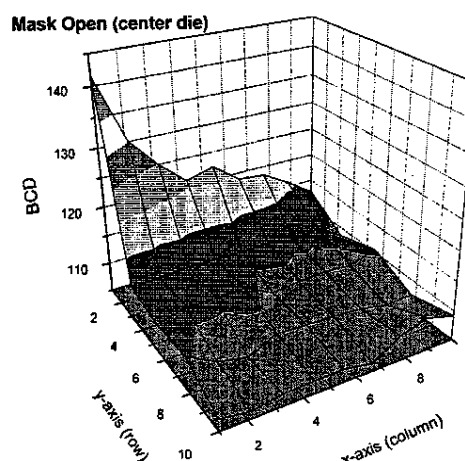
Figure 13: Die mapping of the bottom CD of GC Mask Open 110nm test structures.

### 3.5 Production Testing

An important prerequisite for accurate measurement of grating structures by scatterometry, is that films below the grating are unpatterned. However, there is one important feature associated with the optical characteristics of the Gate Control stack. The $WSi_x$ layer is highly absorbing and effects resulting from layers below the $WSi_x$ layer, are not seen at wavelengths shorter than approximately 600nm. This offers the possibility of measuring grating structures within the Gate Control active die area, provided the appropriate wavelength range is selected.

The presence of a grating structure within the die area of a 140nm DRAM device allows us to assess the performance of both the measurement technique and the associated hardware, in the volume production environment. So, high volume production tests were performed at two points in the process: (i) GC Litho 140nm, and (ii) GC Mask Open 140nm. As the existing production lines are based on 140nm technology node, the recipes created on the basis of the previously described results, were adapted. The following key adjustments were made in both applications: (i) the parameter limits within the regression library had to be altered in order to allow measurement at the larger line width, (ii) the film stacks associated with either application, are slightly different at 140nm, new dispersion files were created for the 140nm photoresist and the SiON layer, (iii) the recipes were run over the wavelength range 300nm to 600nm in order to suppress any contribution from layers or patterning below the $WSi_x$ layer.

The measurement was implemented in the 140nm DRAM process flow directly before CD-SEM linewidth measurements using the same measurement locations on both systems. This allows a direct comparison of the SCD results to those of the established standard CD metrology. Furthermore two unpatterned locations per die were measured to track the suitability of the film stack model (see section 3.6). Effectively seven sites per die, five die per wafer and two wafers per lot were measured.

In the first phase of the production test about 85 lots were measured after GC Litho. To assess the behaviour of the scatterometry measurement, the TCD, MCD and BCD were monitored and compared to the standard measurement used for process monitoring, the BCD as measured by CD-SEM.

From Figure 14 it is seen that (i) the BCD as measured by Spectra-CD, is close to the target line width of the technology. This is not so with the CD-SEM measured BCD where a measurement offset must be applied, (ii) the standard deviation of all data points is approximately equal when comparing CD-SEM BCD and Spectra-CD MCD. The larger standard deviation reported for Spectra-CD BCD and TCD is caused by error propagation resulting from calculation of these parameters from the original measured basis parameters, (iii) comparison of the CD-SEM BCD and Spectra-CD MCD shows a high degree of correlation between the two measurements (see Figure 9) If an offset [Spectra-CD TCD/ MCD/ BCD - CD-SEM BCD] is calculated, the standard deviation of the SCD MCD to CD-SEM BCD is lowest (< 1 nm).

In a second phase of the production test about 50 lots were measured after GC Mask Open. The format of the GC Mask Open production test was identical to that used for GC Litho. The model in this case was more complicated than the simple trapezoid lithography shape. Here we had three stacked trapezoids of different materials (see section 3.3) plus a fixed bottom rounding.
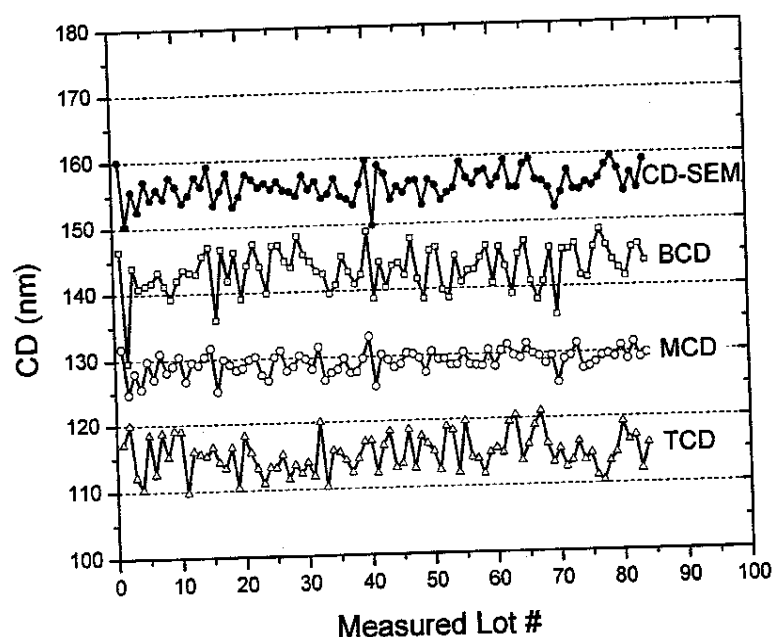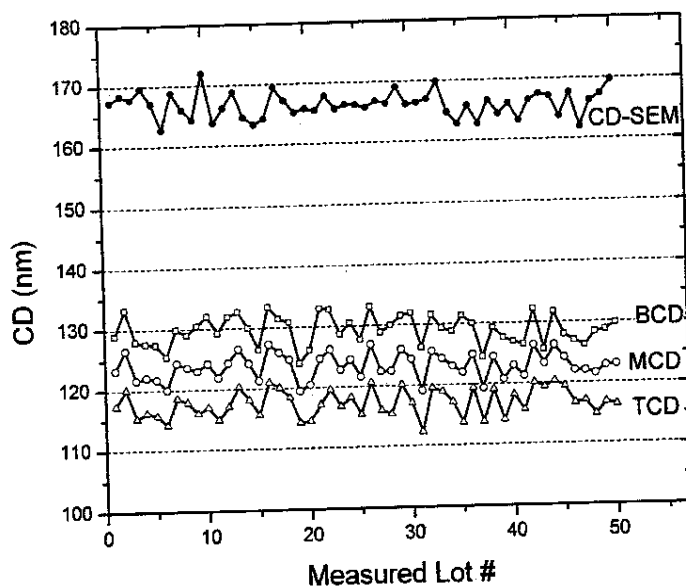
Sigma of all datasets:

CD-SEM
2.0 nm

SCD BCD
3.3 nm

SCD MCD
1.6 nm

SCD TCD
2.8 nm

Figure 14: BCD, MCD, TCD as measured by Spectra-CD for GC Litho 140nm. Comparison with that reported by CD-SEM. Each datapoint represents a single location close to the wafer center. SCD and CD-SEM data are from the same wafers.

From Figure 15 it is seen that (i) the BCD as measured by SCD, is again close to the target line width of the technology while the offset to the CD-SEM measured BCD has increased, (ii) the standard deviation of all data points is approximately equal when comparing CD-SEM BCD and Spectra-CD MCD. The standard deviation reported for Spectra-CD BCD and TCD are only slighly larger, (iii) the sidewall angle has changed to higher values (smaller BCD-TCD difference). A direct comparison of the CD-SEM BCD and Spectra-CD MCD is not possible for GC Mask Open because the date are from the same lots but from different wafers. However the correlation between GC Litho and GC Mask Open is already shown in section 3.4 (Field Mapping).



Sigma of all datasets:

CD-SEM
2.1 nm

SCD BCD
2.5 nm

SCD MCD
2.1 nm

SCD TCD
2.2 nm

Figure 15: GC Mask Open 140 nm. MCD, BCD as measured by Spectra-CD. Comparison with that reported by CD-SEM. Each datapoint represents a single location close to the wafer center. Note that SCD and CD-SEM data are from the same lots but from different wafers.

## 3.6 Effect of Filmstack Variations on the CD Measurement

For maximum accuracy Scatterometry as a model based measurement technique requires accurate film dispersion and stack models. Filmstacks for STI or Oxide Trench applications contain "well known" materials and provide good conditions for optical measurements (homogeneous materials, smooth interfaces). However the DRAM Gate Stack used in this investigation contains a Si-rich SiON layer as well as a $WSi_x$ layer. Especially the $WSi_x$ dispersion modeling is quite challenging because this layer is opaque in most of the usable wavelength range (250nm to 600nm). On the other hand there is a strong correlation between the SiON top layer and the underlying Nitride layer because of a similar n&k dispersion in the visible wavelength range (400nm to 800nm). In order to avoid correlation effects the SiON layer was fixed at its nominal value. In addition the $WSi_x$ and SiON layers may show some variation of their optical properties depending on process conditions.

The n&k dispersions of Resist, ARC, SiON, $Si_3N_4$ and Polysilicon were confirmed using SE data taken on test wafers (single layers on silicon, except for polysilicon which has an underlying oxide layer). The n&k dispersion of $WSi_x$ was modeled in the complete Gate Stack which may result in unphysical n&k behaviour. However this approach allows us to compensate for interface roughness, graininess (see Figure 8 b) and other material related effects. The complete filmstack model was tested and showed typical GOF values for this kind of application. The filmstack model finally used for the CD measurements gave low GOF values ($\chi2$ based GOF $\approx$ 0.4) compared to GOFs observed in applications such as STI ($\chi2$ based GOF $\approx$ 0.8) on unpatterned measurement areas.

The production test for the 140nm GC Litho process was used to track the GOF values on two unpatterned areas (FTA sites) over a long period of time and to investigate the influence of filmstack variations on the SCD measurements. GOF variations are visible wafer-to-wafer as well as lot-to-lot indicating variations in the optical properties of the stack materials (most likely $WSi_x$ or SiON) or thickness deviation from the nominal value for layers with fixed thickness. Similar GOF behavior was observed on both unpatterned locations (Up/Down area). The GOF range on the gratings is comparable to that on the FTA sites, however there is no obvious GOF correlation between the grating and the unpatterned locations (see Figure 16). In addition the SCD data seems not to be affected by these stack variations. The correlation to the CD-SEM measurement remains unchanged.
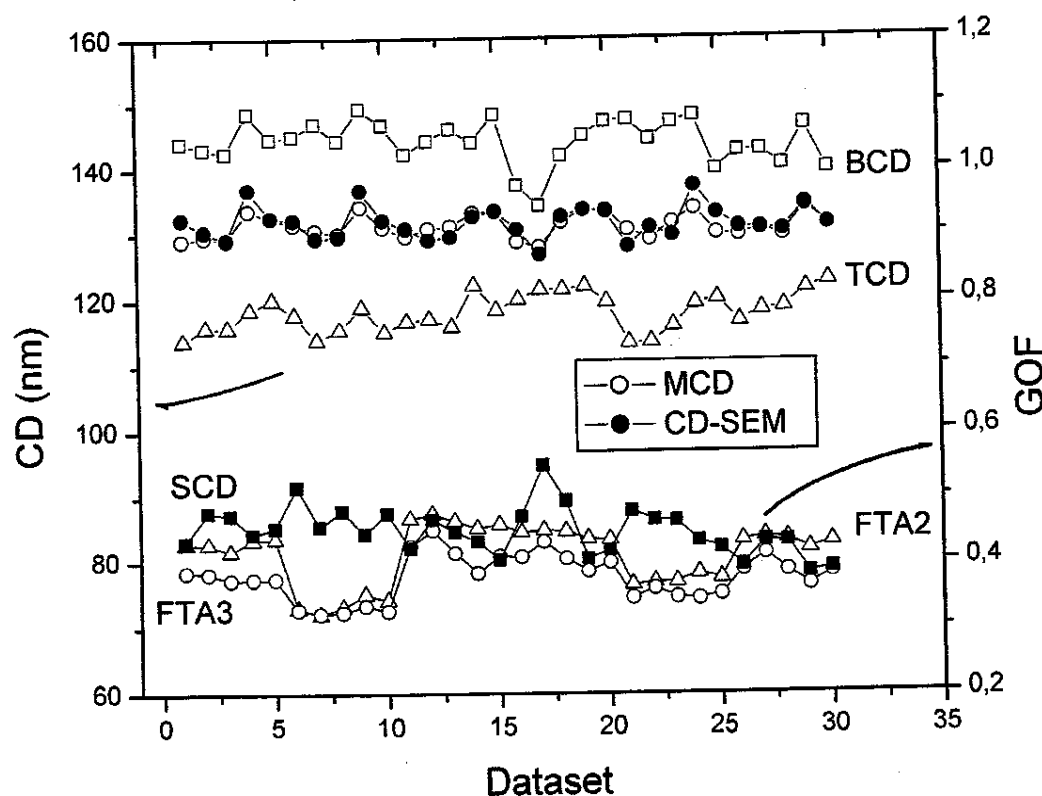


Figure 16: Examples for GOF variations (right Y-axis) for the two unpatterned FTA sites and the grating. The corresponding CD values (left Y-axis) for both SCD and CD-SEM (offset-corrected) are shown as well. Each data point represents the field center of a die. 3 lots are shown with 2 wafers per lot and 5 die per wafer.

## 4. CONCLUSION

We have shown that for the 110nm technology $WSi_x$ Gate process, a single trapezoid shape model can be used to characterize process variations arising under high volume production conditions or created in FEM applications. For focus/exposure conditions outside the process window more advanced shape models including top and bottom rounding effects are required for the accurate description of the line shapes.

From field mapping we see that SCD gives higher precision compared to CD-SEM. The origin of this we attribute to measurement area. SCD averages over a number of lines while the CD-SEM is sensitive to local line width variations. Therefore SCD has advantage for DRAM Gate process control compared to CD-SEM.

As scatterometry is a model based technique, sensitivity to n&k variations in the stack materials would be expected. For the GC Litho application we observe GOF variations in the filmstack model. However such variations have no significant influence of on the CD measurement.

## 5. REFERENCES

[1]     J. Sturtevant *et. al.*, *CD control challenges for sub 0.25 μm patterning*, SEMATECH DUV Lithography Workshop, Austin, TX, Oct. 16-18, 1996.

[2]     Xinhui Niu, *An Integrated System of Optical Metrology for Deep Submicron Lithography*, Ph.D. thesis, University of California, Berkeley, 1999.

[3]     Xinhui Niu, N. Jakatdar, B. Junwei, and C.J. Spanos , *Specular Spectroscopic Scatterometry*, IEEE Transactions on Semiconductor Manufacturing **14**(2), p.97-111, 2001.

[4]     A.C. Diebold, *Challenges Facing 3D Information Extraction by CD-SEM and Scatterometry*, Proceedings of the SPIE – Int. Soc. Opt. Eng. **4275**, Santa Clara, p.1-7, 2001.

[5]     G.G. Barna. *Sensor Integration into Plasma Etch Reactors of a Development Pilot Line*, Journal of Vacuum Science & Technology B (Microelectronics and Nanometer Structures) 12(4), p.2860-7, 1994.

[6]     C.C.Baum et al., *Scatterometry for Post-Etch Polysilicon Gate Metrology*, SPIE Microlithgraphy Conference 1999, Proc. SPIE 3677, p.148, 1999.

[7]     C.J. Raymond, M. Littau, R. Markle, M. Purdy, *Scatterometry for Shallow Trench Isolation (STI) Process Metrology*, Proceedings of the SPIE – Int. Soc. Opt. Eng. **4344**, p.716-25, 2001.

[8]     J. Allgair, P. Herrara, *Spectroscopic Optical Metrology for Process Characterization and Control*, Microlithography World **11**(1), p.12-16, 2002.

** TOTAL PAGE. 14 **

# Exhibit E

**KLA Tencor**
Accelerating Yield

| Products | Support | News | Events | Company | Investors | Careers | Contact | Keep Me Posted |

**PRODUCTS**

**Current Products**
- Semiconductor Products
  - By Solution
    - Defect Control Solutions
    - Metrology Solutions
      - CD Metrology
      - Substrate and Surface Metrology
      - Overlay
      - Films
    - Lithography
    - Transparent Films & Substrates
  - By Process
  - Back End
- Data Storage Products
  - Wafer Test
  - Head Test
  - Media Test

**K-T Certified (Used, Refurbished Products)**

Request Literature >     Contact M

**RELATED PRODUCTS**
- ASET-F5x
- ProDATA
- SpectraFx

# SpectraCD 200

### Inline Automated CD and Profile Metrology

- Improved precision and matching specifications exceed ITRS requirements
- High throughput and short move-acquire-measure (MAM) time allow for increased sampling plans, critical to 300mm wafer manufacturing
- Profile measurements are non-destructive, reducing or even eliminating costly wafer cross-sections
- Both thin-film and 3D profile data can easily be collected in the same wafer run through a seamless recipe setup approach
- Measurement feedback, including 2D/3D contact holes, improves process control for applications such as shallow trench isolation (STI)

The SpectraCD™ 200 is a non-destructive, inline optical CD metrology system with the precision, throughput and sensitivity to meet the requirements for the 90nm and 65nm nodes. The SpectraCD 200 system delivers high-throughput feature profile information and film-thickness data in a single tool, making it the industry's lowest cost-of-ownership (CoO), production-worthy CD metrology system. Combining accurate 3D modeling for yield-critical structures such as contact holes, with process enabling precision (to 0.5nm) and tool-to-tool

matching (to 1nm), SpectraCD 200 provides IC manufacturers with the critical information needed to accurately predict yield and transistor performance inline. This allows fabs to detect process-drift excursions early in the process flow and minimize the cost per good die.

**Complete CD Control Platform**
SpectraCD (inline spectroscopic CD metrology), ProDATA (lithography data analysis) and PROLITH (lithography simulation) provide a complete CD solution capable of improving pattern transfer quality, bin yield, and device performance.

**RELATED INFORMATION**

- **SpectraCD 200 Product Overview**
  (English, 153 KB)

- **Related Articles >**

Products | Support | News | Events | Company | Investors | Career
Home | Contact | Keep Me Posted | Ask KLA-Tencor

# Exhibit F

ELSEVIER

# Generalized spectroscopic ellipsometry and Mueller-matrix study of twisted nematic and super twisted nematic liquid crystals

J.N. Hilfiker[a,*], B. Johs[a], C.M. Herzinger[a], J.F. Elman[b], E. Montbach[b,c], D. Bryant[c], P.J. Bos[c]

[a]*J.A. Woollam Co., Inc., 645 M Street, Suite 102, Lincoln, NE 68508, USA*
[b]*Eastman Kodak Company, Kodak Research Labs, Imaging Materials Division, Rochester, NY 14650, USA*
[c]*Kent State University, Liquid Crystal Institute, Kent, OH 44242, USA*

## Abstract

Generalized spectroscopic ellipsometry (g-SE) and Mueller-matrix (MM) measurements are applied to twisted nematic (TN) and super twisted nematic (STN) displays. Transmitted measurements near normal incidence are used to extract twist, $\phi(d)$, and anisotropy for each display type. Angle-dependent measurements are used to determine tilt distribution, $\theta(d)$. Oblique angle measurements allow characterization of both ordinary and extraordinary indices. Finally, the liquid crystal layer thickness is accurately determined from coherent interference oscillations.
© 2004 Elsevier B.V. All rights reserved.

*Keywords:* Generalized spectroscopic ellipsometry; Mueller-matrix; Anisotropic materials; Liquid crystals

## 1. Introduction

TN and STN are the most common liquid crystal (LC) display types. Both rely on proper director orientation for the uniaxial LC molecules. The molecules twist through the film to orientations at top and bottom established by alignment layers. In addition, the LC director is tilted at each interface (pre-tilt) to avoid disclination. The overall LC director profile is important to final device performance.

Generalized spectroscopic ellipsometry (g-SE) has been applied to LC characterization. Measurements at normal incidence first studied twist and anisotropy ($\Delta n$) in cholesteric LCs [1]. Angle-dependent measurements have demonstrated sensitivity to tilt profiles in LC polymer films [2]. Researchers have also used 'renormalized' transmission ellipsometry to study TN display properties [3,4]. This measurement approach is similar to g-SE in that it includes the off-diagonal Jones matrix elements. In this work, we apply transmission g-SE and transmission MM measurements to TN and STN displays.

*Corresponding author. Tel.: 1-402-477-7501x127; fax: +1-402-477-8214.
*E-mail address:* jhilfiker@jawoollam.com (J.N. Hilfiker).

## 2. Experiment

Both a TN and STN liquid crystal display are characterized. Fig. 1 shows the display sample structure. Each display consists of an LC molecule sandwiched between glass substrates. The inner face of each glass substrate is coated first with indium tin oxide (ITO) conductive layer and then a polyimide alignment layer. The alignment layer was rubbed to induce anisotropy that orients the LC molecules. The LC will twist between substrates to match the direction of top and bottom alignment layers, $\phi_{top}$ and $\phi_{bottom}$, respectively. In this manner, different display types can be controlled. For TN displays, the total LC twist, $\phi_{top} - \phi_{bottom}$, is 90°. For STN displays, twist is between 180 and 225°. In addition to the LC twist, there is a pre-tilt ($\theta$) of the LC director from each substrate plane to avoid disclination. The tilt will vary with depth through the film. The cell gap for each display is controlled by Mylar spacers. The TN and STN films have nominal LC thickness of 4.8 and 3.6 $\mu$m, respectively. Different LC molecules are used for each display type as the amount of anisotropy must match the display design.

The LC molecules orient to form anisotropy. To fully describe an ellipsometry measurement transmitted through this type of material requires the off-diagonal Jones matrix elements [5]:
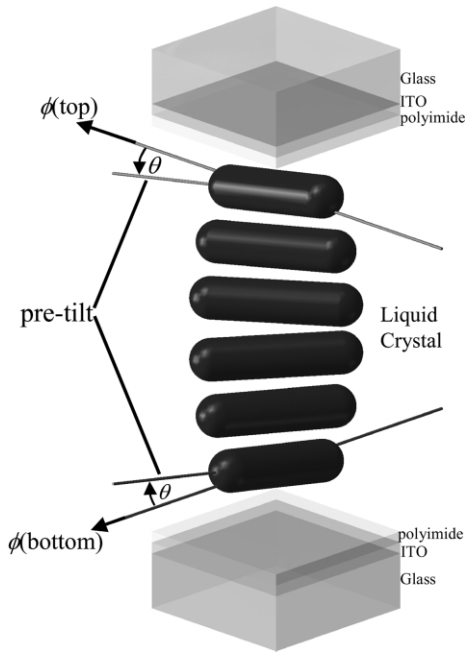
Fig. 1. Basic structure for both the TN and STN display. The LC layer is sandwiched between glass substrates that are coated with ITO and polyimide. The LC twists through the film between a bottom and top orientation, $\phi$. In addition, the LC molecules are tilted at each interface by an angle, $\theta$.

$$\begin{bmatrix} E_p \\ E_s \end{bmatrix}_{\text{OUT}} = \begin{bmatrix} t_{pp} & t_{sp} \\ t_{ps} & t_{ss} \end{bmatrix} \begin{bmatrix} E_p \\ E_s \end{bmatrix}_{\text{IN}} \tag{1}$$

Generalized ellipsometry measurements consist of three ellipsometry ratios:

$$\rho = \tan(\Psi) e^{i\Delta} = \frac{t_{pp}}{t_{ss}} \tag{2a}$$

$$\rho_{ps} = \tan(\Psi_{ps}) e^{i\Delta_{ps}} = \frac{t_{ps}}{t_{pp}} \tag{2b}$$

$$\rho_{sp} = \tan(\Psi_{sp}) e^{i\Delta_{sps}} = \frac{t_{sp}}{t_{ss}} \tag{2c}$$

If the sample or measurement is also depolarizing, then it may be necessary to use Mueller-matrix measurements, as the Jones matrix is not valid for partially polarized light. The Mueller-matrix maps the Stokes parameters for incoming to outgoing light using a $4\times4$ notation [5]:

$$\begin{bmatrix} S_0 \\ S_1 \\ S_2 \\ S_3 \end{bmatrix}_{\text{OUT}} = \begin{bmatrix} M_{11} & M_{12} & M_{13} & M_{14} \\ M_{21} & M_{22} & M_{23} & M_{24} \\ M_{31} & M_{32} & M_{33} & M_{34} \\ M_{41} & M_{42} & M_{43} & M_{44} \end{bmatrix} \begin{bmatrix} S_0 \\ S_1 \\ S_2 \\ S_3 \end{bmatrix}_{\text{IN}} \tag{3}$$

Measurements in this study were taken on a rotating analyzer ellipsometer that incorporates an adjustable compensator before the sample [6]. This provides access to eleven Mueller-matrix elements normalized to $M_{11}$. The fourth row is not accessible without a retarder after the sample. The sample is controlled to both positive and negative angles of incidence. The detector is situated on an independent rotational stage that can move to collect the transmitted, reflected, or scattered light beam.

## 3. Strategy

Both g-SE and MM measurements were acquired in transmission to characterize the TN and STN displays. Transmission-type measurements are preferred because there is a lower percentage of unwanted incoherent reflections collected from the glass substrates [7] and larger overall signal intensity is collected compared to reflection measurements. The higher signal intensity is due to the design of these display types to work with transmitted light—typically exhibiting more than 90% transmission and less than 10% reflection.

There are many unknown material properties for this type of complex sample. The large number of unknown
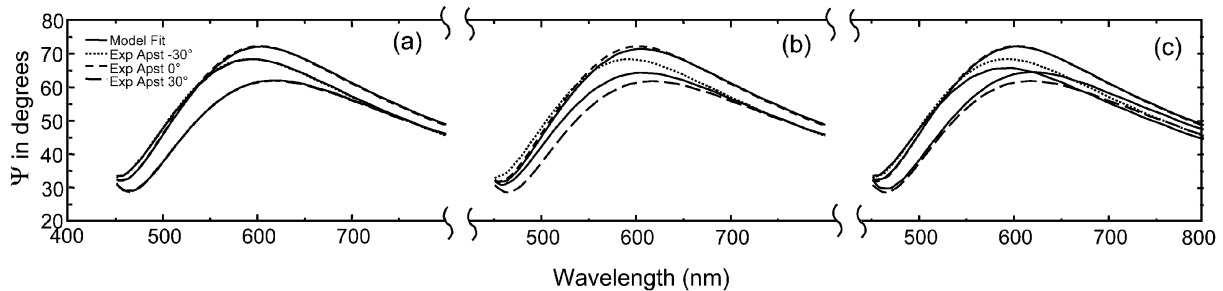


Fig. 2. The tilt distribution for STN display is determined from measurements near normal incidence. The final model (a) assumes a sinusoidal tilt distribution and is able to match data curves from both positive and negative angles of incidence. If no tilt is assumed (b), the model produces the same curve for positive and negative angles. If a constant tilt is fit (c) to the experimental curves, there is separation between positive and negative model curves, but not adequate to match the experiment.

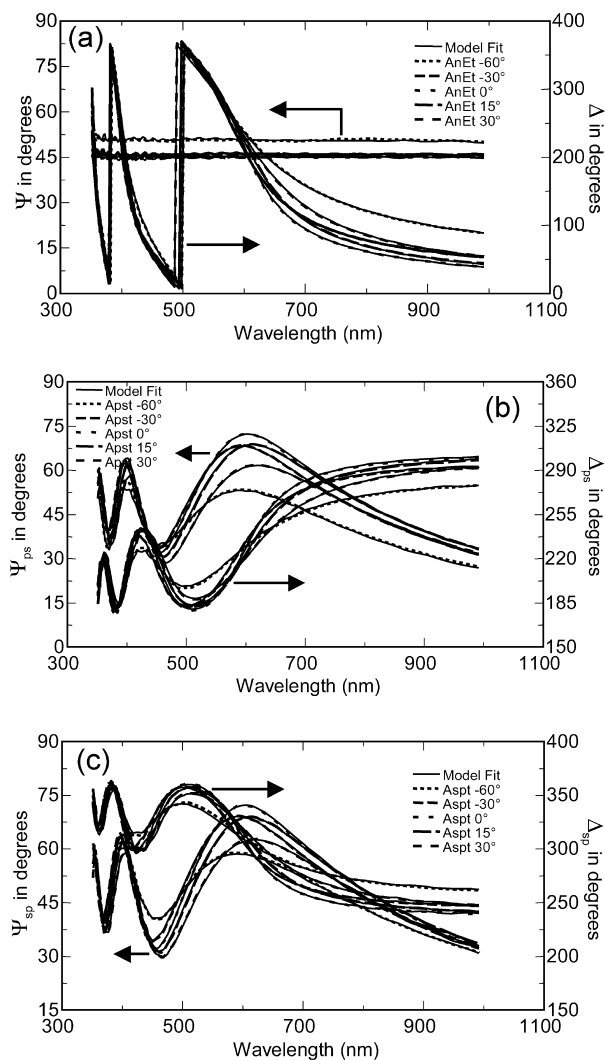*J.N. Hilfiker et al. / Thin Solid Films 455–456 (2004) 596–600*



Fig. 3. Generalized SE data measured from the STN display show excellent agreement to (a) diagonal Ψ and Δ and (b, c) all off-diagonal Ψ and Δ measurements.
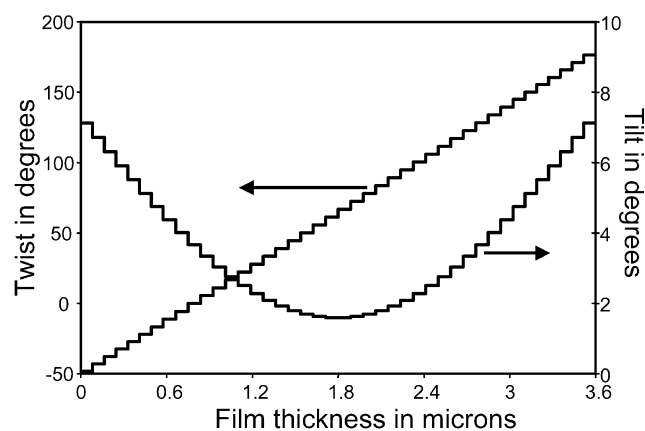


Fig. 4. Final twist and tilt distribution determined for the STN display. The model divides the LC layer into 42 slabs to allow the twist and tilt to vary through the film.

ordinary and extraordinary ray traveling through the LC layer help to determine the anisotropy ($\Delta n$) and in-plane orientation of the LC. For both TN and STN materials, the in-plane orientation twists as a function of film depth—thus we need to characterize $\phi(d)$. This was accomplished by dividing the LC layer into a large number of slabs with functional variation in the optical axis between slabs through the LC thickness. The number of slabs is chosen to approximate a smooth transition of each parameter through the film without encumbering the fit algorithm. Each display was split into 42 layers for this study. The overall twist profile was described with a linear relationship with the orientation at each polyimide alignment layer ($\phi_{\text{bottom}}$ and $\phi_{\text{top}}$) varied in the fit:

$$\phi(d) = \phi_{\text{bottom}} + (\phi_{\text{top}} - \phi_{\text{bottom}})d \qquad (4)$$

Third, the near-normal angles are included in the fit to determine the LC pre-tilt. The tilt is also a function of depth through the liquid crystal film. Measurements

parameters is uniquely determined by acquiring g-SE data over a wide range of incident angles in transmission through the display. Certain material properties are isolated at specific angles of incidence. For example, the anisotropy and twist distribution can be determined from normal incidence measurements, without sensitivity to the isotropic layers, LC pre-tilt or LC index. Data analysis progressed as follows.

First, the substrate and isotropic films are characterized from test samples to determine optical constants for soda lime glass, ITO and polyimide. The thickness and optical constants of ITO and polyimide are fixed in future measurements.

Second, measurements of the display at normal incidence are fit to isolate the anisotropic layer without being affected by the isotropic layers or the absolute index of any material. Strong interference between the
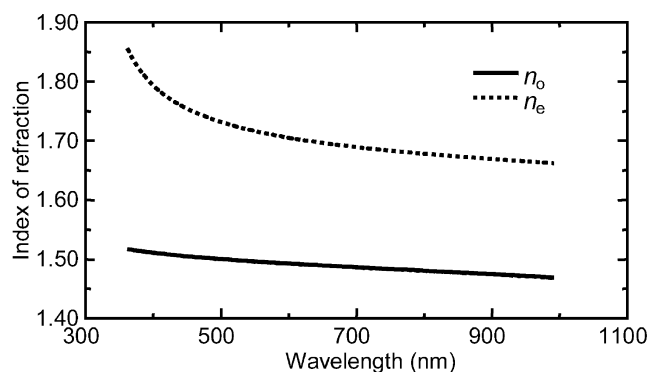


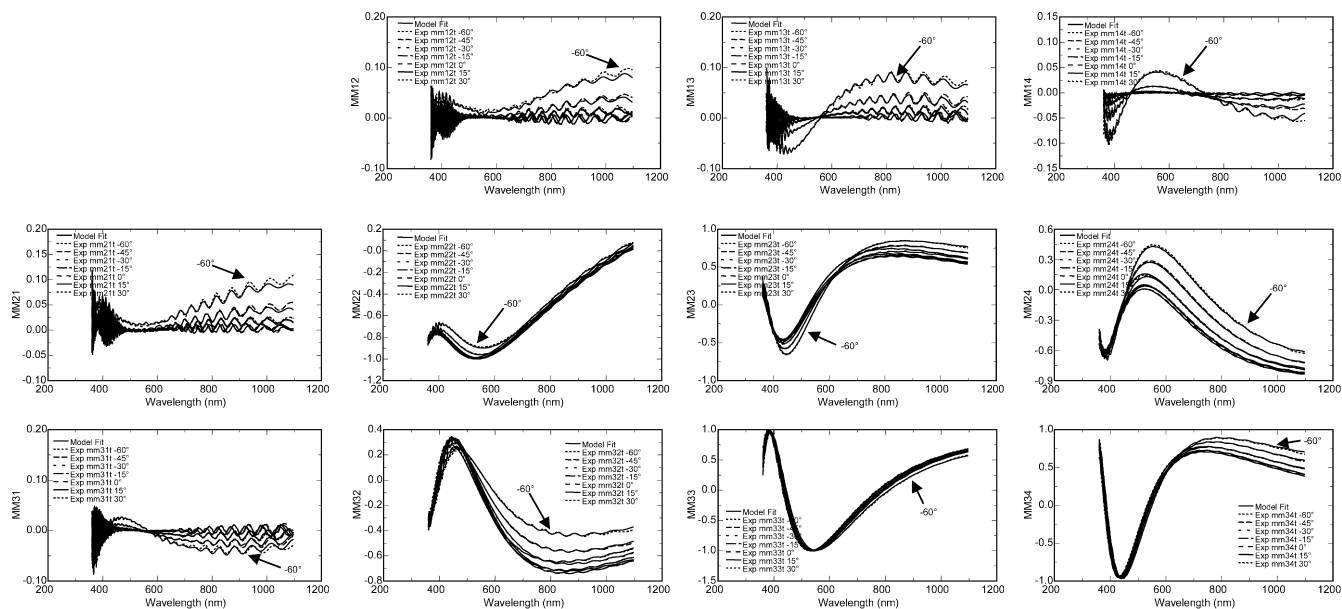Fig. 5. Final ordinary and extraordinary refractive index determined for the STN liquid crystal film.

Fig. 6. Mueller-matrix measurements over a range of angles (−60 to +30) and corresponding fit to describe a TN display. Because there is little tilt in this display, the equal negative and positive angles result in very similar data.

at both positive and negative angles of incidence determine the tilt distribution, $\theta(d)$. The functional variation of tilt profile depended on the display and is discussed later for both TN and STN results.

Fourth, oblique angles are included in the data analysis to help determine the LC index. These angles also help to fine-tune the isotropic layer thicknesses in the LC structure. However, correlation between parameters needs to be cautiously monitored – especially at more oblique angles that introduce stronger depolarizing effects from incoherent interference within the glass substrates.

Fifth and finally, all data were simultaneously included in a fit to allow all fit parameters to adjust to best match the entire data set.

## 4. STN results

Generalized SE measurements of the STN display provide the anisotropy, ordinary and extraordinary refractive index, LC twist and tilt distributions. Measurements involved g-SE in transmission from 360 to 1000 nm at six angles of incidence: −60, −30, −15, 0, +15 and +30°.

Both positive and negative angles near normal incidence are measured to determine the tilt distribution through the LC film. Because the experimental data are not symmetric about normal incidence, the LC molecule must be tilted from the substrate plane. Fig. 2 demonstrates sensitivity to tilt distribution for the STN display. The final fit shown in Fig. 2a matches experimental off-diagonal g-SE data at −30, 0 and 30° angles of



Fig. 7. The high frequency oscillations easily distinguished in three Mueller-matrix elements measured at 60° incident angles are fit to determine the TN film thickness.
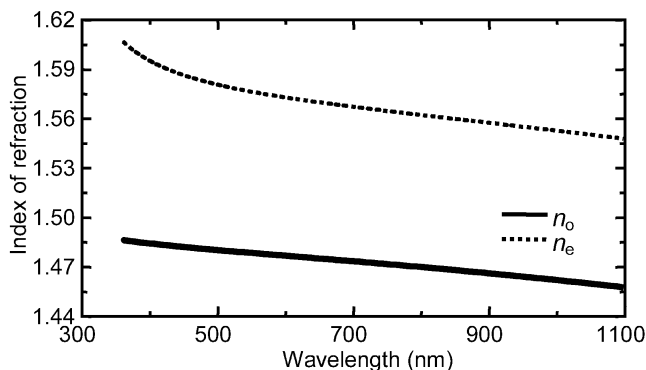


Fig. 8. Final ordinary and extraordinary refractive index determined for the TN liquid crystal film.

incidence. Final model assumes a sinusoidal tilt distribution with the same tilt at each substrate interface and less tilt at the film center. The distribution was described as:

$$\theta(d) = \theta_{edge} - \theta_{diff} \cdot \sin(\pi d), \tag{5}$$

with final fit values for the STN display of: $\theta_{edge} = 7.55°$ and $\theta_{diff} = 5.8°$.

If no tilt is assumed for this material, the positive and negative angles should be equivalent, as shown in the model of Fig. 2b. If a constant tilt is assumed through the film, the model for positive and negative angles separate, but are not in adequate agreement to experimental curves (Fig. 2c).

The final model is in good agreement with all g-SE measurements over a wide range of incident angles. Fig. 3 shows g-SE measurements from all angles ($-60$, $-30$, $-15$, $0$, $+15$, and $+30°$) along with the corresponding model fit. The model successfully determines the LC tilt and twist distribution shown in Fig. 4. Finally, the resulting ordinary and extraordinary LC refractive indices are shown in Fig. 5. Both ordinary and extraordinary indices are modeled using a sum of zero-broadened oscillator terms for ultraviolet (UV) and infrared (IR) contributions, as:

$$\varepsilon(E) = \varepsilon_{offset} + \left( \frac{A_{UV}}{E_{UV}^2 - E^2} \right) + \left( \frac{A_{IR}}{E_{IR}^2 - E^2} \right) \tag{6}$$

The infrared oscillator was fixed at $E_{IR} = 0.001$ eV, while $E_{UV}$, $A_{UV}$, $A_{IR}$ and $\varepsilon_{offset}$ were allowed to fit. The LC thickness is not determined because the coherent interference within the LC layer is not noticeable. This is likely due to smearing of the oscillations from a non-uniform film thickness and index matching between layers.

## 5. TN results

A similar characterization approach was used for the TN display. However, depolarization in this display required Mueller-matrix measurements, as discussed in more detail in a companion paper [8]. Data were measured from 350 to 1100 nm at seven angles of incidence ($-60$, $-45$, $-30$, $-15$, $0$, $+15$ and $+30°$). The final model uses a sum of zero-broadened oscillators for ordinary and extraordinary LC indices, as previously described in Eq. (6). In this display, the pre-tilt is small (approx. 1.5°) with no discernible variation through the film. The twist is again modeled with a linear distribu-

tion where top and bottom orientations are fit. Fig. 6 shows the MM curves as function of wavelength and angle of incidence. The corresponding model fit is in excellent agreement with all curves. For this sample, the LC thickness is determined via match to the coherent interference oscillations. The final fit thickness is 4.752 μm, which is in agreement to the nominal Mylar spacer thickness of 4.8 μm. Fig. 7 shows three measured MM curves for the 60° incident angle, which demonstrate the match to coherent interference oscillations. In this figure, the low frequency oscillations are due to anisotropy, while the higher frequency oscillations are due to the layer thickness. These oscillations are not very pronounced because of index matching between the LC and surrounding materials. The final LC optical constants are presented in Fig. 8.

## 6. Conclusion

Complete characterization of TN and STN displays is demonstrated by transmission measurements of g-SE and MM data. Measurements over a wide range of angles are acquired to insure correct modeling of the many liquid crystal properties; including ordinary and extraordinary refractive index, twist distribution and tilt distribution of the liquid crystal director. In addition, the presence of coherent oscillations in the TN display allowed characterization of the liquid crystal film thickness. Measurement angles are very important, as certain material properties can be isolated or enhanced at specific angles of incidence. The Mueller-matrix measurements were only required for the TN display, which also exhibited significant depolarization. Otherwise, generalized SE is completely adequate for full characterization.

## References

[1] M. Schubert, B. Rheinlander, C. Cramer, H. Schmiedel, J.A. Woollam, C.M. Herzinger, B. Johs, J. Opt. Soc. Am. A 13 (9) (1996) 1930–1940.
[2] C. Benecke, H. Seiberle, M. Schadt, Jpn. J. Appl. Phys. 39 (2000) 525–531.
[3] N. Tanaka, M. Kimura, T. Akahane, Jpn. J. Appl. Phys. 41 (2002) L1502–L1504.
[4] N. Tanaka, M. Kimura, T. Akahane, Jpn. J. Appl. Phys. 42 (2003) 486–491.
[5] B. Johs, J.A. Woollam, C.M. Herzinger, J. Hilfiker, R. Synowicki, C.L. Bungay, SPIE Proc. CR72 (1999) 29–58.
[6] VASE with AutoRetarder from J.A. Woollam Co., Inc.
[7] J.F. Elman, J. Greener, C.M. Herzinger, B. Johs, Thin Solid Films 313/314 (1998) 814–818.
[8] J.N. Hilfiker, C.M. Herzinger, T. Wagner, A. Marino, G. Delgais, G. Abbate, Thin Solid Films, submitted.

# Exhibit G

ELSEVIER

# VUV and IR spectroellipsometric studies of polymer surfaces

John A. Woollam [a,b,*], Corey Bungay [b], James Hilfiker [b], Tom Tiwald [b]

[a] *Department of Electrical Engineering, Center for Microelectronic and Optical Materials Research, University of Nebraska, Lincoln, NE 68588-0511, USA*
[b] *J.A. Woollam Co., Inc., 645 M Street, Lincoln, NE 68588-0511, USA*

**Abstract**

This article reviews applications of spectroscopic ellipsometry (SE) in polymers and irradiated polymers. SE has long been used to determine optical constants, layer thicknesses in multi-layer stacks and microstructure (voids, alloy fraction, or mixed phase composition). Modern spectroscopic ellipsometers now cover a range from 140 nm ($\approx$9 eV) in the vacuum ultraviolet to 100 $\mu$m (100 cm$^{-1}$) in the far infrared. Examples of ellipsometric measurements for irradiated and un-irradiated thin film and bulk polymers, and biological materials are presented. Analysis yields index of refraction and dispersion, optical absorption and optical anisotropy as studied by "generalized ellipsometry". Both ex situ and in situ ellipsometry are discussed, as are future trends and opportunities.
© 2003 Elsevier B.V. All rights reserved.

*Keywords:* Polymers; Vacuum ultraviolet; Visible; Infrared spectroscopic ellipsometry; Optical anisotropy; Depth profiles

## 1. Introduction

Ellipsometry uses light of known polarization incident on a surface under study and detects the polarization state of the reflected (or transmitted) light [1–4]. Incident light is usually linearly polarized and reflected light has elliptical polarization, as illustrated in Fig. 1, where coordinates of incoming field vector $E$ are the p- and s-polarizations. The plane of incidence is defined by the incident and reflected beams and sample normal. Spectroscopic ellipsometry (SE) data can be acquired from vacuum ultraviolet to far infrared. SE measures ratios of intensities as polarization is modulated, often by rotating a polarizer, analyzer, or achromatic retarder [5,6]. Data are expressed as functions of a complex variable, where $\Psi$ and $\Delta$ contain the amplitude and phase information, respectively.

The ellipsometric data $\Psi$ and $\Delta$ are acquired over a broad spectral range, often at several angles of incidence. In each spectral range different properties of materials are learned. However, the data must be analyzed to obtain useful information. An optical model representing the assumed physical geometry and microstructure is developed, and Fresnel reflection coefficients calculated, allowing predictions of $\Psi$ and $\Delta$ to compare with measured values. Model parameters, such as $n$, $k$ and thickness, vary in regression until the comparator function, such as mean square error, is minimized. The resulting parameters are the "best

---

* Corresponding author. Present address: J.A. Woollam Co., Inc., 645 M Street, Lincoln, NE 68588-0511, USA. Tel.: +1-402-477-7501x227; fax: +1-402-477-8214.
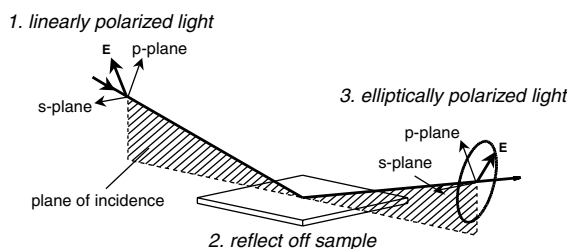*E-mail address:* jwoollam@jawoollam.com (J.A. Woollam).

Fig. 1. Geometry for spectroscopic ellipsometry measurements. Light of known polarization state is incident at selected accurately known angles of incidence to the sample normal, and the polarization state of the reflected light is determined (sometimes transmitted polarized light). Data are taken over a wide spectral range.

fit'' values of $n$ and $k$, surface roughness, layer thickness, alloy fractions, etc. SE is also sensitive to index grading from the surface into a material, laterally inhomogeneous properties, multi-constituent materials mixed on an atomic scale, as well as optical anisotropy [2,3,7]. This paper illustrates a few recent examples of polymer SE studies.

For years ellipsometry used monochromatic laser sources. However, by mid-1980s commercial ellipsometers were available for visible, near-ultraviolet and near-infrared wavelengths. Recently commercial SE has been extended to mid-infrared (33 μm) and vacuum ultraviolet spectral ranges. SE is used in fundamental scientific studies of materials, as well as process control and metrology in production. It is used either ex situ, where the material under study is brought to the instrument, or in situ, where the instrument monitors and/or controls a process [8].

Often optical constants $n$ and $k$ are unknown parameters at hundreds of wavelengths, resulting in large numbers of fit parameters in regression. More convenient are dispersion relations, greatly reducing unknowns. The Cauchy relation is often applied to polymers in regions of total transparency ($k = 0$), where the index dispersion is represented by a simple empirical equation, with only three parameters. Fits between experimental and calculated $\Psi$ and $\Delta$ must be close, otherwise the model does not properly represent the physics. For many dielectrics the Cauchy model often works well in the visible. In the ultraviolet, $k$ is not zero and its mathematical shape must be represented by

another model. Likewise, oscillator models work well to represent infrared absorptions due to vibrational state coupling [9]. An advantage of oscillators in the infrared is ability to do line-shape analysis to provide chemical bond information. Other dispersion relations are discussed elsewhere [9–11].

There has been considerable work on spectro-ellipsometric studies of modified polymers, not related to examples discussed below, and a selected few are referenced [12–15]. With this introduction, example SE results on polymers are presented.

## 2. Polymer degradation in the space environment

Spacecraft in low earth orbit are exposed to atomic oxygen, ultraviolet radiation, contamination from out-gassing spacecraft materials and various size particles impacting with a range of energies [16,17]. Thus studies of degradation mechanisms for candidate space materials are on-going. Figs. 2 and 3 show SE results from Kapton polyimide exposed to ultraviolet [18]. The UV source was a xenon arc lamp. Because air absorbs light with wavelengths shorter than 190 nm, and calibrated intensity from the lamp showed linear increase from zero at 190 nm to 80 W/cm$^2$ nm at 450 nm. Kapton is transparent at wavelengths longer than 450 nm, thus damaging radiation in our case is due to light from 190 to 450 nm.
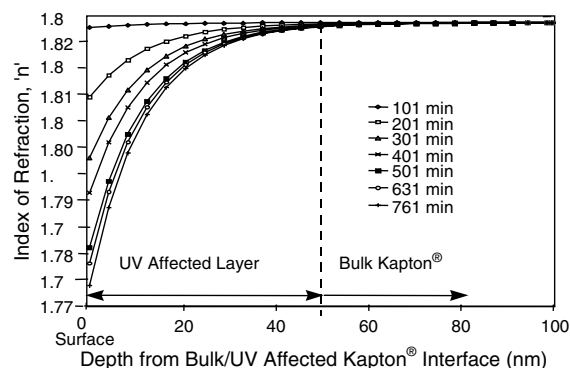


Fig. 2. Index of refraction versus depth into Kapton after a series of exposures times to radiation with strong ultraviolet component (UV source described in text).
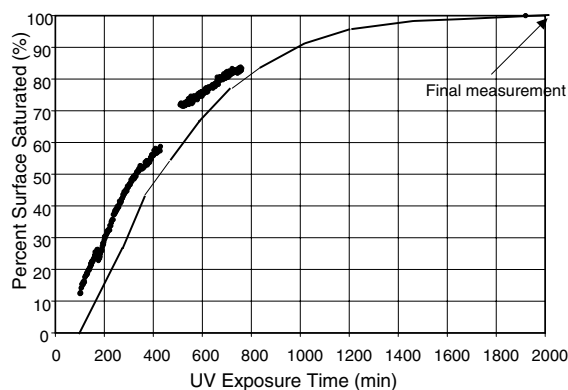
37



Fig. 3. Percent surface conversion of Kapton towards final saturated value, as a function of exposure time to UV radiation.

In situ SE data were taken continuously during exposure. Several mathematical models representing the index of refraction depth profile were tried. Best fits were found using a simple exponential variation. The depth profile of UV irradiated Kapton for a series of exposure times is given in Fig. 2. Notice that damage in Kapton extends to about 50 nm depth for all exposure times. This depth depends on optical properties of the particular polymer. As exposure time increases the surface is further damaged until saturating to a final value. In Fig. 3 this is after 1900 min exposure. This is explained by Fig. 4, where $n$ and $k$ are plotted for exposed and unexposed Kapton. Note that the absorption coefficient (defined by Beers law) equals $4\pi k$ divided by wavelength, and that the reciprocal of the absorption coefficient is ap-
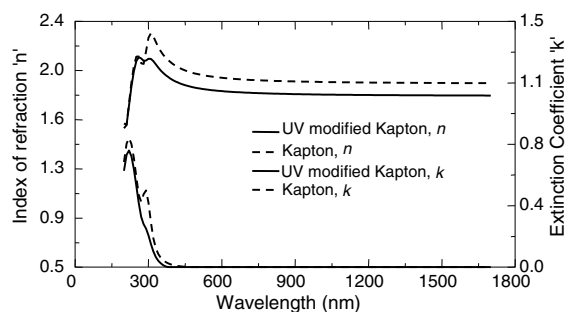
proximately the depth of penetration of light (the distance at which intensity drops to $1/e$ from its value at the surface). Damage is maximum between 200 and 300 nm wavelengths where absorption, and therefore damage, are maximum. Based on $k$ from 0.4 at 250 nm to 0.8 at 200 nm (Fig. 4), the penetration depth is between 20 and 50 nm. Fig. 2 shows the index profile is $1/e$ towards saturation in the 20–30 nm region. Thus SE derived optical constants of irradiated polymers reveal the mathematical profile of damage depth. Other examples of SE depth profiling can be found in literature [19].

## 3. Optical anisotropy and infrared examples in polymers

Generalized ellipsometry (GE) was discussed in the 1970s, but became practical only after recent theory and software advances. GE allows analysis of materials where $n$ and $k$ depend on direction of light propagation, generally not the same as sample geometry [1,20]. It assumes non-zero off-diagonal components for the Jones matrix, and uses the following relationship:

$$\begin{bmatrix} p_{out} \\ s_{out} \end{bmatrix} = \begin{bmatrix} r_{pp} & r_{sp} \\ r_{ps} & r_{ss} \end{bmatrix} \cdot \begin{bmatrix} p_{in} \\ s_{in} \end{bmatrix},$$

where $r_{pp}$ and $r_{ss}$ are the Fresnel reflection coefficients for p- and s-polarized components of polarization. $p_{in}, s_{in}, p_{out}$ and $s_{out}$ are input and output in Jones vector analysis. For optically anisotropic materials $r_{ps}$ and $r_{sp}$ Fresnel coefficients are non-zero. For isotropic materials, pure p- or pure s-polarization continue as pure p- or s-. In anisotropic materials there is conversion between p- and s-polarizations. Ellipsometric data over a wide spectral range, at several incidence angles, and with the sample rotated to several in-plane angles are typically required [21].

Fig. 5 shows GE analysis results to obtain the infrared extinction coefficient for polystyrene. Note significant energy shift of absorption bands between in-plane and out-of-plane. The 2920 cm$^{-1}$ band is due to C–H stretch, with higher energies for out-of-plane. Likewise, Fig. 6 shows results of GE analysis for poly(ethylene terephthalate)



Fig. 4. Spectral dependence of Kapton optical constants before and after UV exposure.

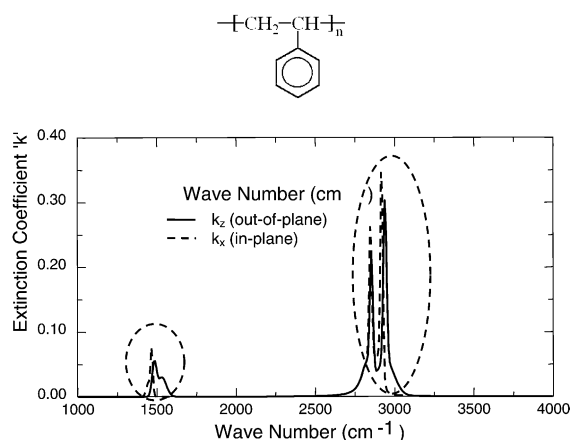*J.A. Woollam et al. / Nucl. Instr. and Meth. in Phys. Res. B 208 (2003) 35–39*



Fig. 5. Polystyrene infrared extinction coefficient. Circled regions show in-plane and out-of-plane optical constants shifted due to optical anisotropy.
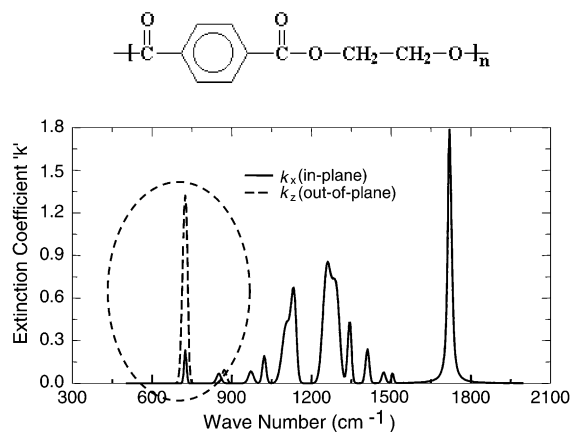


Fig. 6. Extinction coefficient for poly(ethylene terephthalate) (PET) obtained from infrared ellipsometry data, showing presence of optical anisotropy.

(PET). Note large differences at about 720 cm$^{-1}$. This peak is due to the $CH_2$ rocking mode which is more strongly excited for motion out of the sample plane. Kramers–Kronig consistency requires $n$ and $k$ both to be affected by chemical bonding anisotropy in the resonant response spectral region. Thus, infrared SE yields considerable directionally dependent bonding chemistry information. Infrared SE can be obtained on single molecular layers, e.g. proteins, due to high thin film sensitivity.

## 4. Future directions for spectroscopic ellipsometry in polymers

This short review introduced several SE applications, including UV irradiated polymers. Kapton was chosen as an example of research on materials in the space environment. New infrared optically anisotropic polymer results were presented.

Space limitations did not permit vacuum ultraviolet result discussion. Commercial vacuum UV ellipsometers recently became available and are used extensively for 157 nm lithography development, including polymer photoresists and antireflective coatings [22–24]. Vacuum UV SE is "wide open" for scientific studies, as all polymers exhibit multiple resonant-type absorptions in the UV, most of which have been little studied, and physics and chemistry largely unexplained.

Anisotropy and quantitative $n$ and $k$ optical constant lineshape analysis can now be done in the infrared, a largely unexplored area. Line shape analysis can potentially determine molecular concentrations and chemical environment in ultrathin polymers, including bio-molecules. Applications of such capability should be extensive.

Another largely unexplored area is using rotating compensator SE to measure Mueller matrix elements including depolarization, to study surface roughness, patterning and coherence. This capability is now available from vacuum UV to mid-IR.

Fast in situ SE provides opportunities for in situ studies of rapid polymer changes during processing. The example presented here was a simple experiment in atmosphere, but in situ SE has been done in vacuum chambers with variable temperature sample mounts and in liquid process chambers. Polymers can be studied during chemical or physical changes, such as cross-linking, curing, bleaching and many other examples.

## Acknowledgements

## References

[1] R.M.A. Azzam, N.M. Bashara, Ellipsometry and Polarized Light, North Holland Press, Amsterdam, 1977.

[2] J.A. Woollam, B. Johs, C.M. Herzinger, J. Hilfiker, R. Synowicki, C. Bungay, in: Critical Reviews of Optical Science and Technology, Optical Metrology, CR72, SPIE Publishing, Bellingham, WA, 1999, p. 3.

[3] B. Johs, J.A. Woollam, C.M. Herzinger, J. Hilfiker, R. Synowicki, C. Bungay, in: Critical Reviews of Optical Science and Technology, Optical Metrology CR72, SPIE Publishing, Bellingham, WA, 1999, p. 29.

[4] H.G. Tompkins, W.A. McGahan, Spectroscopic Ellipsometry and Reflectivity, "A User's Guide", John Wiley and Sons, New York, 1999.

[5] R.W. Collins, Rev. Sci. Instr. 61 (1990) 2029.

[6] B.D. Johs, U.S. Patent # 5,872,630 A2, 1999.

[7] J.F. Elman, J. Greener, C.M. Herzinger, B. Johs, Thin Solid Films 313 (1998) 816.

[8] B. Johs, J. Hale, N.J. Ianno, C.M. Herzinger, T. Tiwald, J.A. Woollam, Proc. SPIE 4449 (2001) 41.

[9] F. Wooten, Optical Properties of Solids, Academic Press, NY, 1972, p. 52.

[10] G.E. Jellison Jr., F.A. Modine, Appl. Phys. Lett. 69 (1996) 371.

[11] B.D. Johs, C.M. Herzinger, U.S. Patent # 5,796,983, 1995.

[12] S. Vallon, B. Drevillon, J.C. Rostaing, Thin Solid Films 233 (1993) 256.

[13] S. Vallon, A. Hofrichter, B. Drevillon, J.E. Klembert-Sapieha, L. Martinu, F. Poncin-Epaillard, Thin Solid Films 290 (1996) 68.

[14] S. Vallon, B. Drevillon, F. Poncin-Epaillard, J.E. Kemberg-Sapieha, L. Martinu, J. Vac. Sci. Technol. A 14 (1996) 3194.

[15] S. Vallon, B. Drevillon, F. Poncin-Epaillard, Appl. Surf. Sci. 108 (1997) 177.

[16] J.I. Kleiman, R.C. Tennyson (Eds.), Protection of Materials and Structures from the Low Earth Orbit Space Environment, Kluwer Academic Publishers, Dordrecht, The Netherlands, 1999.

[17] Proceedings of the 8th International Symposium on Materials in a Space Environment, 5th International Conference on Protection of Materials and Structures from the LEO Space Environment (Centre National D'tetudes Spatiales, Toulouse, France, 2000), European Space Agency Publications Division, Noordwijk, The Netherlands, 2000.

[18] C. Bungay, T.E. Tiwald, M.J. Devries, B.J. Dworak, J.A. Woollam, Polym. Eng. Sci. 40 (2000) 300.

[19] T.E. Tiwald, D.W. Thompson, J.A. Woollam, J. Vac. Sci. Technol. B 16 (1998) 312.

[20] M. Schubert, B. Rheinlander, J.A. Woollam, B. Johs, C.M. Herzinger, J. Opt. Soc. Am. A (1996) 875.

[21] J. Hilfiker, C. Bungay, C.M. Herzinger, U.S. Patent 6,441,902 B1, 2002.

[22] Proceedings of the Conference on Optical Microlithography XV, SPIE 4691, Society for Photo-optical and Instrumentation Engineers, Bellingham, WA, 2002.

[23] R.H. French, J. Feldman, F.C. Zumsteg, M.K. Crawford, A.E. Feiring, J. Gordon, V.A. Petrov, F.L. Schadt III, R.C. Wheland, E. Zhang, Progress in Materials Development for 157 nm Photolithography: Photoresists and Pellicles, 14th ed., Semiconductor Fabtech, ICG Publishing, London, 2001.

[24] T. Wagner, J.N. Hilfiker, T.E. Tiwald, C.L. Bungay, S. Zollner, Phys. Stat. Sol. 188 (2001) 1553.

# Exhibit H

# Emerging applications of Spectroscopic Ellipsometry

Spectroscopic Ellipsometry (SE) is routinely used to measure optical coatings. Improvements in accuracy, speed, and spectral coverage have increased its utility. Emerging areas utilize the versatility and functionality of SE for single- and multi-layer stacks.

Spectroscopic Ellipsometry (*SE*) is a non-destructive technique routinely used to measure refractive index and film thickness for optical coatings. It is similar to spectrophotometric (*R/T*) measurements in that both measure the properties of light upon reflection or transmission from a coating or stack. Whereas *R/T* measurements collect the light *intensity*, ellipsometry measures the *polarization* change. While less intuitive than intensity, the change in polarization measured by ellipsometry has a few distinct advantages:

- polarization contains more information than intensity – both amplitude and phase;
- ellipsometry is more sensitive to material details such as index gradients, surface and interfacial regions;
- phase provides enhanced sensitivity to ultra-thin layers less than 10nm thick; and

- polarization is easier to measure with accuracy and precision.

## REFRACTIVE INDEX AND COATING THICKNESS

The most common SE application is the accurate measurement of thin films to determine thickness and refractive index. The measurement will collect reflections from the coating *surface* along with light that has travelled through the film and reflects from the coating-substrate *interface*.

The two light beams recombine to produce a change in total polarization. Film thickness and refractive index can be determined from this change. In Spectroscopic Ellipsometry the polarization change is measured at many wavelengths, providing a "spectrum" of data. As the wavelength varies, so does the interaction between surface and interface light beams, causing periodic "interference" oscillations in the ellipsometric (polarization) spectrum. The shape and frequency of the interference pattern contains information about refractive index, film thickness and additional details of the film microstructure. Additional information can be gathered by varying the angle of incidence, since this changes the path length of the light travelling through the various films. *SE* is commonly used to measure a wide variety of optical coatings; including fluorides, oxides, nitrides, carbides, and more.

A common example using SE is for the accurate measurement of Indium Tin Oxide (ITO) on glass. Figure 1 shows a data spectrum collected with an SE system from the ultraviolet (UV) to the near infrared (NIR). ITO coatings are interesting over this range, as they change from dielectric-behaviour to metallic-behaviour. In the visible, the ITO film is transparent and the data spectrum is dominated by interference oscillations. However, these oscillations stop at longer NIR wavelengths when the ITO coating becomes absorbing. In this region, the light is absorbed by free-carriers. The free-carrier absorption in NIR region can be used to optically measure the ITO resistivity. Another interesting feature of ITO films is that due to processing, it is rare for the free-carrier absorption to be constant through the film. Thus, to properly describe the shape of the data spectrum requires a resistivity gradient. Figure 1 also shows the measured optical constants for the ITO layer at top and bottom of the film, showing the large variation in NIR absorption, which also couples into the index shape.

## EMERGING AREA

### *Combined measurements*

Although *SE* and *R/T* measurements contain similar information, they can be complementary. The combination of *SE* and Transmission Intensity (*%T*) has been used with semi-absorbing coatings. The *SE* measurement provides sensitivity to thickness and index, while benefiting from the sensitivity of *%T* to low amounts of absorption. Recently, variable angle *SE* measurements have been complemented by variable angle *%T* to measure anisotropic colour filter layers. More advanced data combinations involve *SE* measurements taken in reflection from front and back surfaces along with *SE* and *%T* transmitted through the sample. This wealth of information is necessary to characterize complex layers, such as

phase-shifting photomasks – where the coating is both absorbing and intentionally graded to provide the optimum performance. Due to the similarities between *SE* and *R/T* measurements, they can often be measured with the same instrument. Figure 2 shows a Variable Angle Spectroscopic Ellipsometer configured for both reflected and transmitted measurements over a wide range of wavelengths and angles.

### *Anisotropic materials*

Plastic substrates, such as PET and PEN are becoming increasingly popular. Optical characterization of these materials is complicated by the substrate anisotropy ($nx \neq ny \neq nz$). The direction-dependent optical properties can introduce data oscillations from interference between the ordinary and extraordinary light rays that travel different paths through the substrate. Unfortunately, these oscillations may hide the optical coating information. The easy solution is to eliminate the substrate anisotropy interference by collecting only the light reflecting from the coated surface. This can be accomplished by: 1) spatially separating the front and backside beams, which would require a very small spot given the typical plastic substrate thickness, or 2) suppressing the back-
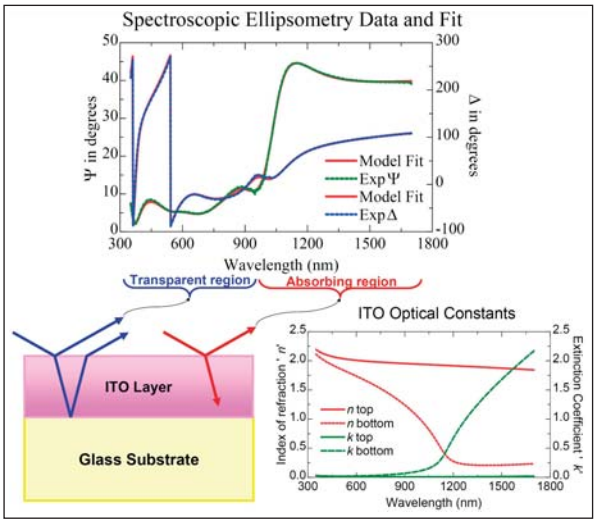


**Fig. 1 -**
**SE Measurement of ITO coating on glass provides thickness information from the transparent region and resistivity information from the absorbing region. The resistivity of the ITO layer was also found to vary through the film depth as shown by the optical constants at surface (top) compared to substrate interface (bottom)**
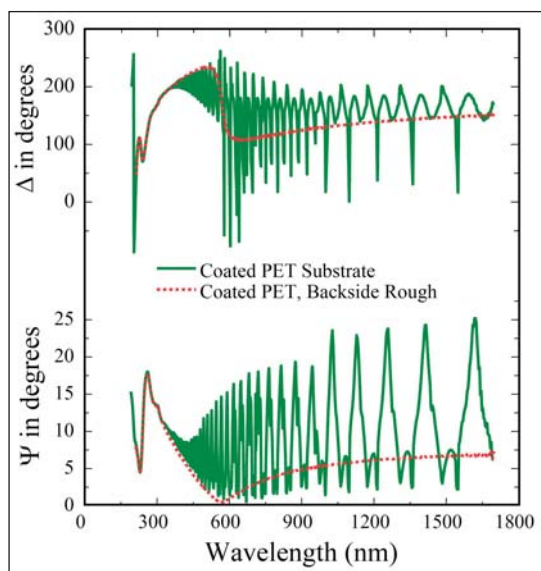
# J. A. WOOLLAM



**Fig. 3 - Comparison of two ellipsometry measurements of coated PET substrate. When the backside of PET substrate is smooth, the data are dominated by high-frequency oscillations from the substrate anisotropy. When backside is rough, these high-frequency oscillations are eliminated to leave only the data features pertaining to the surface coating**

side reflection. Two techniques are common for suppressing backside reflections – the use of index matching materials to minimize this reflection, and roughening the backsurface to scatter the backside reflection. Figure 3 shows data collected from a coated PET substrate with and without backside reflections. Because of the "anisotropy" effects in the substrate of the data set with backside smooth (green curves), it is difficult to recognize the coating oscillation. With the backside rough (red curves), the high frequency oscillation is eliminated, allowing easy and accurate identification of the coating properties.

In a research lab, it may be acceptable to roughen the backside of anisotropic substrates. However, it is impractical to avoid collection of the backside reflections in many industrial environments. Thus, substrate anisotropy becomes part of the experiment. New *SE* measurement technologies have been developed to aid the measurement of anisotropic substrates. Generalized Spectroscopic

Ellipsometry (*g-SE*) provides six measured values compared to the two terms of standard ellipsometry. The additional four values are related to cross-polarization that only occurs for anisotropic materials. The *g-SE* method has been used to analyze a wide variety of anisotropic materials, including bulk crystals and plastic substrates.

Mueller-Matrix Spectroscopic Ellipsometry (*MM-SE*) is an even more general measurement method that describes the reflection or transmission with up to 16 measured values. For most samples, there is significant redundancy in the Mueller-matrix. For highly complex samples which are both Anisotropic and Depolarizing, there are 7 distinct values. *MM-SE* has been applied to liquid crystal characterization to successfully measure the anisotropic optical properties and "twisting" behaviour of the LC layer.

### Infrared spectroscopic ellipsometry

Historically, it has been difficult to accurately measure optical coatings in the infrared, which means that coating designs have relied on incomplete or inaccurate index and extinction coefficients found in the open literature. The open literature values are particularly questionable for thin films since the processing conditions can strongly affect optical properties. The optical components of an IR spectroscopic ellipsometer (*IR-SE*) – polarizers, retarders, light sources, detectors, etc. – are far from ideal. Innovative construction and calibration methods have allowed *IR-SE* to achieve the high accuracy required for successful thin film measurements.

In the last decade, IR-SE has been used to measure thickness and the mid- and far-IR optical properties ($2 < \lambda < 33\mu m$) of a number of single and multi-layer films stacks. This has

allowed better prediction and control of the mid-infrared Reflectance, Transmittance and Emissivity of film-substrate structures. *IR-SE* has been used to study both passive and active thermal control; for example, silver, tin oxides, electrochromic coatings, have all been measured. Figure 4 shows an IR-SE measurement of $TiO_2$ coating on float glass, along with the determined IR optical properties. $TiO_2$ has photocatalytic properties that are useful for self-cleaning windows. IR-SE can also be sensitive to water and other contaminants which may be incorporated in films or present on the film surface.

### Large area uniformity

To produce Thin Film Transistor (TFT) screens, it is important to uniformly coat glass panels with the related thin films over large dimensions. To monitor the layer thickness uniformity on large glass panels, an ellipsometer mapping table was setup at Unaxis in Trübach under the direction of Dr. Sam Broderick. A compact SE moves over the glass panel as shown in Figure 5.

This development was made feasible by 3 features of modern elli-

**Fig. 4 - Experimental SE data covering from the UV to IR for a TiO2 coated glass substrate. This data is used to accurately determine the TiO2 optical constants (n and k) – as shown**
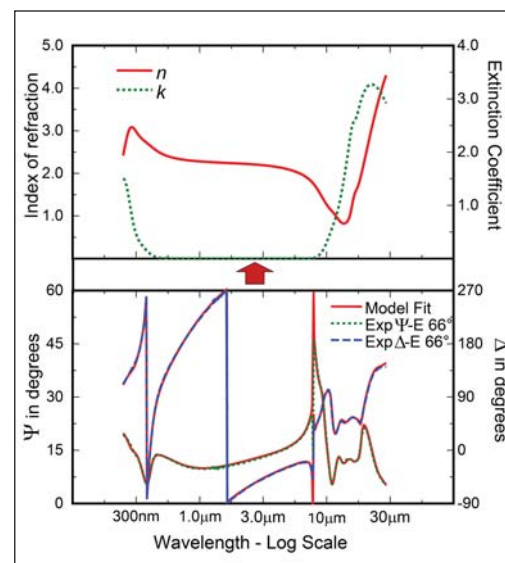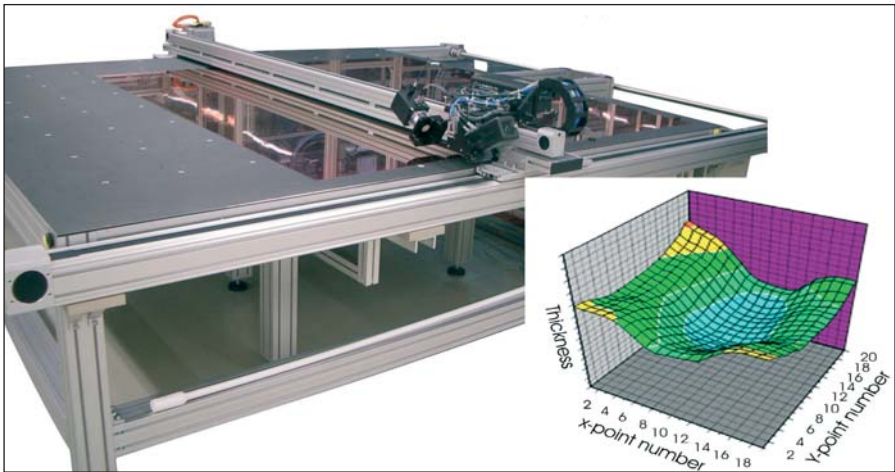
**Fig. 5 - Large-area mapping SE used to test film uniformity on large glass panels**

psometer technology: 1) compact optical design, 2) fast measurement speed, and 3) rotating compensator technology that allows accurate measurement with glass substrates. A panel can be scanned within minutes to provide the thickness profile. In addition, the ellipsometer can measure variation of the optical constants to provide layer 'quality' information to the process engineer.

*Industrial integration*

In situ *SE* measurements have been demonstrated with a large variety of processes, including Molecular Beam Epitaxy (MBE), Atomic Layer Deposition (ALD), Sputtering, Evaporation, Etching, and more.



**Fig. 6 - SE designed to work with roll-to-roll coatings by implementing a double-bounce method**

However, the hardware integration is not always trivial. The substrates are often in constant motion, which requires rapid data acquisition and often a "triggering" method. It may also be difficult to approach the sample using a standard configuration with the source and detector at equal-yet-opposite angles. An innovative solution for web-coatings involves aligning the source and detector nearly parallel to each other in a single housing. The light beam exits the housing as shown in Figure 6 and reflects from the web. It is then incident on a mirror and returns to the same housing after bouncing a second time from the web. In this manner, coatings can be monitored on flexible roll-to-roll substrates.

For multi-layer applications, it can be beneficial to collect *SE* data after each new coating. This is possible with some planetary deposition chambers,

where the sample can return to the measurement location. For other process designs, it may be helpful to use multiple *SE* systems. For example, Von Ardenne has incorporated a measurement system for in-line monitoring of multi-layer dielectrics on metal bands. Multiple *SE* systems are positioned after each layer deposition to provide accurate measurement of all layer thicknesses. Each *SE* communicates the current 'result' to the next ellipsometer in the process so it can analyze the new top layer with pre-determined results for the underlying structure. Figure 7 shows a typical Von Ardenne system with multiple ellipsometers mounted at key positions in the process.
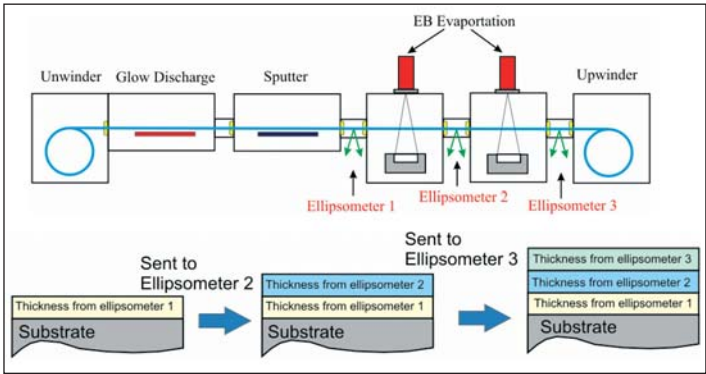


**Fig. 7 - Multiple SE systems are established on a large processing chamber to study multilayer coatings at different steps during processing. Each SE system can feed the current information to the next SE system to be used as the basis for characterization when the sample reaches the next system**
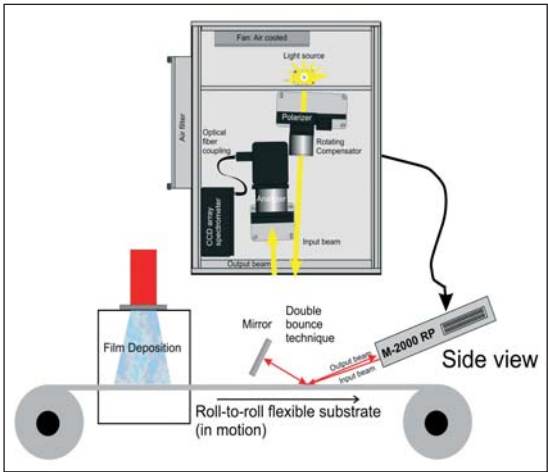
# Exhibit I

# SPECTROSCOPIC ELLIPSOMETRY ANALYSIS OF InGaN/GaN AND AlGaN/GaN HETEROSTRUCTURES USING A PARAMETRIC DIELECTRIC FUNCTION MODEL

J. Wagner, A. Ramakrishnan, H. Obloh, M. Kunzer, K. Köhler, and B. Johs[*]

Fraunhofer-Institut für Angewandte Festkörperphysik, Tullastrasse 72,
D-79108 Freiburg, Germany, wagner@iaf.fhg.de;
[*]J. A. Woollam Co., Inc., 645 'M' Street #102, Lincoln, Nebraska 68508

## ABSTRACT

Spectroscopic ellipsometry (SE) has been used for the characterization of AlGaN/GaN and InGaN/GaN heterostructures. The resulting pseudodielectric function spectra were analyzed using a multilayer approach, describing the dielectric functions of the individual layers by a parametric oscillator model. From this analysis, the dielectric function spectra of GaN, $Al_xGa_{1-x}N$ ($x \leq 0.16$), and $In_{0.13}Ga_{0.87}N$ were deduced. Further, the dependence of the $Al_xGa_{1-x}N$ band gap energy on the Al mole fraction was derived and compared with photoluminescence data recorded on the same material. The SE band gap data are compatible with a bowing parameter close to 1 eV for the composition dependence of the $Al_xGa_{1-x}N$ gap energy. Finally, the parametric dielectric functions have been used to model the pseudodielectric function spectrum of a complete GaN/AlGaN/InGaN LED structure.

## INTRODUCTION

Reproducible growth of high-quality (AlGaIn)N heterostructures requires, because of the rather narrow growth parameter window, fast and efficient characterization of, e.g., layer thickness and composition. Spectroscopic ellipsometry (SE) is a nondestructive optical characterization technique which has been used successfully for the characterization of conventional III-V heterostructures [1-4]. For a quantitative analysis of SE data on group III-arsenide and -antimonide heterostructures, detailed modeling of the pseudodielectric function spectra has been performed employing a multilayer approach, incorporating parametric dielectric function models for the individual layers [2-4]. With respect to the group III-nitrides, SE data and model fits to the dielectric function spectra have been reported so far mostly for bulk-like GaN and AlGaN [5-10]. We have reported recently on the SE characterization of $In_xGa_{1-x}N$ ($x \leq 0.1$) layers on GaN, but no modeling of the pseudodielectric function spectra has been performed to extract the dielectric function spectra of the individual layers [11].

The aim of the present investigation was to characterize hexagonal (AlGaIn)N heterostructures by variable angle SE and to analyze the resulting pseudodielectric function spectra within the framework of a multilayer model based on parametric dielectric functions. Parameterized dielectric function spectra have been derived for GaN, $In_{0.13}Ga_{0.87}N$, and $Al_xGa_{1-x}N$ ($x \leq 0.16$), allowing a direct determination of the composition dependence of the $Al_xGa_{1-x}N$ band gap energy $E_G(x)$. There is an ongoing controversy regarding the deviation of $E_G(x)$ from a linear dependence on x. Recent values for the bowing parameter b, which describes the magnitude of parabolic nonlinearity, range from 0, as derived from photoreflectance measurements for $x \leq 0.2$ [12], to 1.33 eV, as obtained from an absorption study covering the full composition range $0 \leq x \leq 1$ [13]. Another recent paper suggests, based on photoluminescence (PL) data and an extensive survey of previous works, a band gap bowing parameter for $Al_xGa_{1-x}N$ of b=0.62 eV [14].

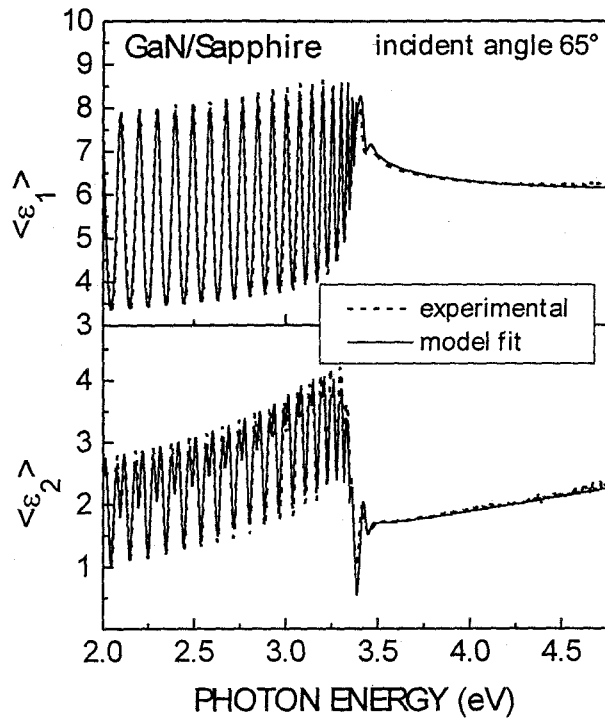*Fig. 1: Real $<\varepsilon_1>$ and imaginary part $<\varepsilon_2>$ of the pseudo-dielectric function spectrum of a 2.5 μm thick GaN layer on sapphire. Experimental data and model fits are indicated by dashed and full lines, respectively.*
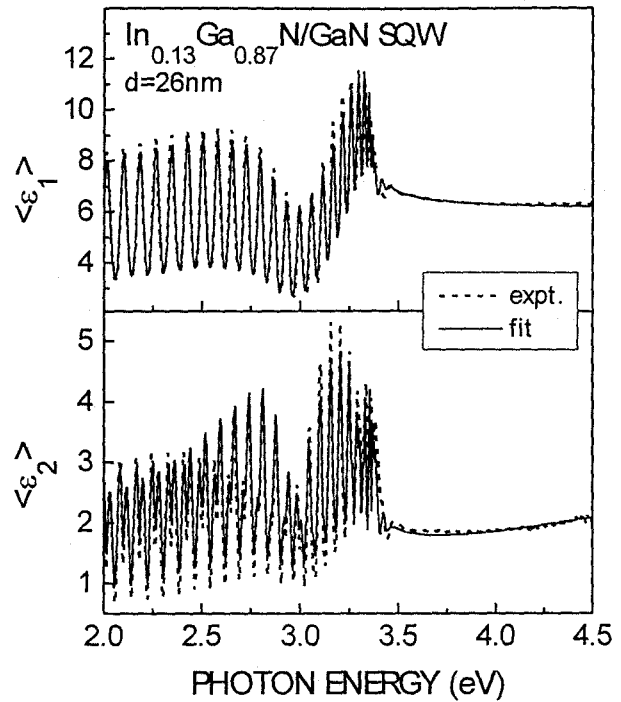
*Fig. 2: Real $<\varepsilon_1>$ and imaginary part $<\varepsilon_2>$ of the pseudo-dielectric function spectrum of a 26 nm thick $In_{0.13}Ga_{0.87}N$ layer embedded between GaN barrier layers. Experimental data and model fits are indicated by dashed and full lines, respectively.*

## EXPERIMENT

The AlGaN/GaN and InGaN/GaN heterostructures as well as a complete GaN/InGaN/AlGaN LED structure used for the present study were grown by low-pressure MOCVD on c-plane 2″ sapphire substrates using a low-temperature GaN nucleation layer. Details on sample growth can be found in Ref. [15]. The AlGaN and InGaN composition was determined by SIMS using appropriate standards calibrated by energy dispersive X-ray analysis (EDX).

Rotating analyzer variable angle SE was used to derive the room-temperature pseudodielectric function spectrum $<\varepsilon>$ of the (AlGaIn)N heterostructures, covering the range of photon energies from 2 to 5 eV. Incident angles of 65°and 75° were used while the polarizer azimuth was kept constant at 30°. Both incident angles gave identical $<\varepsilon>$ spectra, which confirms that the ellipsometry data correspond to an electric field vector perpendicular to the c-axis. For clarity of presentation only $<\varepsilon>$ spectra recorded for an incident angle of 65° will be shown in the following. Samples were further analyzed by PL spectroscopy.

## RESULTS AND DISCUSSION

The real $<\varepsilon_1>$ and imaginary part $<\varepsilon_2>$ of the pseudodielectric function spectrum of a 2.5 μm thick GaN film on sapphire is shown in Fig. 1 together with a parametric model fit to the experimental data. All features present in the experimental spectra are reproduced by the model fit. To match the amplitude of the layer thickness oscillations in the transparency region of the GaN film, a layer thickness uniformity of 0.7% was assumed, which accounts for inhomogeneities of
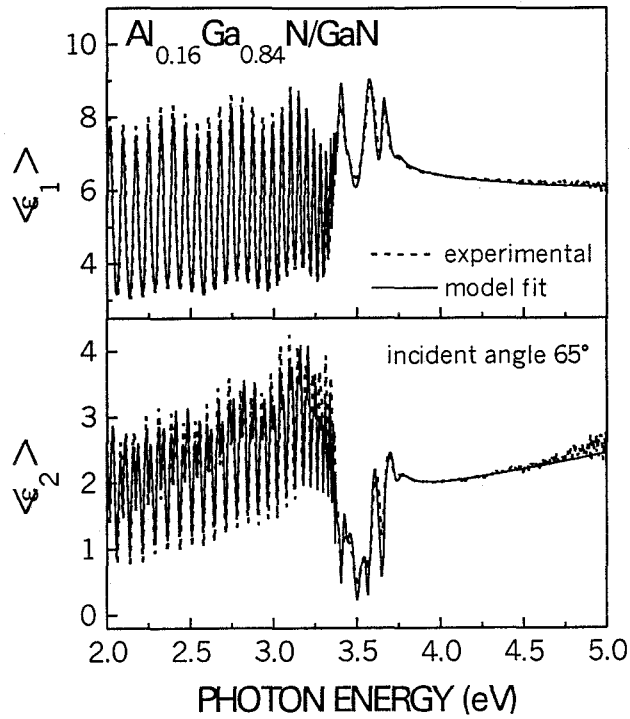
*Fig. 3:   Real $<\varepsilon_1>$ and imaginary part $<\varepsilon_2>$ of the pseudo-dielectric function spectrum of a 600 nm thick $Al_{0.16}Ga_{0.84}N$ layer on GaN. Experimental data and model fits are indicated by dashed and full lines, respectively.*
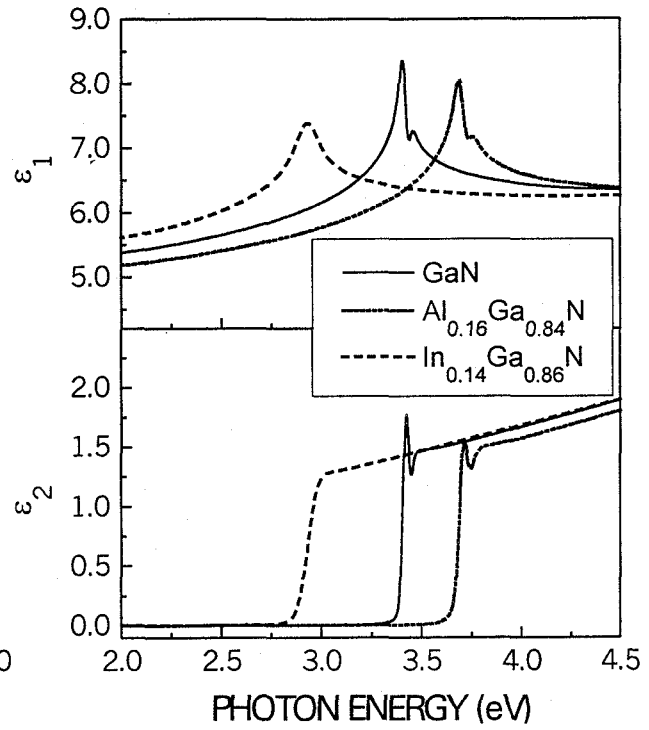
*Fig. 4:   Real $\varepsilon_1$ and imaginary part $\varepsilon_2$ of the parametric dielectric function spectra of GaN, $Al_{0.16}Ga_{0.84}N$ , and $In_{0.13}Ga_{0.87}N$ as deduced from multilayer parametric model fits to SE data.*

film thickness across the area probed by the ellipsometer as well as for imperfections of the GaN/sapphire interface, which also attenuate the interference oscillations. Further, a surface roughness of the GaN film of 0.9 nm was taken into account, which is compatible with atomic force micrographs which yield a RMS roughness of 2 to 3 nm at the most for the present samples.

Fig. 2 shows the $<\varepsilon_1>$ and $<\varepsilon_2>$ spectra of an InGaN/GaN heterostructure, consisting of a 26 nm thick $In_{0.13}Ga_{0.87}N$ layer embedded between a lower, 2.7 µm thick, and an upper, 130 nm thick, GaN barrier layers. From a comparison with the $<\varepsilon>$ spectrum of GaN on sapphire (see Fig. 1) the presence of the InGaN layer is readily detected via the occurrence of minima in both the $<\varepsilon_1>$ and the $<\varepsilon_2>$ spectrum at around 3 eV, which is the band gap energy of the InGaN. For the parametric model fit, also shown in Fig. 2, the GaN dielectric function was taken from the fit in Fig. 1 while the dielectric function spectrum of the InGaN layer was fitted. The InGaN layer thickness measured by SIMS was taken as an input parameter.

Pseudodielectric function spectra $<\varepsilon_1>$ and $<\varepsilon_2>$ of an AlGaN/GaN heterostructure are shown in Fig. 3 along with a parametric model fit. The sample is composed of a 600 nm thick $Al_{0.16}Ga_{0.84}N$ layer grown on top of a 2.77 µm thick GaN layer. The AlGaN layer was covered by 6 nm thick GaN capping layer. Again, the GaN dielectric function was taken from the fit to the GaN-on-sapphire sample and the AlGaN dielectric function was fitted. The parametric model fit nicely reproduces all features present in the experimental spectra. The AlGaN layer thickness deduced from the fit to the SE data of 609 nm is in excellent agreement with that of 594 nm determined by SIMS depth profiling.

The parametric dielectric function spectra $\varepsilon_1$ and $\varepsilon_2$ for GaN, $In_{0.13}Ga_{0.87}N$, and $Al_{0.16}Ga_{0.84}N$, deduced from the above shown fits, are plotted in Fig. 4. For both the GaN and the AlGaN
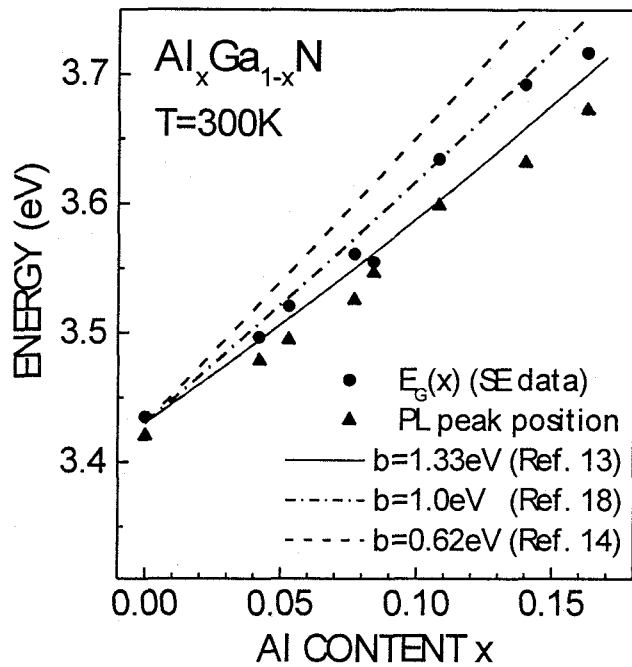
*Fig. 5:  Room-temperature $Al_{0.16}Ga_{0.84}N$ band gap energy $E_G(x)$, as derived from fits to SE data, and PL peak position versus Al content x. Calculated $E_G(x)$ curves, computed for different bowing parameters b given in the figure, are also shown.*

dielectric function spectra an excitonic resonance is resolved superimposed on the spectrum arising from band-to-band continuum transitions. For the model fit, the excitonic resonance was represented by a Gaussian oscillator. For InGaN, in contrast, this resonance is broadened, most likely due to compositional inhomogeneity [16], and just a single peak is present in the $\varepsilon_1$ spectrum.

For a series of $Al_xGa_{1-x}N/GaN$ heterostructures with $0 \leq x \leq 0.16$, the $Al_xGa_{1-x}N$ dielectric function was determined by fitting the SE data. From this analysis, the composition dependent $Al_xGa_{1-x}N$ band gap energy $E_G(x)$ was obtained, as depicted in Fig. 5. Further, PL peak positions recorded on the same series of samples are shown. The PL measurements were carried out at low temperatures (10 K) in order to resolve the AlGaN near band edge PL against the background from corresponding GaN related emission, which was difficult for room-temperature PL spectra in particular for low Al mole fractions. The resulting low-temperature PL peak energy was then down-shifted rigidly by 64 meV to account for the temperature induced band gap shift when going from 10 K to 300 K [17]. The data shown in Fig. 5 indicate a certain Stokes shift between $E_G(x)$ derived from the SE data and the PL peak position, which increases slightly with increasing Al mole fraction and thus increasing compositional disorder.

For comparison, also calculated $E_G(x)$ curves are shown, computed for representative bowing parameters of b=0.62 eV [14], b=1.0 eV [18], and b=1.33 eV [13]. For the room-temperature band gap energies of GaN and AlN values of 3.43 and 6.2 eV, respectively, were taken [13]. The composition dependence of the PL peak energy can be reproduced with a bowing parameter of b=1.3 eV, when allowing for a small rigid low-energy shift of the PL peak energy relative to the calculated $E_G(x)$. The $E_G(x)$ data obtained from the analysis of the SE data, in contrast, indicate a somewhat smaller bowing parameter closer to b=1.0 eV than b=1.33 eV. No fit for b to the present $E_G(x)$ data was attempted because of the limited composition range covered by the present set of samples.

## CONCLUSION

Spectroscopic ellipsometry in conjunction with a parametric dielectric function based multilayer model has been applied to the analysis of (AlGaIn)N heterostructures. Model dielectric functions for GaN, AlGaN, and InGaN have been derived. Further, the composition dependence of the $Al_xGa_{1-x}N$ band gap energy ($x \leq 0.16$) has been deduced from the present SE data. Based on the parametric model dielectric functions, the measured pseudodielectric function spectrum of complete (AlGaIn)N QW LED structures and GaN/AlGaN layer sequences suitable for the fabrication of modulation doped field effect transistors could also be modeled, yielding fit values for the individual layer thicknesses in close agreement with those obtained by SIMS depth profiling.

Thus the present study demonstrates the potential of spectroscopic ellipsometry for the analysis of layer thickness and composition in group III-nitride based device structures.

## ACKNOWLEDGMENTS

## REFERENCES

1. C. Pickering, R. T. Carline, M. T. Emeney, N. S. Garawal, and L. K. Howard, Appl. Phys. Lett. **60**, 2412 (1992).
2. C. M. Herzinger, H. Yao, P. G. Snyder, F. G. Celli, Y.-C. Kao, B. Johs, and J. A. Woollam, J. Appl. Phys. **77**, 4677 (1995); C. M. Herzinger, P. G. Snyder, F. G. Celli, Y.-C. Kao, D. Chow. B. Johs, and J. A. Woollam, *ibid.* **79**, 2663 (1996).
3. U. Weimar, J. Wagner, A. Gaymann, and K. Köhler, Appl. Phys. Lett. **68**, 3293 (1996).
4. J. Wagner, J. Schmitz, N. Herres, G. Tränkle, and P. Koidl, Appl. Phys. Lett. **70**, 1456 (1997).
5. S. Logothetidis, J. Petalas, M. Cardona, and T. D. Moustakas, Phys. Rev. B **50**, 18017 (1994).
6. J. Petalas, S. Logothetidis, S. Boultadakis, M. Alouani, and J. M. Wills, Phys. Rev. B **52**, 8082 (1995).
7. G. Yu, H. Ishikawa, M. Umeno, T. Egawa, J. Watanabe, T. Jimbo, and T. Soga, Appl. Phys. Lett. **72**, 2202 (1998).
8. T. Kawashima, H. Yoshikawa, S. Adachi, S. Fuke, and K. Ohtsuka, J. Appl. Phys. **82**, 3528 (1997).
9. A. B. Djurisic and E. H. Li, Appl. Phys. Lett. **73**, 868 (1998); J. Appl. Phys. **85**, 2848 (1999).
10. A. B. Djurisic, A. D. Rakic, P. C. K. Kwok, E. H. Li, M. L. Majewski, and J. M. Elazar, J. Appl. Phys. **86**, 445 (1999).
11. J. Wagner, A. Ramakrishnan, D. Behr, H. Obloh, M. Kunzer, and K.-H. Bachem, Appl. Phys. Lett. **73**, 1715 (1998).
12. T. J. Ochalski, B. Gil, P. Lefebvre, N. Grandjean, M. Leroux, J. Massies, S. Nakamura, and H. Morkoc, Appl. Phys. Lett. **74**, 3353 (1999).
13. W. Shan, J. W. Ager III, K. M. Yu, W. Walukiewicz, E. E. Haller, M. C. Martin, W. R. McKinney, and W. Yang, J. Appl. Phys. **85**, 8505 (1999).
14. S. R. Lee, A. F. Wright, M. H. Crawford, G. A. Petersen, J. Han, and R. M. Biefeld, Appl. Phys. Lett. **74**, 3344 (1999).
15. H. Obloh, D. Behr, N. Herres, C. Hoffmann, M. Kunzer, M. Maier, S. Müller, W. Pletschen, B. Santic, P. Schlotter, M. Seelmann-E., K.-H. Bachem, and U. Kaufmann, Proc. 2$^{nd}$ Int. Conf. Nitride Semicond. (Tokushima, Japan, 1997), p. 258.
16. S. Chichibu, T. Azuhata, T. Sota, and S. Nakamura, Appl. Phys. Lett. **70**, 2822 (1997).
17. G. Steude, B. K. Meyer, A. Göldner, A. Hoffmann, F. Bertram, J. Christen, H. Amano, and I. Akasaki, Appl. Phys. Lett. **74**, 2456 (1999).
18. Y. Koide, H. Itoh, M. R. H. Khan, K. Hiramatu, N. Sawaki, and I. Askasaki, J. Appl. Phys. Lett. **61**, 4540 (1987).
19. A. Ramakrishnan, J. Wagner, M. Kunzer, H. Obloh, and K. Köhler, submitted to Appl. Phys. Lett.

1  MILBANK, TWEED, HADLEY & McCLOY LLP
   Mark C. Scarsi (SBN 183926)
2  Chris L. Holm (SBN 249388)
   601 South Figueroa Street, 30th Floor
3  Los Angeles, CA  90017-5735
   Telephone:  (213) 892-4000
4  Facsimile:   (213) 822-5796
   F-N-wg@milbank.com
5
   MILBANK, TWEED, HADLEY & McCLOY LLP
6  Christopher E. Chalsen (*Pro Hac Vice*)
   Michael M. Murray (*Pro Hac Vice*)
7  Lawrence T. Kass (*Pro Hac Vice*)
   1 Chase Manhattan Plaza
8  New York, NY  10005
   Telephone:  (212) 530-5000
9  Facsimile:   (212) 822-5796
   F-N-wg@milbank.com
10
   Attorneys for Plaintiffs,
11 FUJITSU LIMITED and
   FUJITSU MICROELECTRONICS AMERICA, INC.
12
                  UNITED STATES DISTRICT COURT
13               NORTHERN DISTRICT OF CALIFORNIA
                      OAKLAND DIVISION
14

| | |
|---|---|
| 15 FUJITSU LIMITED and<br>FUJITSU MICROELECTRONICS<br>AMERICA, INC., | Case No.   4:06-CV-06613 (CW) (JCS)<br>4:07-CV-03672 (CW)<br>4:08-CV-01254 (CW) |
| 16 | |
| 17 *Plaintiffs and*<br>*Counterclaim-Defendants,* | **PLAINTIFFS' RESPONSES AND OBJECTIONS**<br>**TO THIRD-PARTY DEFENDANT KLA-**<br>**TENCOR CORPORATION'S FIRST SET OF** |
| 18 -against- | **REQUESTS FOR ADMISSIONS TO**<br>**PLAINTIFFS FUJITSU LIMITED AND FUJITSU** |
| 19 NANYA TECHNOLOGY CORP. and<br>NANYA TECHNOLOGY CORP. U.S.A., | **MICROELECTRONICS AMERICA, INC. (1-90)** |
| 20 | |
| 21 *Defendants and*<br>*Counterclaim-Plaintiffs.* | |
| 22 | |
| 23 NANYA TECHNOLOGY CORP. and<br>NANYA TECHNOLOGY CORP. U.S.A., | |
| 24 *Third-Party Plaintiff,* | |
| 25 -against- | |
| 26 KLA-TENCOR CORPORATION, | |
| 27 *Third-Party Defendant.* | |
| 28 | |

1 | **REQUEST FOR ADMISSION NO. 21**:

2 |      Admit that KLA-Tencor cannot be liable for directly infringing any Asserted Claim under

3 | 35 U.S.C. §271(a).

4 | **RESPONSE**:

5 |      In addition to its General Objections, Fujitsu objects to this Request as premature because

6 | it seeks contentions. As discussed in its General Objections, Fujitsu proposes that the parties

7 | exchange contention responses on a mutually agreeable date. Fujitsu also objects to this Request

8 | as requiring Fujitsu to form legal conclusions in order to respond, including but not limited to

9 | requiring interpretation of claims and/or claim terms that are subject to construction by the Court

10 | and are therefore not yet defined, and as seeking privileged information.

11 | **REQUEST FOR ADMISSION NO. 22**:

12 |      Admit that Fujitsu has not accused KLA-Tencor of directly infringing any Asserted Claim

13 | in this case under 35 U.S.C. §271(a).

14 | **RESPONSE**:

15 |      Admitted.

16 | **REQUEST FOR ADMISSION NO. 23**:

17 |      Admit that a computer database was known prior to December 28, 1995.
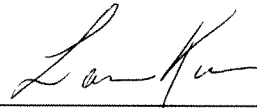
18 | **RESPONSE**:

19 |      In addition to its General Objections, Fujitsu objects to this Request as vague and as

20 | requiring Fujitsu to speculate as to the meaning of the term or phrase "a computer database was

21 | known". Fujitsu also objects to this Request as seeking information in the custody, possession, or

22 | control of persons or entities other than Fujitsu. Fujitsu also objects to this Request as premature

23 | because it seeks contentions. As discussed in its General Objections, Fujitsu proposes that the

24 | parties exchange contention responses on a mutually agreeable date. Fujitsu also objects to the

25 | Requests as premature to the extent they seek information that is properly the subject of expert

26 | reports and discovery.

27

28

FUJITSU'S RESPONSES AND OBJECTIONS TO      -17-            06-cv-06613 (CW)
KLA's 1st SET OF REQUESTS FOR ADMISSION
Confidential - Outside Counsel Eyes Only

1    information.  Subject to and without waiving the foregoing objections, and to the extent Fujitsu

2    understands this Request, denied.

3    Dated:   June 30, 2008          By:   _____
                                            MILBANK, TWEED, HADLEY & McCLOY LLP
4                                           Mark C. Scarsi (SBN 183926)
                                            Chris L. Holm (SBN 249388)
5                                           601 South Figueroa Street, 30th Floor
                                            Los Angeles, CA  90017-5735
6                                           Telephone:(213) 892-4000
                                            Facsimile: (213) 822-5796
7                                           F-N-wg@milbank.com

8                                           MILBANK, TWEED, HADLEY & McCLOY LLP
                                            Christopher E. Chalsen (Pro Hac Vice)
9                                           Michael M. Murray (Pro Hac Vice)
                                            Lawrence T. Kass (Pro Hac Vice)
10                                          1 Chase Manhattan Plaza
                                            New York, NY  10005
11                                          Telephone:(212) 530-5000
                                            Facsimile: (212) 822-5796
12                                          F-N-wg@milbank.com

13                                          Attorneys for Plaintiffs,
                                            FUJITSU LIMITED and
                                            FUJITSU MICROELECTRONICS AMERICA, INC.
14

15

16

17

18

19

20

21

22

23

24

25

26

27

28